Optimal Operation of Power Distribution Feeders with Smart Loads

by

Abolfazl Mosaddegh

A thesis
presented to the University of Waterloo
in fulfillment of the
thesis requirement for the degree of
Doctor of Philosophy
in
Electrical and Computer Engineering

Waterloo, Ontario, Canada, 2016

I hereby declare that I am the sole author of this thesis. This is a true copy of the thesis, including any required final revisions, as accepted by my examiners.

I understand that my thesis may be made electronically available to the public.

Abstract

Distribution systems have been going through significant changes in recent years, moving away from traditional systems with low-level control toward smart grids with high-level control, with improved technologies in communications, monitoring, computation, and real-time control. In the context of smart grids, Demand Response (DR) programs have been introduced so that customers are able to control and alter their energy consumption in consideration with distribution system operators, with benefits accruing to both customers and Local Distribution Companies (LDCs).

This thesis focuses on the integration of DR with the intelligent operation of distribution system feeders. Thus, it proposes a mathematical model of an unbalanced three-phase distribution system power flow, including different kinds of loads and other components of distribution systems. In this context, an unbalanced three-phase Distribution Optimal Power Flow (DOPF) model is proposed, which includes the models of lines, transformers, voltage-based loads, smart loads, Load Tap Changers (LTCs), and Switched Capacitors (SCs), together with their respective operating limits, to determine the optimal switching decisions for LTCs, SCs, and control signals for smart loads, in particular, Energy Hub Management System loads and Peaksaver PLUS^{TM} loads. Hence, Neural-Network-based models of controllable smart loads, which are integrated into the DOPF model are proposed, developed, and tested.

Since the DOPF model has different discrete variables such as LTCs and SCs, the model is a Mixed-Integer Non-Linear Programming (MINLP) problem, which presents a considerable computational challenge. In order to solve this MINLP problem without approximations and ad-hoc heuristics, a Genetic Algorithm (GA) is used to determine the optimal control decisions of controllable feeder elements and loads. Since the number of control variables in a realistic distribution system is large, solving the DOPF for real-time applications using GA is computationally expensive. Hence, a decentralized system with parallel computing nodes based on a Smart Grid Communication Middleware (SGCM) system is proposed. Using a "MapReduce" model, the SGCM system executes the DOPF model, communicates between the master and the worker computing nodes, and sends/receives data amongst different parts of the parallel computing system. When large number of nodes are involved, the SGCM system has a fast performance, is reliable, and is able to handle different fault tolerance levels with the available computing resources.

The proposed approaches are tested and validated on a practical feeder with the objective of minimizing energy losses and/or energy drawn from the substation. The results demonstrate the feasibility of the developed techniques for real-time distribution feeder

control, highlighting the advantages of integration of smart loads in the operation of distribution systems by LDCs.

Acknowledgements

First and foremost, I would like to express my sincere gratitude to my supervisors, Professor Claudio A. Cañizares and Professor Kankar Bhattacharya, for their continuous support to my PhD study and research, for their patience, motivation, enthusiasm, and immense knowledge. Their guidance helped me in my research and writing of this thesis. It was my privilege to complete my studies under their supervision.

My sincere thanks also goes to Professor Hongbing Fan from the Department of Physics and Computer Science, Wilfrid Laurier University, Waterloo, for his generous guidance with implementation of the Smart Grid Communication Middleware (SGCM) for power system applications. Without his support, it would not have been possible to conduct this research.

I thank the University of Waterloo, Natural Sciences and Engineering Research Council (NSERC) Smart Microgrid Research Network (NSMG-Net), Hydro One Networks, Energent Inc., Milton Hydro Distribution, the Ontario Power Authority (OPA), and the Ontario Center of Excellence (OCE) for their funding and support of this work.

I would like also to thank my PhD committee members for their encouragement, insightful comments and inputs: Professor Bala Venkatesh from the Department of Electrical and Computer Engineering, Ryerson University, Toronto, Canada; Professor Ian Rowlands from the School of Environment, Resources and Sustainability, University of Waterloo; Professor Mehrdad Kazerani and Professor Sagar Naik from the Department of Electrical and Computer Engineering, University of Waterloo.

My heartfelt thanks and endless appreciation to my family and in-laws for their unconditional support, love, care, and encouragement. To my beloved wife, Sana, no amount of thanks will be enough for the way you have supported me over these years. Thank you all, for being there for me throughout my ups and downs.

I also appreciate the help and support of Professor Benjamin Jeyasurya from the Department of Electrical and Computer Engineering, Memorial University of Newfoundland, St. John's, Canada, during my research under his supervision.

I thank my current and past colleagues from the Electricity Market Simulation and Optimization Laboratory (EMSOL): Sumit, Ehsan, Indrajit, Isha, Mehrdad, Nafeesa, Behnam, Victor, Juan Carlos, Mauricio, Mostafa, Bharat, Dario, Fabian, Ivan, Rupali, Felipe, Fabricio, Alfredo, Shubha, Jose, Mariano, Akash, Daniel, Edris, Rajib, Edson, David, Sofia, Chioma, and Nasrin, for all technical discussions, and for all the fun we have had during the last four years. Thank you all, for creating a pleasant and friendly working environment in the lab.

Dedication

I dedicate this work to my beautiful wife, Sana, for her unconditional love and for supporting me spiritually throughout my PhD studies and my life. I also dedicate this work to my parents, my parents-in-law, and my brothers, Reza and Hamed, for their support and encouragement.

Table of Contents

List of Tables

List of Figures

List of Acronyms

AC	Air Conditioner.
ADA	Advanced Distribution Automation.
AMI	Advanced Metering Infrastructure.
CPP	Critical Peak Pricing.
DG	Distributed Generation.
DLC	Direct Load Control.
DLF	Distribution Load Flow.
DMS	Distribution Management System.
DOPF	Distribution Optimal Power Flow.
DR	Demand Response.
DSA	Distribution System Automation.
DSM	Demand Side Management.
EA	Evolutionary Algorithm.
EHMS	Energy Hub Management System.
EMS	Energy Management System.
GA	Genetic Algorithm.
GHG	Greenhouse Gas.
HAN	Home Area Network.
HAS	Home Automation System.
HEM	Home Energy Management.
HVAC	Heating, Ventilation, and Air Conditioning.

I/O	Input/Output.
ID	Identification.
IESO	Independent Electricity System Operator.
ILC	Interruptible Load Control.
IP	Internet Protocol.
ISO	Independent System Operator.
KCL	Kirchhoff's Current Law.
LDC	Local Distribution Company.
LMA	Levenberg-Marquardt Algorithm.
LP	Linear Programming.
LTC	Load Tap Changer.
MILP	Mixed-Integer Linear Programming.
MINLP	Mixed-Integer Non-Linear Programming.
MIP	Mixed-Integer Programming.
MPC	Model Predictive Control.
MSE	Mean Squared Error.
NAN	Neighbourhood Area Network.
NLP	Non-Linear Programming.
NN	Neural Network.
OPA	Ontario Power Authority.
OPF	Optimal Power Flow.
PCT	Programmable Communicating Thermostat.
PEV	Plug-in Electric Vehicle.
PLC	Programmable Logic Controller.
PLC	Power Line Carrier.
PS+	Peaksaver PLUS™.
PSO	Particle Swarm Optimization.
PV	Photo-Voltaic.
RTO	Regional Transmission Organization.
RTP	Real-Time Pricing.

SC	Switched Capacitor.
SCADA	Supervisory Control and Data Acquisition.
SGCM	Smart Grid Communication Middleware.
SRLS	Smart Residential Load Simulator.
STATCOM	Static Synchronous Compensator.
TCP	Transmission Control Protocol.
TOU	Time of Use.
TSO	Transmission System Operator.
VVC	Voltage/Var Control.
WAN	Wide Area Network.

Nomenclature

Indices

c	Nodes, $c = 1, ..., N_N$.
dc	Delta-connected fixed capacitors.
dcc	Delta-connected controllable capacitor banks.
di	Delta-connected constant current loads.
dl	Delta-connected loads and capacitors, $dl = dc, dcc, di, dp, dz$.
dp	Delta-connected constant power loads.
dz	Delta-connected constant impedance loads.
e	Nodes, $e = 1, ..., N_N$.
fc	Per-phase controllable tap changers.
h	Time interval, $h = 1, ..., 24$.
i	Input layer nodes, $i = 1, ..., N_I$.
k	Set of objective functions, $k = 1, ..., 4$.
l	Series elements, $l = fc, sw, tr, wr$.
lf	Feeder line, $lf \in wr$.
lr	Series elements whose receiving ends are connected to node n.
ls	Series elements whose sending ends are connected to node n.
n	Nodes, $n = 1, ..., N_N$.
nd_W	Worker-nodes, $nd_W = 1, ..., Nd$.
o	Output layer nodes, $u = 1, ..., N_O$.
o	Output layer nodes, $u = 1, ..., N_O$.
p	Phases, $p = a, b, c$.
pp	Phase-to-phase, $pp = ab, bc, ca$.
r	Receiving-end.
r_n	Receiving-ends connected at node n.
s	Sending-end.
s_f	Substation node, $s_f \in n$.
s_n	Sending-ends connected at node n.

sw	Switches.
tr	Transformers, $tr = tr1, tr2, tr3, tr4, tr5$.
$tr1$	Delta - grounded wye step-down transformers.
$tr2$	Ungrounded wye - delta step-down transformers.
$tr3$	Grounded wye - grounded wye transformers.
$tr4$	Delta - delta transformers.
$tr5$	Open wye - open delta transformers.
u	Hidden layer nodes, $u = 1, ..., N_H$.
wr	Conductors/Cables.
yc	Wye-connected fixed capacitors.
ycc	Wye-connected controllable capacitor banks.
yi	Wye-connected constant current loads.
yl	Wye-connected loads and capacitors, $yl = yc, ycc, yi, yp, yz$.
yp	Wye-connected constant power loads.
yz	Wye-connected constant impedance loads.
Parameters	
A_l, B_l, C_l, D_l	Three-phase ABCD parameter matrices; A_l and D_l are dimensionless, B_l in [kΩ], and C_l in [μS].
b_{ec}	Susceptance or imaginary part of Y_{ec} from node e to node c [μS].
C^{max}	Total number of capacitor blocks available in capacitor banks.
$CAP_{ycc/dcc,n,p/pp}$	Fixed number of capacitor blocks in capacitor banks.
CR	Cross-over rate.
EN	Elite off-spring selection.
G	Maximum number of generations in Genetic Algorithm (GA).
g_{ec}	Conductance or real part of Y_{ec} from node e to node c [μS].
G_m	GA generations/iterations.
H	Output of hidden layer neuron.
$\overline{I}_{lf}$	Maximum feeder current limit [A].
$\overline{I}_l$	Maximum line current limit [A].
$I^{sp}_{yi/di,n,p/pp}$	Load current at specified power and nominal voltage [A].
$I_{inj_{l,p,t}}$	Injection current [A].
MR	Mutation rate.
N	Transformer turn ratio.
N_H	Number of neurons in the hidden layers.
N_I	Number of neurons in the input layers.
N_N	Total number of nodes.
N_O	Number of neurons in the output layers.

N_O	Number of neurons in the output layers.
Nd	Distributed nodes in the Middleware System.
$P^g_{n,p,h}$	Generated active power [kW].
P_{cons}	Target active power demand [kW].
P_{lim}	Active power demand limit [kW].
$P_{yl/dl,n,p/pp}$	Load active power [kW].
PS	Population size.
$Q^g_{n,p,h}$	Generated reactive power [kVar].
$Q_{yl/dl,n,p/pp}$	Load reactive power [kVar].
R_{max}	Maximum allowable value of R [kWh].
R_{min}	Minimum allowable value of R [kWh].
SV	Stall generation limit.
$T^{max}_{n,p}$	Maximum hours of Programmable Communication Thermostat (PCT) operation [h].
$\overline{TAP}_{p,fc}$	Maximum tap changer position.
$TAP_{p,fc}$	Fixed tap position.
$\underline{TAP}_{p,fc}$	Minimum tap changer position.
TL	Termination time limit [min].
U	The 3×3 identity matrix.
$\overline{V}$	Maximum voltage limit [kV].
$V^{sp}_{n,p/pp}$	Specified nominal voltage [kV].
$\underline{V}$	Minimum voltage limit [kV].
W	Weight of the connection between hidden and output layer neurons.
W	Weight of the connection between hidden and output layer neurons.
$X_{yl/dl,n,p/pp}$	Reactance of a capacitor [kΩ].
Y_{ec}	Nodal admittance matrices of the power system from node e to node c [μS].
Y_l	Load admittance at specified power and nominal voltage [μS].
$Yprim$	An admittance of power delivery or power conversion elements at OpenDSS simulator [μS].
$Ysyst$	System admittance matrix at OpenDSS simulator [μ].
Z_l	Load impedance at specified power and nominal voltage [kΩ].
α_k	Peak demand factor.
β	Peak load penalty factor.
$\gamma_{max_{n,p,h}}$	Maximum allowable value of peak demand cap [kW].
$\gamma_{min_{n,p,h}}$	Minimum allowable value of peak demand cap [kW].
δ	Bias of hidden layer neurons.

$\Delta Q_{ycc,n,p}$	Size of each capacitor block in capacitor banks [kVar].
ΔT_{fc}	Per-unit voltage change for each tap changer position.
$\theta^{sp}_{yi/di,n,p/pp}$	Specified load power factor angle [rad].
θ_h	Ambient temperature [°C].
σ_h	Time of Use (TOU) Tariff [$/MWh].
ω	Weight of the connection between input and hidden layer neurons.
Ω	Bias of output layer neurons.
Variables	
$cap_{ycc/dcc,n,p/pp}$	Number of capacitor blocks switched on.
E_{drawn}	Energy drawn from the substation [kWh].
E_{loss}	Energy losses [kWh].
F	Objective function [kWh].
$I_{n,p,l}$	Current phasor [A].
J_1	Energy losses [kWh].
J_2	Energy drawn from the substation [kWh].
P_{feeder}	Feeder active power [kW].
Ps	Simulated active power demand for Energy Hub Management System (EHMS) Micro-hub loads [kW].
Psl	Simulated active power demand for Peaksaver PLUS^{TM} (PS+) loads [kW].
R	Sum of peak demand cap signals [kWh].
t	Time interval of OpenDSS simulator [s].
$tap_{p,fc}$	Tap position.
$V_{n,p,l}$	Voltage phasor [kV].
$\gamma_{n,p,h}$	Peak demand cap [kW].
$\mu_{n,p,h}$	Binary ON/OFF signal for PCT setpoints of Air Conditioners (ACs).
ϕ	Angle of phasor voltage [rad].

Chapter 1

Introduction

1.1 Motivation

With the continued growth in global population, the world's energy consumption is expected to increase significantly over time. A 56% increase in global energy consumption between 2011 and 2035 is expected, with a 93% increase in electricity generation and 66% increase of world electricity demand projected for the same period. Renewables and nuclear are expected to be the most important energy sources, which have been increasing by 2.5% per year [1]. In Ontario, Canada, the peak load and energy demand are expected to increase by 25% and 26%, respectively over the period of 2014-2033 [2], which requires augmenting transmission lines and generation capacity of the system.

Climate change is the most important environmental issue associated with fossil-fuel-based electricity generation. The world petroleum and other liquid fuels consumption is estimated to increase from 176 to 243.1 quadrillion BTU, with an average annual increase of 1.1% [3]. Hence, to reduce the impact of global warming by reducing Greenhouse Gas (GHG) emissions from fossil-fuel-based generation and also meet the rapidly increasing demand, there is a need for cleaner energy sources in the system. Energy conservation, energy management, and renewable energy resources are among the different possible alternatives. For example, Ontario is the first jurisdiction in North America to completely remove all coal-fired electricity generation [4]. However, building new transmission lines and generation is costly, and hence, finding effective and intelligent methods to manage and reduce the peak load and energy demand are important.

The need to make the grid more reliable and efficient, driven by economic growth and climate change concerns, has led to the development of smart grids, which incorporates

technologies and advanced applications including Demand Side Management (DSM) and Distributed Generation (DG) units. In smart grids, customers have the ability to use electricity more efficiently through smart metering and intelligent controls, based on new communication infrastructure, information management, and automated control technologies [5]. One of the basic components of these smart grids is the Advanced Metering Infrastructure (AMI), which includes "smart meters" to provide two-way communication between utilities and customers. As a result, controllable smart loads are being introduced in distribution networks, which allow developing and implementing Energy Management Systems (EMSs) for customers and distribution feeders, with smart meters having the ability to measure energy consumption in real-time and also providing usage information. With these capabilities, both utilities and customers can communicate, observe, and control their specific needs [6]. In this context, advanced communication, control, and measurement technologies at both customer and feeder levels facilitate and enhance DSM and Demand Response (DR) programs, which allow customers' involvement in the operation and control of the distribution system [7].

DR programs have been and continue to be implemented in order to alter and control the demand shape through Local Distribution Company (LDC) requests, incentive signals, and/or external signals such as price or weather signals. Among different contributions to the realization of a smart grid in Ontario [8–11], the Energy Hub Management System (EHMS) project was initiated in April 2008 with the purpose of developing and implementing smart EMSs for commercial/institutional, agricultural, industrial, and residential customers [12, 13], as well as for distribution feeders, and is geared towards improved communications, control, and real-time information for customers and utilities. From the customers' point of view, the objective of EMSs is to reduce the cost of energy consumption and/or carbon footprint, whereas utilities have additional concerns such as load shifting, peak load reduction, and improvement in the quality of service. Based on these different objectives, energy management of distribution feeders has been discussed at two levels in the context of EHMS: the micro-hub level, which concentrates on customers operation, optimization, and control, and the macro-hub level, which deals with utility concerns, communicates with all groups of micro-hubs, and operates from the perspective of LDCs [12, 13].

In Ontario, Canada, a target to reduce the peak demand was set to 6,300 MW by 2025 through DSM, DR, and demand control programs [14]. In this context, a voluntary Peaksaver PLUS^{TM} (PS+) program was introduced by the Ontario Power Authority (OPA)[1] to reduce Air Conditioner (AC) demand in the residential and small commercial sector,

[1]The OPA was merged into the Independent Electricity System Operator (IESO) on January 1, 2015.

and hence reduce the system peak load during the summer by slightly increasing the AC temperature setpoints of the smart thermostats.

The need to minimize energy consumption and reduce peak load in smart distribution systems is the focus and motivation of this work, which proposes a Distribution Optimal Power Flow (DOPF) model at the feeder level, consisting of an unbalanced three-phase distribution system power flow, and including different kind of loads and other components of distribution systems such as lines, transformers, voltage-based loads, Neural Network (NN)-based smart loads, Load Tap Changers (LTCs), and Switched Capacitors (SCs), together with their respective operating limits, to determine the optimal switching decisions for LTCs, SCs, peak demand caps for EHMS smart loads, and Programmable Communicating Thermostat (PCT) ON/OFF signals for PS+ smart loads. With the presence of controllable smart loads, DR is considered in the model in order to reduce the system peak load and also study the effect of smart loads in the DOPF model, which is expected to be beneficial from the perspective of both LDCs and customers.

1.2 Literature Review

This section reviews the state-of-the-art of the relevant techniques and technologies on which the presented research is based. Thus, an overview is presented next of Distribution Management System (DMS), Distribution System Automation (DSA), DSM, DR, and distributed computing approach to DOPF.

1.2.1 Distribution Management Systems and Distribution System Automation

Reliability and power quality at the distribution level are the focus of DSA, which provides options for computation, communication, and control of distribution systems in real time. Since the 1970s, the concept of DSA appeared in the literature, together with improvements in monitoring, control and communication technologies [15]. The evolution of DSA can be categorized into three main stages, as follows [16]:

1. Positioning central processor controllers with distributed sensors in different areas to collect data; Programmable Logic Controllers (PLCs) were the earliest devices.

2. Integration of PLCs in the network using a new communication architecture.

3. Intelligent DSA, in which the intelligence is decentralized and embedded into software components. The hardware system (i.e., the distributed computing system) should be able to deal with the required computational burden.

Distribution systems have been changing in recent years, moving away from traditional systems with low-level control toward smart grids with high-level control, based on improved technologies in communication, monitoring, computation, and real-time control. EMSs and their application to distribution systems, referred to as DMSs, are essential to the smart grid. EMSs in power grids have traditionally supervised and controlled high/medium voltage transmission systems and power plants, whereas DMSs have dealt with medium/low voltage distribution systems [17]. DMSs have the following objectives [18]:

- Maintain the system in good conditions under bus voltage and line or transformer constraints.
- Try to achieve unity power factor at the feeders.
- Minimize power losses in lines and transformers.
- Minimize the injected active power, i.e., energy drawn and peak demand, at the substation transformer.
- Manage reactive power to improve system voltage and minimize losses.
- Maximize revenue, i.e., maximize the difference between the cost of electricity production from load DG units and energy sales to customers.

Voltage and reactive power control in distribution systems are two important aspects of DSA and DMS, which have been traditionally carried out by LTCs, SCs, fixed capacitors, and step-voltage regulators. LTCs and step-voltage regulators are voltage-control devices, while SCs and fixed capacitors can regulate both voltage and reactive power. All these traditional Voltage/Var Control (VVC) devices operate locally with stand-alone controllers to improve voltage profiles and reduce energy losses. These devices lack continuous monitoring and automatic reconfiguration systems, hence optimal operation cannot be guaranteed under all circumstances. To this effect, Mixed-Integer Non-Linear Programming (MINLP) models have been proposed to determine the discrete settings of LTCs and SCs in an optimal integrated VVC approach [19–24].

Overall, VVC problems can be divided into two main categories: rule-based and network-model-based [18]. The rule-based methods, which use real-time measurements, have been

applied to control discrete devices such as SCs and LTCs, wherein the key factors for determining the discrete settings are rules and operator experience [24–29]. In [25], a decoupled VVC problem is presented, assuming a weak coupling between the voltage and reactive power, which decouples the control problem into two independent sub-problems, in which LTCs control the voltage, while SCs control the reactive power. In [24], the authors apply the VVC approach to minimize active power mismatches between simulated and real results from DR programs, proposing an MINLP problem to find the optimal size and location of Static Synchronous Compensator (STATCOM) and/or optimal values of LTCs. In [26], the authors propose a solution of the VVC problem for different levels of measurement and communication infrastructure in the distribution system. In [27,28], by using Benders' decomposition, the MINLP VVC problem is solved with LTCs and SCs as integer variables, while reactive power of DG units are considered as continuous variables. In [27], the authors separate the discrete and continuous variables, decomposing the problem into a Non-Linear Programming (NLP) sub-problem with fixed discrete variables and a Mixed-Integer Linear Programming (MILP) master problem; the master problem is a relaxed MINLP problem, and it updates the discrete variable iteratively until the bounds for continuous variables are contained within a fixed tolerance. The authors suggest their method is close enough to the optimal solution, which can be considered as a practical model in distribution systems; however, there is no guarantee to arrive at the global optimal solution with this approach. In [28], the general VVC problem is decomposed into two sub-problems: the "volt sub-problem" which is a Mixed-Integer Programming (MIP)-based master problem, and the "var sub-problem", which is an MILP problem. The sub-problems are solved by Benders' decomposition with the objective of minimizing the system real power losses. Compared to [27], this method determines the optimal value of integer variables (i.e., the reactive power from DG units), while [27] proposes a range for the reactive power from DG units. Since rule-based methods are useful when wide-area measurements are not available (i.e., the solution is obtained based on off-line studies) and the VVC control is just based on local measurements, the optimal solution for systems is not guaranteed; hence, frequent changes in the settings of those controllers are proposed in [29] to account for seasonal load variations and reconfiguration of the system.

Network-model-based VVC methods are based on different parameters such as the topology of a distribution system, system configuration, measurements, and statistical data. Typically, to obtain the optimal solution in these methods, the Distribution Load Flow (DLF) and the DOPF models are used, where DLF equations are considered as constraints in the DOPF model. To solve the network-model-based VVC problems for larger systems and to reduce the computational costs, heuristic methods such as NN techniques [20, 30], computational cost reduction [29, 31], and decoupling of the VVC problem

into sub-problems [22, 23] have been proposed. In [20], NN and fuzzy dynamic programming techniques are combined in order to speed up the VVC computations. Because of the lack of sensors and accurate measurements in distribution systems, state estimators are inadequate to assess distribution system variables such as active and reactive powers; hence, the VVC real outputs are not close enough to the optimal values of DOPF problems. In [30], an NN model is used to reduce this error and have a better estimation, which is necessary for proper functioning of Advanced Distribution Automation (ADA) systems.

In [29], a fast DLF is proposed to reduce the computational costs, and in [31], a fast gradient technique in combination with a heuristic method, which is compared with conventional methods, is introduced, and the results show that the proposed technique increases the run-time by about 30-35 times. However, approaches with enumerative techniques are good enough to deal with smaller systems with limited number of LTCs and SCs. In [32–35], the authors consider the DLF equations as constraints in the DOPF model, and relax the MINLP problem into an NLP problem by rounding the discrete variables to their closest integer values and applying the quadratic penalty approach. Reducing the complexity of the DOPF model reduces the computational burden and makes it suitable for real-time applications. The authors also consider the limits on the number of daily switching operations of SCs and LTCs in the DOPF solution, because of the maintenance costs of these controllers, but the drawback of rounding continuous variables into discrete variables is that the solution may be sub-optimal, because of the discrete nature of those variables. The same authors in [36] propose a Genetic Algorithm (GA) approach to determine the optimal solution of VVC-based DOPF problem, and the results are compared with a heuristic approach in terms of both optimality and computational burden as an NLP problem, arguing that the GA-based DOPF solution yields superior solution in terms of optimality but at larger computational costs; the heuristic method is shown to reduce the run-time of the DOPF model, although with sub-optimal solutions.

Based on the above discussion, this thesis focuses on improving existing DOPF techniques for real-time applications. Thus, since the DOPF model has different discrete variables such as LTCs and SCs that make it an MINLP problem, it presents a considerable computational challenge, particularly for the practical application discussed here. In order to solve this MINLP problem without approximations and ad-hoc heuristics, and also to have a superior optimal solution, the Evolutionary Algorithm (EA) approach of GA is used to solve the DOPF model. GA is preferred in this work, amongst other EA approaches, because it is possible to run the DLF for each individual GA chromosome independently, and hence, it can be easily parallelized for the real-time applications considered in this study. Thus, the distributed computing approach referred to as Smart Grid Communication Middleware (SGCM) is used here to reduce the computational burden of the DOPF model,

which is particularly suitable for the proposed GA-based DOPF solution approaches.

1.2.2 Demand Side Management and Demand Response

Since the late 1970s, DSM has been used to refer to a set of end-user measurements, plans, implementations, and methods that impact the attitude of customers and the shape of the load curve [37]. The efficient use of energy and incentive tariffs such as Real-Time Pricing (RTP) and Time of Use (TOU) tariffs are part of DSM. Peak clipping, valley filling, load shifting, and flexible load shaping are among the DSM strategies. Generally, DSM can be classified as follows [38]:

- Energy efficiency and conservation.
- Strategic load growth.
- DR.

Energy efficiency and conservation refers to programs that result in reduction in energy consumption by specific end-use systems or devices, typically, without any impact on the provided services. Energy consumption is reduced by substituting the existing system with more energy-efficient technologies; designing buildings in an efficient way and efficient lighting programs are two examples of this approach [39]. In contrast, strategic load growth essentially refers to increasing the load levels through electrification in a strategic way.

DR programs have been introduced so that customers can control and alter their energy consumption, with benefits accruing to both customers and LDCs [34]. Many DR programs are based on the relation between electricity price and demand. A review since 1970 shows the following realizations of DR programs [40]:

1. *Frequency-based schemes*: Load shedding has been proposed as a method to restore the frequency of a system to a normal value. For example, in [41], a central DR algorithm is used to minimize the number of load shedding operations for frequency restoration, and in [42], some "responsive end-user devices" are introduced at the residential level for the frequency control of the system.
2. *Direct control of utility devices*: Voltage reduction in order to conserve energy has been proposed in the literature [43–46]. Protection relays such as fuses and reclosers and remote controller relays are also considered for DSM in [47].

3. *Direct control of customers' devices*: Timer-based switches have limited applicability in DR, but utilities have no control on these devices, and if a contingency occurs in the system, the device cannot be isolated automatically. Remote systems based on Power Line Carriers (PLCs), internet, and radio wave systems make end-users' devices controllable within a distribution system.

4. *Cost-based controls*: Introduction of different tariffs encourage customers to consider the way they use power. Through proper pricing mechanisms, end-users can be encouraged to reduce their energy use and reduce their energy costs. TOU pricing, Critical Peak Pricing (CPP), and RTP are among the incentive tariffs used to indirectly control the user behaviour, as follows:

   - TOU pricing: Constant rates are defined for periods of time, with lower prices at off-peak periods and higher prices at peak-demand periods. In [48], the Ontario TOU pricing is discussed, suggesting additional modifications to make the TOU pricing appropriate for different seasons.
   - CPP: These tariffs represent a transition from a static TOU tariff to a dynamic tariff scheme, with a flexible pre-determined period of time during critical system conditions (i.e., when the system is stressed). Different optimal strategies based on interests of utilities and customers are suggested for CPP in [49].
   - RTP: Changing utilities' energy prices in real-time can motivate customers to respond to pricing signals and hence reduce their costs. In [50], two important requirements for the implementation of RTP are mentioned: a suitable infrastructure and well-informed end-users who respond to pricing signals. Some examples of suitable infrastructure are Home Automation Systems (HASs), Home Energy Management (HEM), and Home Area Network (HAN), which allow energy consumption scheduling and ADA devices to assist in real-time monitoring, scheduling, and control [51–53].

5. *Market-based controls*: Some organizations such as Regional Transmission Organizations (RTOs), Independent System Operators (ISOs), and Transmission System Operators (TSOs) encourage customers to take part in distribution systems control by using DG sources. The main use of these sources has been in emergency conditions; however, customers are now being paid to participate in DR actions. In this context, DG sources can be considered as providers of energy and ancillary services in distribution systems [54, 55].

6. *Model-based controls*: Load response can be accomplished by using model-based predictive control algorithms. The architecture of such systems can be divided into

centralized and decentralized schemes. Model Predictive Control (MPC) is based on centralized methods. For example, in [12, 56, 57], the model schedules appliances for residential customers; in [58], solar Photo-Voltaic (PV) power for electrical thermal appliances is maximized; and in [59], an MPC algorithm with different kind of tariffs is proposed to optimize distributed energy resources like PV in residential sites. Given the increasing number of controller devices in smart grids, decentralized approaches based on multi-agent control systems are being researched. For example, an automated DR technique is proposed in [60] based on a global coordinator (aggregator) that addresses privacy and security concerns. The authors propose a uniform interface for management of distributed energy resources in terms of their energy capabilities that can be attributed to different markets and services; these resources are then aggregated in order to deliver energy services to these markets.

In the present research, the impact and use of existing DSM and DR techniques for distribution feeder management is studied. Thus, two different NN-based controllable smart load models are developed for both EHMS micro-hubs and PS+ smart loads, to integrate them into the DOPF model to optimally control LTCs and SCs, and send optimal peak demand cap signals for EHMS loads and ON/OFF signals to PCTs for PS+ loads. The impact and use of these controllable loads by LDCs to control the load profile at the feeder level is analyzed in order to optimize energy consumption and reduce peak demand over a desired horizon.

1.2.3 Distributed Computing Approach to DOPF

An increase in the number of controller devices in smart grids is a significant challenge in the operation of distribution systems. In particular, with the presence of smart controller loads, the need to quickly update the operation strategy of controllable devices is necessary. In this context, real-time optimization applications such as the DOPF are required. Therefore, distributed computing approaches to solve DOPF models have been proposed in the literature. In [61–63], a central multi-processor server/computer unit is used to obtain the DOPF solution without any decomposition of the model. In [61], probable scenarios around the forecasted wind power are determined and the real-time DOPF for different scenarios runs in parallel. In [62], possible generation and size of DG units are obtained from a Monte Carlo method, and then using a multi-core MATLAB® program, each core is responsible to run the DLF of individual set of variables. In [63], a Jacobian-based sensitivity approach is developed for the purpose of distribution energy management of distribution systems; the authors proposed that by decreasing the time window, the computation time

exponentially increases, and by using the multi-core processors with 5000 cores, the average computation time considerably reduces. Although multi-core or multi-processor units can reduce run-times, the program speed cannot be increased because of the limited number of cores of the processor units. Furthermore, in case of computer failures, there is a need to re-run the whole program.

Another category of a distributed computing approach consists on DOPF models being decomposed into sub-problems, with each sub-problem being independently run on a computing node of a distributed computing system [64–66]. Thus, in [64], the model, which is in a tree structure is decomposed into sub-tree problems, with each sub-problem searching for loss minimization independently. In [65], the distribution system is decomposed into three different levels, namely, primary main feeders, single-phase laterals, and secondary systems; an optimization model is then formulated for each sub-network, while the results are coordinated to find the optimal solution of the network. In [66], the network is decomposed into two sub-areas, with the output of DG units being optimized independently in each sub-area; a global power flow is then calculated based on the results of those sub-areas. Although the distributed computing approach with decomposition models can reduce the run-time, because of the decomposition, the DOPF solution may be sub-optimal.

In this work, in order to reduce the computational burden of the DOPF model with GA-based solution and make it suitable for real-time applications, a distributed computing platform is proposed based on the SGCM system [67], since this system is designed for smart grid applications including data acquisition, monitoring, and distributed computing. As per [67], the system is built on top of a reconfigurable interconnection network computing platform, and provides reliable, secure, and fast performance two-way communication among nodes of utility servers, energy hubs, and smart sensors/controllers. Similar to Hadoop [68–70], which is a distributed computing platform for MapReduce models [71], the SGCM uses proprietary protocols on top of the Transmission Control Protocol (TCP)/Internet Protocol (IP) for inter-communication of computing components. However, unlike Hadoop, the SGCM uses programmable data paths to distribute/collect data to/from computing nodes running distributed computers, while Hadoop uses a chained pipe to distribute files to different data nodes in a cluster. Hence, the SGCM has the same functionality for solving MapReduce problems as Hadoop does, but in a customized approach. By using different servers/computers with different port specifications, independent computing nodes, which can independently run the DOPF model, are defined. Without using any approximation or decomposition in the DOPF model, the full model can be run on different computing nodes, and in a master-slave structure, the optimal results can be obtained. Furthermore, the reliability of the SGCM is higher than other computing systems, because in case of computer failures, just the computers/ports which

are faulty fail, while the system as whole continues solving the model, isolating the faulty computing nodes.

1.3 Research Objectives

Based on the aforementioned literature review and associated discussions, the followings are the main objectives and contribution of the research proposed in this thesis:

- Implement a power flow model of an unbalanced three-phase distribution system, referred to as a DLF, including controllable smart loads and other components of distribution systems. The DLF model needs to be a stand-alone executable program that can be used on different platforms (i.e., the Windows, Linux, and Mac), for its implementation in the proposed distributed computing approach. The proposed DLF is solved in the OpenDSS simulator [72].
- Develop NN-based models of EHMS micro-hub and PS+ controllable loads, and integrate them into the DLF model, to realize appropriate DOPF models with the objectives of minimizing energy loss and peak demand over a desired horizon.
- Develop a GA-based solution approach for the DOPF model to find optimal switching of control devices such as LTCs, SCs, peak demand caps on EHMS micro-hub loads, and thermostat signals on PS+ loads, and develop a "MapReduce" model, using a distributed computing approach on an SGCM system [73], to reduce the computational time of the GA-based model to make it suitable for real-time applications.
- Test the developed DOPF model on a practical test feeder in order to demonstrate and validate the proposed method for practical applications.

1.4 Thesis Outline

The remainder of the thesis is organized as follows:

- Chapter 2 presents a review of the main background topics for this research. Thus, a brief background on DSA, DMS, and centralized VVC problems is first presented, followed by a discussion on load modeling and load management programs in the context of DSM and DR. A detailed explanation of EHMS and PS+ loads is also presented,

followed by a discussion on mathematical programming models and their solution approaches. The distributed computing approach based on the SGCM system is also introduced and explained. Finally, detailed mathematical models of distribution system components for the DLF model are described.

- Chapter 3 discusses the algorithm for solving an unbalanced three-phase DLF model. Two distribution feeders, namely, the IEEE 13-node test feeder and a practical test feeder are employed to test and validate the model. Thereafter, the implementation of GA-based DOPF model is explained, together with a discussion on the need to decrease the run-time of the DLF using the OpenDSS simulator. The integration into the DOPF of an NN-based EHMS micro-hub controllable smart loads is then discussed. Finally, analyzing the results obtained from different realistic case studies and scenarios in a practical distribution feeder are presented.

- Chapter 4 presents the modeling of controllable smart loads using an NN technique, and demonstrates its application to existing controllable PS+ loads. The mathematical NN model of PS+ loads and its integration into the DOPF model are also discussed. Finally, the results of applying the proposed DOPF model to a practical distribution feeder for different scenarios are discussed, and the effect of the optimal management of PS+ loads is analyzed.

- Chapter 5 presents the main conclusions and contributions of this thesis, and identifies some directions for the future work.

Chapter 2

Background Review

2.1 Introduction

This chapter reviews the main background topics of this research. Thus, Section 2.2 presents a brief background on DSA, DMS, and centralized VVC problems. Section 2.3 discusses load modeling and load management programs in the context of DSM and DR, followed by a discussion of the EHMS and PS+ loads. A brief descriptions of different mathematical programming models and solution approaches are presented in Section 2.4. In Section 2.5, the SGCM architecture and an application of the SGCM for distributed computing approaches is introduced and explained. Finally, detailed models of distribution system components for DLF studies are described in Section 2.6.

2.2 Distribution System Automation and Distribution Management System

DSA and DMS are defined and briefly reviewed in Section 1.2.1. In this section, details on these topics that are particularly relevant to this work are presented and discussed.

2.2.1 Distribution System Automation

DSA can be categorized into two functions: monitoring and control. For monitoring, a Supervisory Control and Data Acquisition (SCADA) system is used, and its main functions

are to read meters at different locations in the system, record the condition of the system at different places, and report any abnormalities (automated meter reading). The control functions include switching operations, system protection, and more recently, remote load control, and remote connection/disconnection [15].

DSA functions can be divided into two levels: customer and system. For customer-level functions, communication devices are needed for remote monitoring and control of loads, whereas system-level functions are mostly installed at main feeders and substations [74]. The main DSA functions are as follows [74, 75]:

- Fault isolation, outage location, service restoration and overload detection.
- Feeder reconfiguration and transformer load balancing.
- Extension of transformer lifetime.
- Recloser/Breaker monitoring and control.
- Control of SCs for VVC.
- Voltage regulation through voltage regulators.
- Substation transformer LTC control.
- Distribution system monitoring and SCADA interfaces.
- Automation of circuit reconfiguration.
- Faster fault detection and fault isolation with enhanced monitoring and communication systems.
- Integration of AMI in DSA.
- Reconfiguration of the system to improve protection schemes.
- Integration of DG units in distribution systems.
- Hardware and software infrastructure improvements for DSA.

Based on above discussion, to fully implement DSA, the following are important goals [74]:

- Improve the operational efficiency of the distribution system with the following installed components:

1. VVC devices to reduce loss along feeders.
2. Sensors to report equipment issues.
3. Standards development based on cost and loss reduction.

- Manage peak loads.
- Predict equipment failure.
- Restore the system after failure.

Rapid changes in distribution systems have introduced new challenges for DSA implementation [76, 77], thus;

- DG units, which are connected to the grid, can affect the reliability of the distribution system, specially in networks with high DG penetration.
- Implementation, administration, and integration of energy storage system have considerable impact on DSA strategies.
- By introducing new infrastructure and technologies such as sensors and DG units, modern distribution systems attain some characteristics of transmission systems such as bi-directional power flow, and non-radial network topologies.
- Disasters such as earthquakes, tsunamis, and hurricanes should be considered in DSA design to improve the reliability and reduce service interruptions.
- Due to different equipments, technologies, policies, standards, and resources, a globally uniform prescription for DSA implementation may not be possible.

2.2.2 Distribution Management System

Traditional VVC in conventional distribution systems is carried out by local controllers with LTCs and SCs, as shown in Figure 2.1. Lack of two-way communication devices, central controllers, and wide-area measurement facilities have been some of the limitations of these systems [78]. However, recent improvements in communication, control, and measurement technologies are transforming conventional distribution systems into what is now called the smart grid. An important part of these smart grids are smart loads, which include HAS and HEM systems [12, 79, 80]. Automatic and remote controller switches for

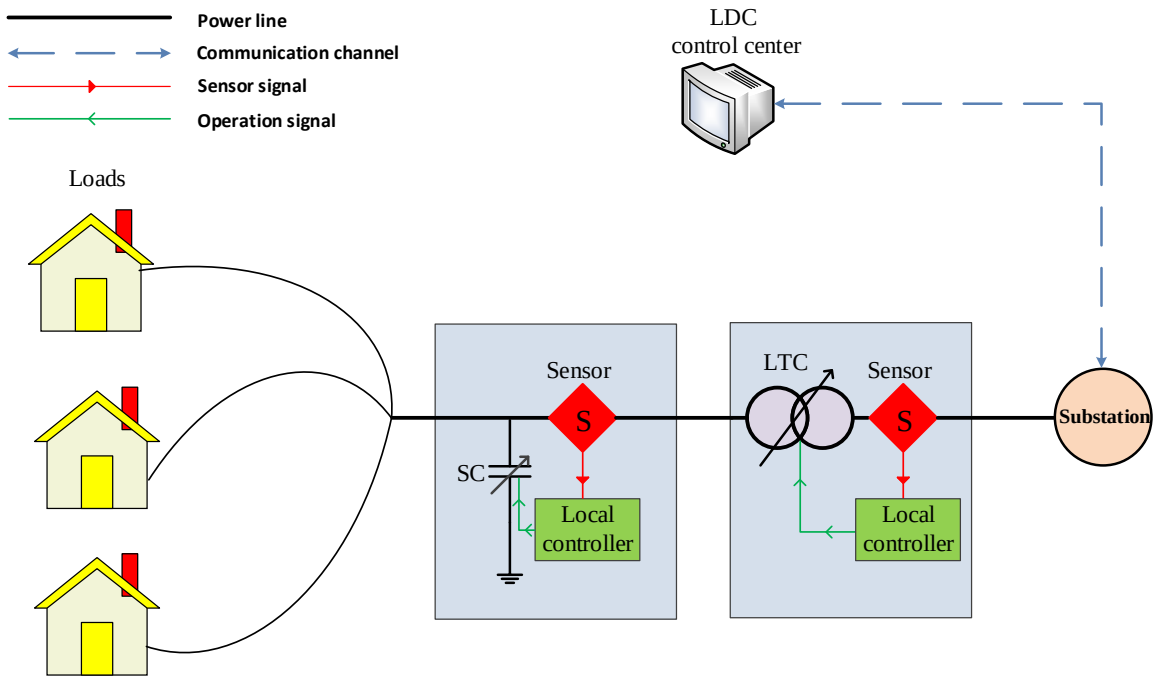

Figure 2.1: A conventional distribution system with local controllers for LTCs and SCs [78].

lights, setpoints for thermostats, window covers, and various other electrical systems and apparatus are among the features of these systems. Figure 2.2 presents a typical smart distribution system, depicting the improvements in communication and control infrastructure, where a central controller collects load data internally from switches, thermostat setpoints, sensors, measurement devices, and plug-in modules such as audio/video systems and security systems, and collects external data such as weather and energy price forecasts, which may be received fully or partially along with other measurements by the LDC through the AMI. In the AMI, a number of neighbours communicate with the LDC through their smart meters, in a so-called Neighbourhood Area Network (NAN), and send their data to the utility's Wide Area Network (WAN) [81].

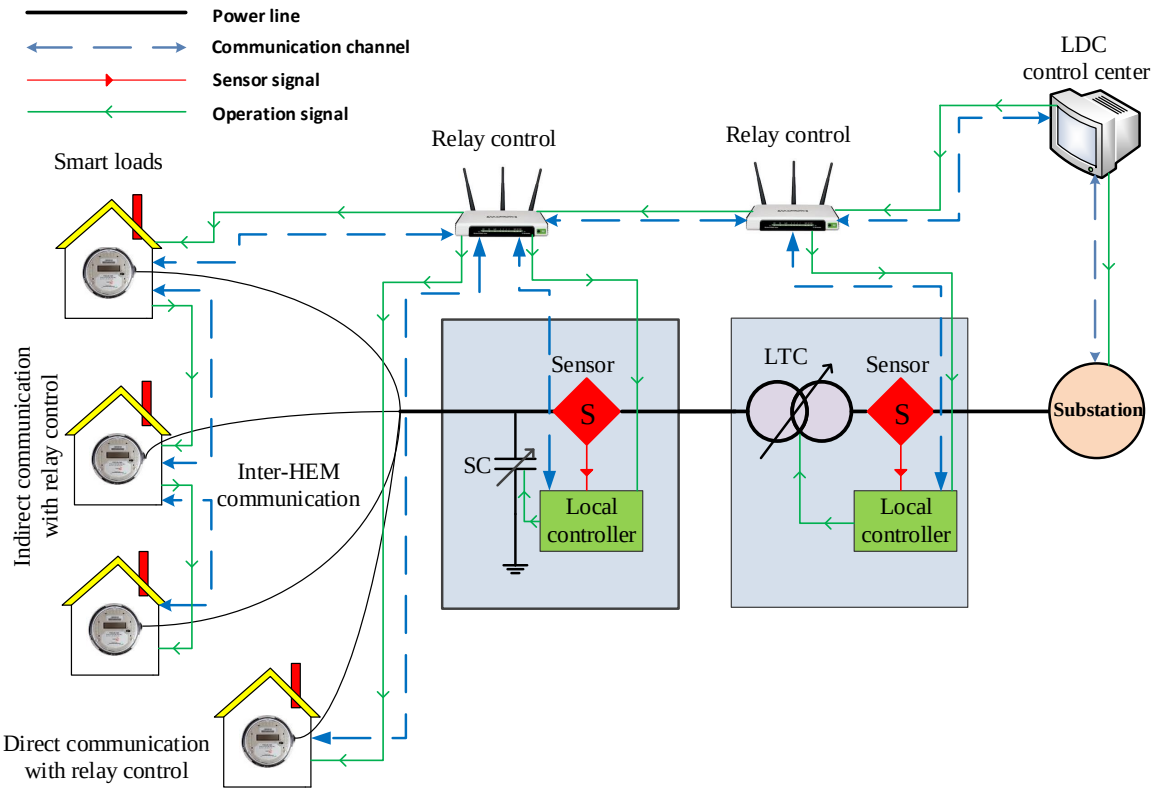

Figure 2.2: A typical distribution system with evolving communication and control infrastructure [18].

2.2.3 Centralized Volt/Var Control

As mentioned in Section 1.2.1, voltage and reactive power control in distribution systems have traditionally been performed by LTCs, SCs, fixed capacitors, and step-voltage regulators. LTCs and step-voltage regulators are voltage-control devices, while SCs and fixed capacitors can regulate both voltage and reactive power [34]. Fixed capacitors are mostly used to cover minimum reactive power requirements in distribution systems, while SCs are added to the system to manage the load variations over the day.

The aforementioned local controllers have no significant effect on system loading. Since peak loads can be up to 2-3 times the average load, and up to 10 times the minimum load [18], to properly manage such load variations, centralized control techniques for VVC

have been proposed in the literature [18, 19, 26–29, 82–85]. VVC has mainly been designed to maintain voltages within an acceptable range and to minimize energy losses. However, other objectives may be used, such as maintaining unity power factor at the substation node and minimizing the energy drawn from the substation [18]. In general, a centralized VVC problem can be defined as follows [82, 83]:

$$\text{Minimize:} \qquad F = \sum f(I, V, tap, cap) \tag{2.1a}$$

Subject to:

- Power flow equations:

$$P_e^g - P_e = \sum_{c=1}^{N_N} |V_e||V_c|[g_{ec}\cos(\phi_e - \phi_c) + b_{ec}\sin(\phi_e - \phi_c)] \qquad \forall e \tag{2.1b}$$

$$Q_e^g - Q_e = \sum_{c=1}^{N_N} |V_e||V_c|[g_{ec}\sin(\phi_e - \phi_c) - b_{ec}\cos(\phi_e - \phi_c)] \qquad \forall e \tag{2.1c}$$

- Operating limits on voltages:

$$\underline{V} \leq |V_e| \leq \overline{V} \quad \forall e \tag{2.1d}$$

- Operating limits on branch currents:

$$|I_l| \leq \overline{I}_l \quad \forall l \tag{2.1e}$$

- Operating limits on LTC:

$$\underline{TAP}_{e,fc} \leq tap_{e,fc} \leq \overline{TAP}_{e,fc} \quad \forall e, fc \tag{2.1f}$$

- Operating limits on capacitors:

$$0 \leq cap_e \leq C_e^{max} \quad \forall e \tag{2.1g}$$

where:

$$V_e = |V_e| \measuredangle \phi_e \tag{2.2a}$$

$$Y_{ec}^{sp} = g_{ec} + jb_{ec} \tag{2.2b}$$

All the indices, parameters, and variables in the equations above and throughout this thesis defined in the Nomenclature Section at the beginning of this document.

The solution to the optimization model (2.1a)-(2.1g) yields the optimal tap and capacitor settings that minimize the objective function (2.1a), while meeting all feeder constraints. This mathematical model is the basis for the DOPF model proposed in this thesis.

2.3 Load Modeling with DSM and DR

Monitoring and control of distribution systems through DMS are integral aspects of smart grids, carried out based on various objectives at the feeder level such as VVC, DR, system reconfiguration, and system restoration [18, 24]. Furthermore, at the customer end, real-time monitoring and control, associated with EMSs at residential, industrial, commercial, and/or agricultural sites, are also important features of smart grids [12, 35]. Controllable loads are being integrated into DSA techniques and tools to affect load profiles, with benefits for both customers and LDCs. While reducing energy consumption and costs are of interest to customers, reducing peak load and reshaping load profiles, which increase system sustainability, are mainly of interest to LDCs [12,86]. Hence, studying the behaviour of controllable loads, their impact on the aggregated load profiles, and their integration in optimal distribution system operation is relevant and timely.

2.3.1 Load Modeling

Load modeling plays an important role in power systems. Although there are various measurement devices at the transmission side, unmetered customers on the distribution side have been an issue for DSA. Static load models have been used for various studies in distribution systems [87]. Traditionally, constant impedance or constant power load models have been used [88], but constant impedance (Z), constant current (I), and constant power (P) or ZIP load models have also been reported [89–94]. A ZIP load model considers the variation of load with bus voltage, and its parameters can be fitted to accurately describe the steady-state behaviour of different kinds of loads. Other static load representations such as an exponential model has been reported in [89].

Because of the complexity of controllable loads and insufficient data, it is difficult to use fundamental physical laws for modeling these loads. However, an accurate model of the customer load profiles is necessary for integrating loads in distribution system EMS;

for this purpose, black-box or empirical load models can be used. In such models, a relationship between the inputs and outputs is obtained and represented using mathematical functions [95,96], or by EAs such as NN [86,97], Particle Swarm Optimization (PSO) [98], or GAs [99]. In the present work, an NN is used to accurately model controllable loads, considering the effect of external parameters such as temperature, TOU price, and LDC control signals.

2.3.2 DSM

Load management is classified into two categories: Direct Load Control (DLC) and Interruptible Load Control (ILC). DLC usually deals with residential customers and it refers to programs that can interrupt customer loads with utility's direct control. On the other hand, ILC usually deals with the commercial/institutional and industrial customer loads, and it involves load interruption during peak demand based on an agreement between the utility and the customers. Interruptions can be made directly by utility operators or by customers, based on a utility's request [100]. The objective of these programs are to modify the load shape of the distribution system.

As mentioned in Section 1.2.2, DSM is classified into three major groups. The energy efficiency and conservation category refers to programs that result in reducing energy consumption or energy used by specific end-use systems or devices, typically, without any impact on the provided services. On the other hand, strategic load growth refers to how the programs increase the load levels through "strategic" electrification. Finally, DR programs propose methods to control and alter the customers' energy consumption with incentives or lower-priced electricity [39, 40], with benefits accruing to both customers and the LDC. Thus, peak clipping, valley filling, load shifting, and flexible load shaping are four major objectives of DR programs. These objectives may combine with strategies such as energy efficiency and strategic load growth to make up a DSM program. Figure 2.3 depicts the DSM objectives and strategies in distribution systems. The following is a brief description of the objectives and strategies of DSM programs [101]:

- Peak clipping to decrease the usage during peak loads.
- Valley filling to encourage customers to use their equipment during off-peak load hours. This can improve the overall load factor of the system.
- Load shifting to shift electricity usage from the peak load hours to off-peak hours. The goal is not to reduce the energy consumption in the long term, but to reduce the peak load in the short term, considering the comfort level of the customers.

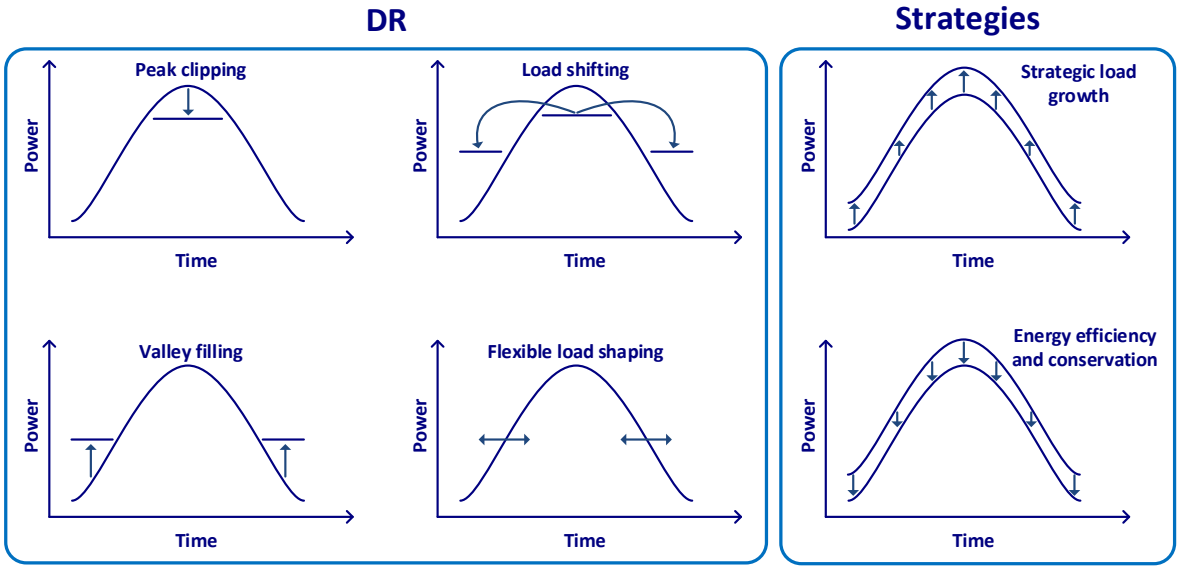

Figure 2.3: DSM objectives in distribution systems [39].

- Flexible load shaping to redistribute the electricity usage during different times.
- Energy efficiency and conservation to decrease electricity costs through equipment's modification or replacement (e.g., improving the residential heat insulation to reduce electricity usage of Heating, Ventilation, and Air Conditioning (HVAC) systems).
- Strategic load growth to increase the load through electrification in a strategic way.

Different DSM techniques have been categorized in [102]; one of the important categories deals with end-use equipment control, which may include, for example:

- AC in residential and commercial package units: remote control cycling, local controllers, thermostat controls, and remote ON/OFF controls.
- AC in commercial and industrial chillers: water column temperature controls, remote control cycling, and capacity reduction.
- Water heater in residential and commercial: remote ON/OFF controls and timers.
- Pumps: timers and remote ON/OFF.

The present research focuses on utility equipment controls, such as LTCs and SCs, while considering of DSM and DR programs. Thus, models of controllable smart loads, in particular EHMS micro-hubs and PS+ loads, as discussed later, are integrated into the proposed DOPF model to minimize the energy drawn from the substation, reduce feeder losses, reduce peak load, and reduce customer costs.

2.3.3 Energy Hub Management System

An "energy hub" can be considered as a node in the power system when the exchange of energy and information with other sources of energy, loads, and external systems occurs. Within an energy hub system, different kinds of energy such as electricity and heat can be converted or conditioned using different combined heat and power technologies such as transformers, turbines, compressors, inverters, and heat exchangers. Based on the services that customers require, the output of the energy hub can be electricity and heating/cooling [103, 104].

In [104–108], the key roles of energy hubs in the future of smart grids are discussed. Thus, the potential of energy hubs to efficiently manage a distribution system for day-ahead operations is discussed in [104]. In [105], a combined optimization of coupled power flows in the presence of different kinds of energy infrastructures such as electricity, gas, and heating systems is proposed. In [106], a method to decompose a multi-carrier Optimal Power Flow (OPF) into separate traditional OPF problems is analyzed. In [107], a model is proposed to manage loads and generators to improve the reliability of energy hubs. Finally, an optimal schedule of an extended energy hub, which includes drivers, renewable DG units, DR, and electrical storages, is presented in [108].

In [12], energy hubs are classified into four major groups: residential, commercial, agricultural, and industrial, based on the way they consume energy. The objectives differ from the point of view of customers and the utility; for customers, one of the most important objectives is to minimize cost. Hence, a two-tier control hierarchy is proposed, separating energy hubs into micro- and macro-hubs; the micro-hub represents a customer at the lower level, and the macro-hub represents the utility at the higher level, with a group of individual micro-hubs communicating with a macro-hub in a two-tier architecture. The mathematical models of residential, commercial, and agricultural micro-hubs are discussed in [13]. An optimal industrial load management model, which can be integrated into the EHMS for real-time management of industrial demand and distribution feeder, is proposed in [34]. The model includes comprehensive models of industrial processes, process inter-dependencies, storage units, process operating constraints, and production require-

ments, and is used for load control and voltage optimization considering the interactions of industrial processes with the operation of distribution feeders.

In macro-hubs, which is the focus of the present research, modeling of the load and DG units are important. In [109–111], some mathematical models are introduced for residential loads. Models of other devices such as Plug-in Electric Vehicles (PEVs) are described in [112]. In [113], the Smart Residential Load Simulator (SRLS), a MATLAB®-based toolbox developed to model and study electric and thermal loads and sources in residential houses, is presented; models of smart thermostats, ACs, furnaces, stoves, washers and dryers, refrigerators, wind turbines, solar PV, and batteries are included in the SRLS. In [114], industrial loads are modeled considering users' comfort levels, dynamic pricing, and generation constraints.

It is noted in [34] that customers have the ability to receive real-time external information from weather stations, market operators, and the LDC, so that micro-hub smart loads internally optimize the load profile. This profile is collected by the LDC from the micro-hub loads together with the system status of the distribution system. All this information is used by the LDC control center in real-time to solve the DOPF, and thus determines the optimal controls for switches, LTCs, and SCs, and to send as well peak demand constraints to micro-hubs to regulate its load accordingly. An overall schematic of an EHMS for different types of energy hubs is presented in Figure 2.4, and Figure 2.5 depicts the micro-hub for different types of loads. Also, Figure 2.6 presents a schematic of the EHMS-based optimal feeder and load control for real-time applications [34].

In this work, a mathematical model of EHMS macro-hubs to optimize the operation of distribution systems is developed. Models of controllable smart loads comprising EHMS micro-hub loads and PS+ loads are developed to study the effect of different types of controllable loads on optimal distribution system operation.

2.3.4 Peaksaver PLUS™ Loads

Among controllable devices, monitoring, supervising, and controlling of HVAC systems in various facilities have been discussed in the literature [116–119]. In particular, the PS+ program in Ontario, Canada, is a voluntary program to reduce AC demand in the residential and small commercial sector [120]. In this program, smart thermostats, referred to as PCTs, are installed to slightly increase the AC temperature setpoints during summer. PS+ loads are currently activated during the summer weekdays (i.e., June to September) for a maximum of 4 hours at anytime, during a day. According to the PS+ rules, PCTs can be activated on average five times per year, up to a maximum of 40 hours, excluding

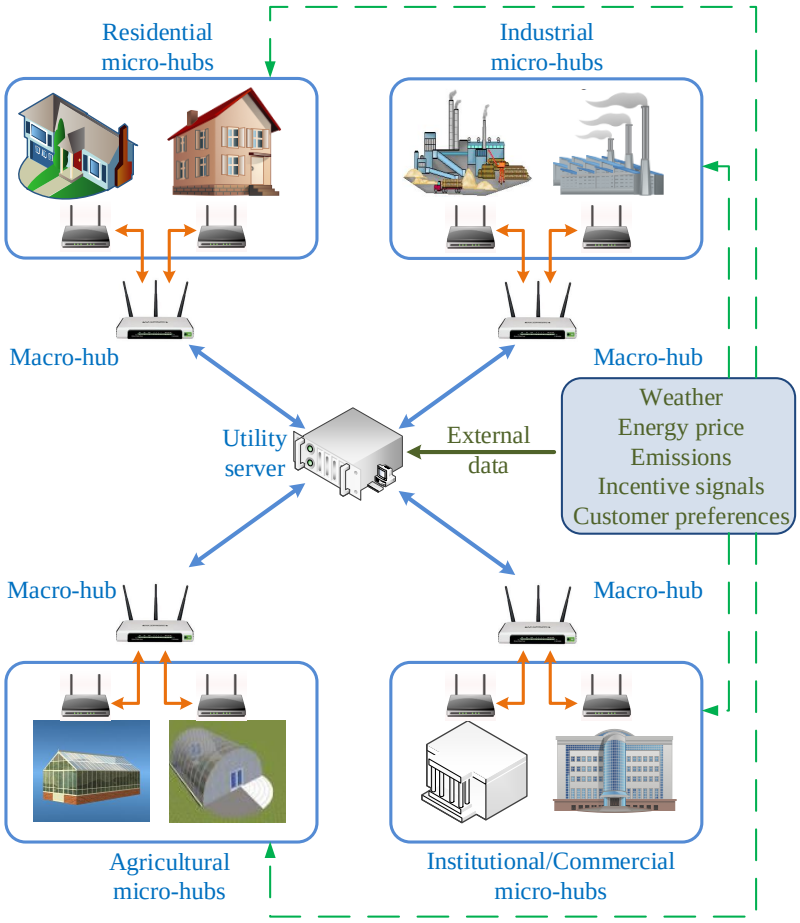

Figure 2.4: Overall schematic of an EHMS [13].

emergencies such as a blackout during summer. Since the AC loads account for about 50% of summer peak residential loads in Ontario, it is estimated in [121] that direct control of AC usage may conserve about 37% of the energy, resulting in savings of $688 million in energy conservation over a 20 year period. Since the demand for electricity in summer is the highest, by automatically adjusting the PS+ smart loads during peak time, the cooling energy use can be reduced by 10% per year [122].

In this thesis, an NN algorithm is used to model EHMS micro-hubs and PS+ smart loads. The NN model is a function approximation tool, which uses external data to estimate

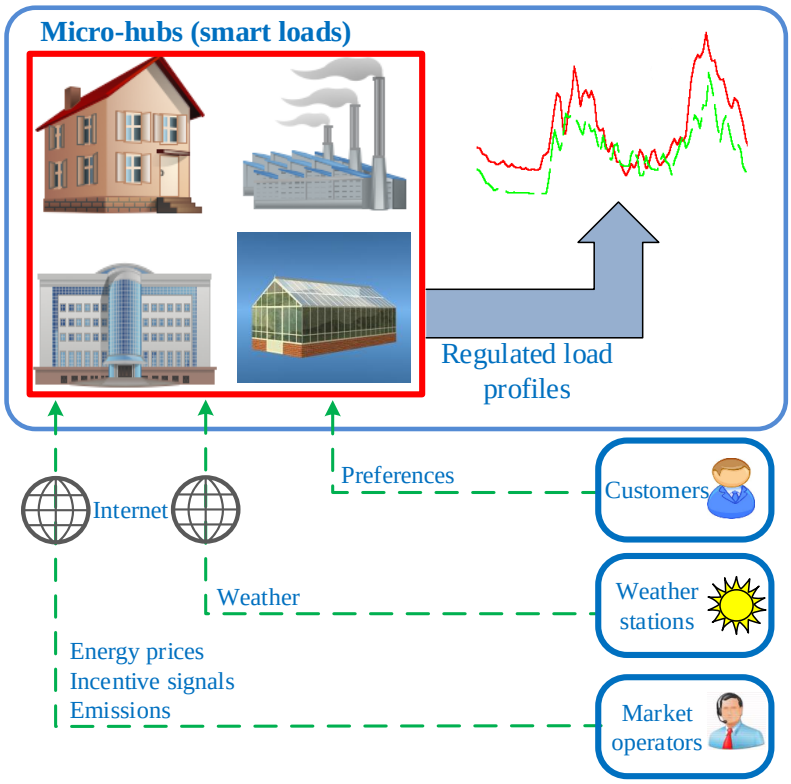

Figure 2.5: EHMS micro-hub for different types of loads [13].

NN parameters. The system is considered as a black-box, which tries to find the best fitted NN parameters that match the outputs with the targets; for this purpose, the NN should be trained to capture the relationship between the input data and related target data. With a feedback loop control, the output of the NN is compared with the target (i.e., the desired output), and the weights and biases are adjusted between neurons to reduce the error. Depending on the complexity of the system, the number of hidden and output layers of the NN may vary.

Figure 2.7 shows the schematic of the overall proposed optimal feeder control with different kinds of loads, including PS+ and EHMS micro-hub smart loads. The LDC will then collect the smart loads profiles together with the status of the distribution feeder, and solve the DOPF model to send optimal control signals to the LTCs, SCs, and smart loads, using a closed-loop MPC approach.

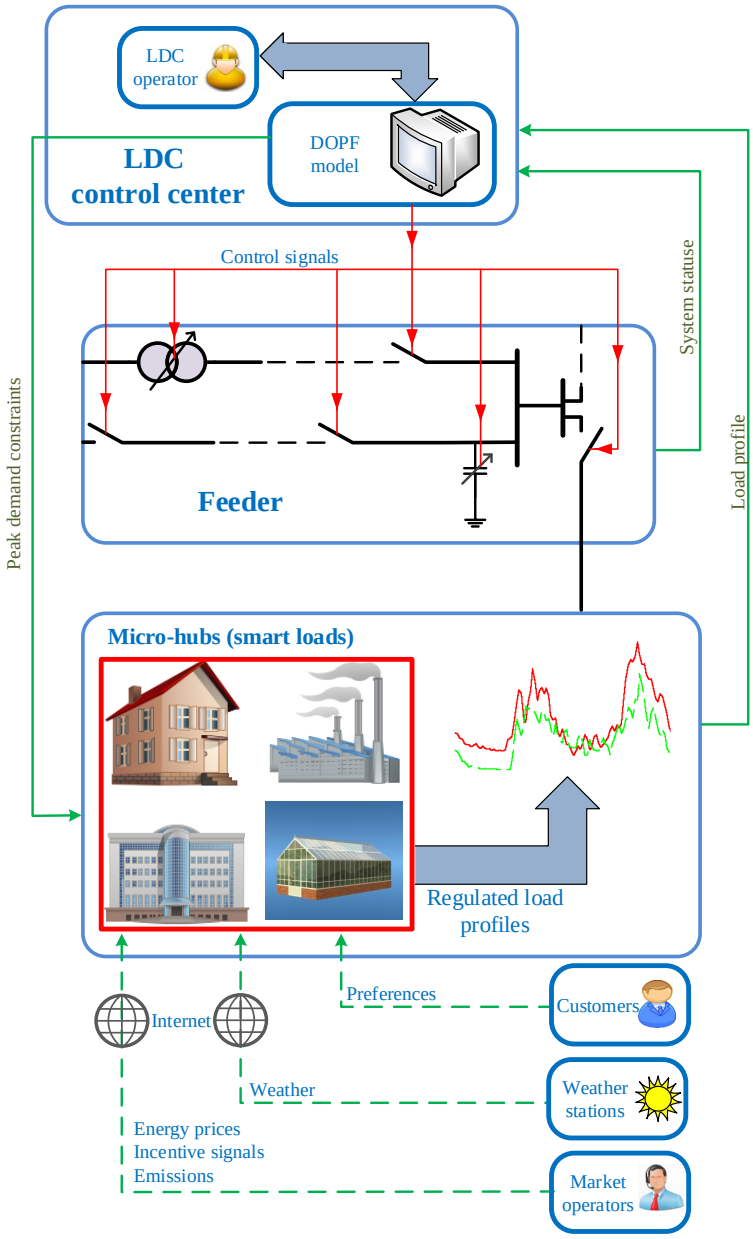

Figure 2.6: Schematic of an EHMS-based feeder and load control [35, 115].

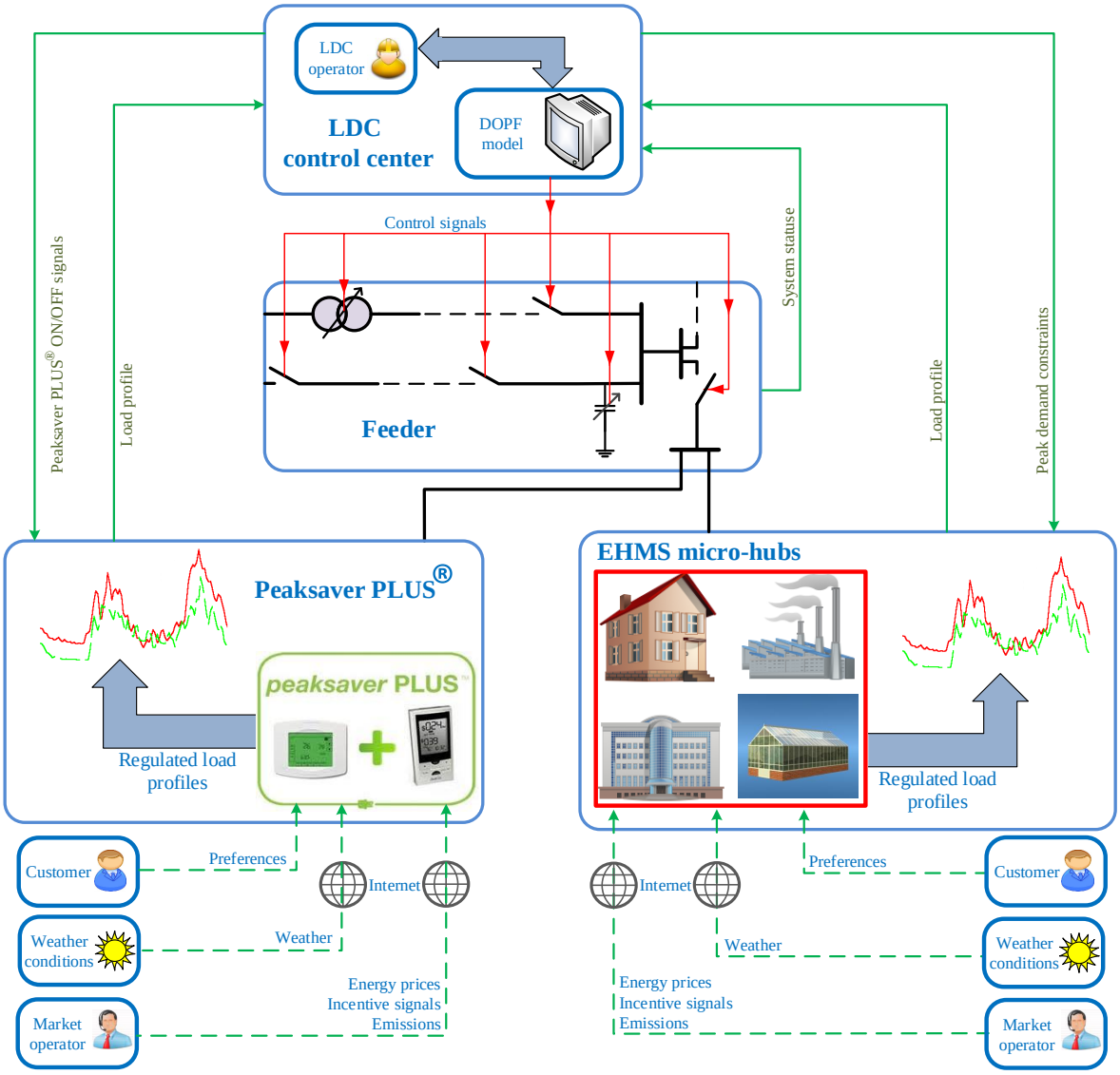

Figure 2.7: Schematic of the proposed optimal feeder control with different kinds of loads.

2.4 System Optimization

2.4.1 Mathematical Programming

Optimization problems seek to obtain the best solution in terms of finding the minimum or maximum of a function subject to various constraints. The general form of an optimization problem can be given as follows:

$$\begin{aligned} \min. \quad & f(x) && && \text{(2.3a)} \\ \text{s.t.}: \quad & g_k(x) = 0, && \forall\, k = 1, 2, \ldots, p && \text{(2.3b)} \\ & h_j(x) \leq 0, && \forall\, j = 1, 2, \ldots, m && \text{(2.3c)} \end{aligned}$$

where x is an n-dimensional decision variable; $f(x)$ is the objective function; $g_k(x)$ is a set of p equality constraints in (2.3b); and $h_j(x)$ is a set of m inequality constraints in (2.3c). The optimum solution of the mathematical program may include (2.3a)-(2.3c) can be found using various methods [123].

Mathematical programming problems can be classified based on the nature of the equations involved in the objective function and the constraints. Accordingly, optimization problems are categorized as linear, non-linear, geometric, and quadratic programming problems. A brief introduction to linear and non-linear programming problems is presented next.

Linear Programming

These problems comprise a linear objective function with a set of linear equality and inequality constraints. The general form of Linear Programming (LP) problems is as follows:

$$\begin{aligned} \min. \quad & f(x) = c^T x && \text{(2.4a)} \\ \text{s.t.}: \quad & Ax \leq b && \text{(2.4b)} \\ & l \leq x \leq u && \text{(2.4c)} \end{aligned}$$

where $x = [x_1\ x_2\ \ldots\ x_n]^T$; l and u are the lower and upper bounds of x; A is an $m \times n$ matrix; c is an n-dimensional column vector; and b is an m-dimensional column vector. The Simplex method and the Interior Point algorithms are commonly used to solve LP problems [123].

Mixed-Integer Linear Programming

These problems are LP problems with some integer or binary variables. The general form of an MILP problem is as follows:

$$\begin{aligned} \min . \quad & f(x,y) = c^T x + d^T y && (2.5a)\\ \text{s.t. :} \quad & Ax + By \leq b && (2.5b)\\ & x \geq 0, \qquad x \in \mathbb{Z} && (2.5c)\\ & y \geq 0 && (2.5d) \end{aligned}$$

where $x = [x_1\ x_2\ \ldots\ x_n]^T$, is an integer non-negative, n-dimensional vector; y is a non-negative, s-dimensional vector with continuous variables; A and B are $m \times n$ and $m \times s$ matrices, respectively; c and d are n- and s-dimensional vectors; and b is an m-dimensional vector. The Cutting Plane and Branch-and-Bound methods are typically used to solve MILP problems [123].

Non-Linear Programming

These problems have a non-linear objective function or at least one non-linear constraint in (2.3a)-(2.3c). The most important solution methods are the Gradient methods, Newton-based methods, Least Square methods, and Interior Point methods [123]. Gradient methods use the search direction based on the slope of the function in order to find the optimal solution; although these methods are general and can solve any size of NLP problems, they may only yield sub-optimal solutions and/or the solution may zigzag near the optimal solution. Newton-based methods are second-order gradient methods that have faster convergence, but are computationally more expensive, since a Hessian matrix and its inverse are needed. Interior Point methods cross the interior of the feasible region and use "barrier functions" to find the optimal solution; a barrier function is a continuous function whose value at a point increases to infinity as the point approaches the boundary of the feasible region.

Mixed-Integer Non-Linear Programming

These problems are NLP problems with at least one integer variable. The Cutting Plane method, Branch-and-Bound method, Balas method, Generalized Penalty Function method, Sequential Linear Integer (discrete) programming methods, and EAs, which are discussed next, are used to solve MINLP problems. The non-linear nature of the DOPF model

renders it an NLP problem, and since LTC or SC switchings are modeled using integer variables, the NLP problem becomes an MINLP problem. In [29, 124–127], MINLP-based models for VVC problems are proposed, heuristic approaches to solve other MINLP-based VVC problems have been reported in [20, 22, 23, 29, 34].

2.4.2 Evolutionary Algorithms

In recent years, many papers have reported algorithms and applications of EAs to solve NLP and MINLP problems. GAs, PSO, and evolution programming strategies are among the different EA-based methods. GAs are based on search algorithms that imitate the process of natural selection. Starting with a "pool of points", referred as chromosomes, the GA searches in a space, which is defined mostly in a binary representation, and compares chromosomes in terms of their fitness/objective to generate a new generation of points. The "cross-over" and "mutation" operators are applied to the parent chromosomes to generate new chromosomes. The cross-over operator selects two random chromosomes; mostly one or two points along their common length are chosen randomly, and they exchange their characteristics to generate two new chromosomes. The mutation operator switches a position randomly within a chromosome to mutate new chromosomes.

It is important to note that GA-based algorithms, like other EA-based algorithms, do not guarantee an optimal solution; however, multi-pass searches in parallel can reduce the probability of falling into sub-optimal traps [128]. Figure 2.8 presents a general GA flowchart. GA-based applications to power system problems have been reported in several papers; thus, in [129–132], GA-based algorithms for the optimal capacitor planning problem are proposed, and in [34, 36, 133], GA-based VVC problems are used. For example, in [34, 36], heuristic and GA-based solution methods to solve the DOPF problem are compared, noting that although the GA-based method yields a better solution, the computational burden is quite significant, making the model unsuitable for real-time applications.

In the present work, as discussed and justified in Section 1.2.1, a GA-based algorithm is used to solve the proposed optimization problem as an MINLP problem, and as discussed in Section 2.5, in order to make the model suitable for real-time applications, an SGCM system is used for parallel computation.

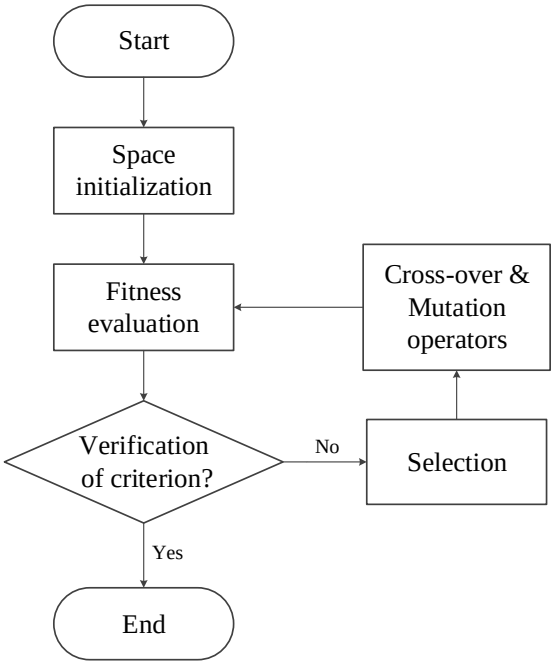

Figure 2.8: A general GA flowchart [128].

2.5 Smart Grid Communication Middleware System

2.5.1 SGCM System Architecture [67]

The SGCM provides a framework for MapReduce model based on distributed computing applications. The framework contains templates to build client, master, and worker components by adding application specific data structures, data file information, "Map" or "Reduce" processes, and work-flow logic. The client component runs on a console to distribute, install, and configure master and worker components on available nodes; it distributes data files to the master-node (i.e., the node with master components installed), and calls master functions to run. The master-node creates jobs in forms of files, sends jobs to worker-nodes (i.e., nodes with worker components installed) for Map or Reduce processes, and tracks jobs. Worker-nodes call Map or Reduce programs to process job files, and send result files to the master-node or other worker-nodes according to the work-flow logic. Since the SGCM framework allows to accommodate more complicated work-flow

logic, it has been used in this work as a template to implement a recursive MapReduce model for the GA-based DOPF solution proposed in this study. Furthermore, in order to reduce the computational burden of the DOPF model with a GA-based solution and make it suitable for real-time applications, the SGCM system is chosen as the preferred platform for a recursive MapReduce model due to its fast performance when large number of nodes are involved; it is light, reliable, and flexible, and is capable of running multiple smart grid applications simultaneously.

The core components of the SGCM system are the nodes and the console. The node is a client and a server program, which can be installed and run on commodity computers and smart devices. As a client, the node is able to make TCP connections to other nodes, and as a server, it waits for a TCP connection and provides services. The node is a virtual router which can forward packets to other nodes. Also, the node is a service provider, on which application modules can be installed. The node is a processor that executes groups of node instructions, which consist of: net instructions for creating structured data path of nodes; file instructions for file Input/Output (I/O) and file transfer; execution instructions for remote function calls; bundle instructions for install/uninstall application modules; and cluster instructions for node cluster discovery and management. The console is a client program used to connect to a node and to launch network commands. The console is a command line interface equipped with script language extended with the command functions. Thus, application deployment, installation, execution, and management can be done by running script console applications.

A typical smart grid application involves multiple computing components on different devices that need to exchange data during the execution of the application. In the SGCM system, computing components are installed as modules on the nodes. Intercommunications of the computing components are realized by structured data paths, which are computed and established by the reconfiguration of nodes. The communication pattern can be one-to-one, one-to-many, many-to-one, or many-to-many. For a typical one-to-many communication request, routing algorithms are used to find an optimal network topology (i.e., a Steiner tree), and a structured data path of the topology is established through reconfiguration of the nodes. The data transfer for the one-to-many communication request is through the data path with an identical net Identification (ID), which avoids data paths interfering with each other when they overlap; thus, the SGCM system supports simultaneous multiple applications. Also, the SGCM system has flexibility to set different fault tolerance levels with available computing resources. For high level of fault tolerance, the system can be configured to run the same job simultaneously on different groups of nodes, and for low level of fault tolerance, the task tracker on the master-node monitors the execution of Map or Reduce process on worker-nodes, and in case of failure, it assigns

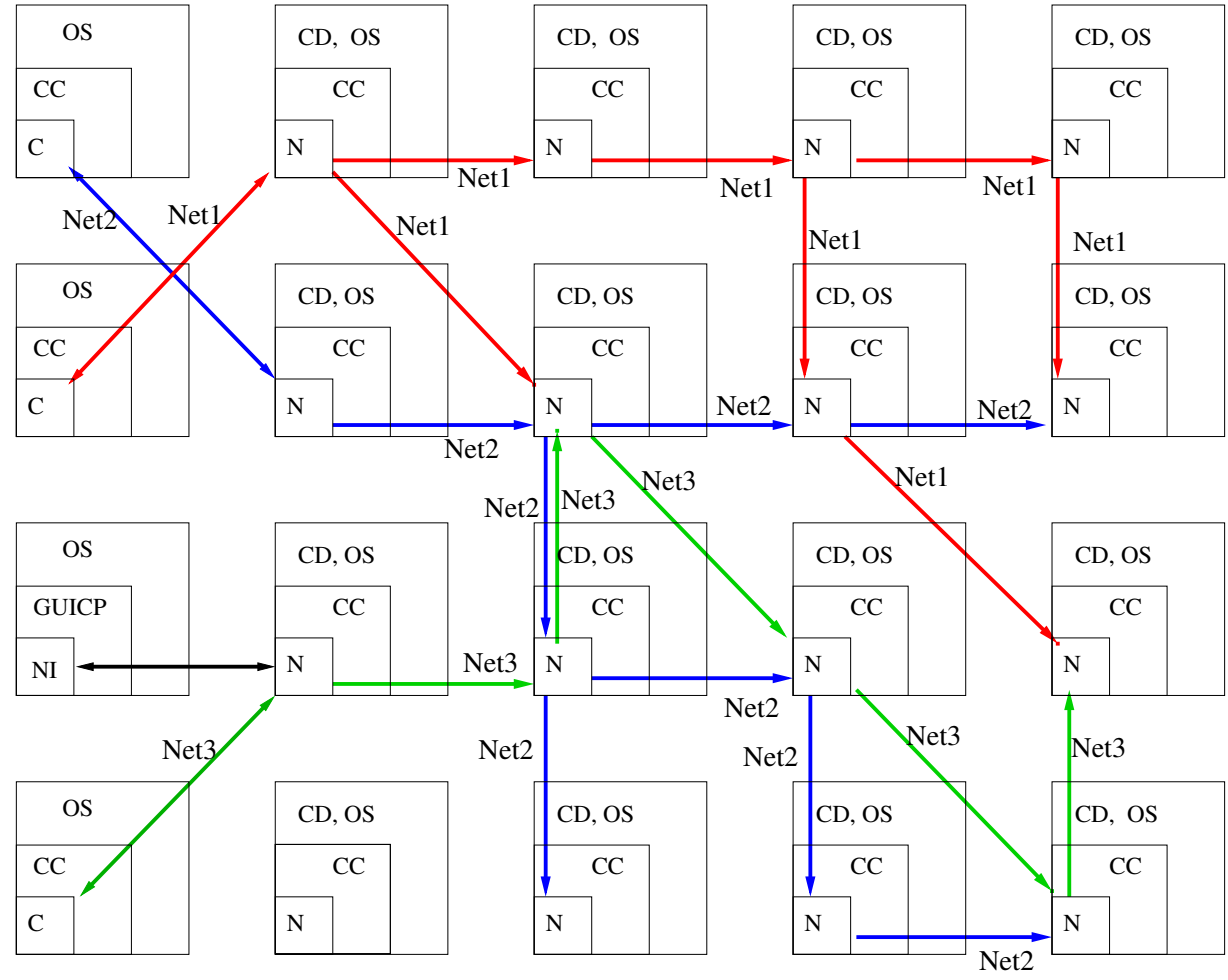

Figure 2.9: Multiple applications running simultaneously on an SGCM system [67].

the task to alternative nodes or re-run the task on the same node. Figure 2.9 illustrates the architecture of SGCM with nodes, a console, and programmable data paths of applications. This architecture and its communication protocols are based on reconfigurable interconnection network computing platform.

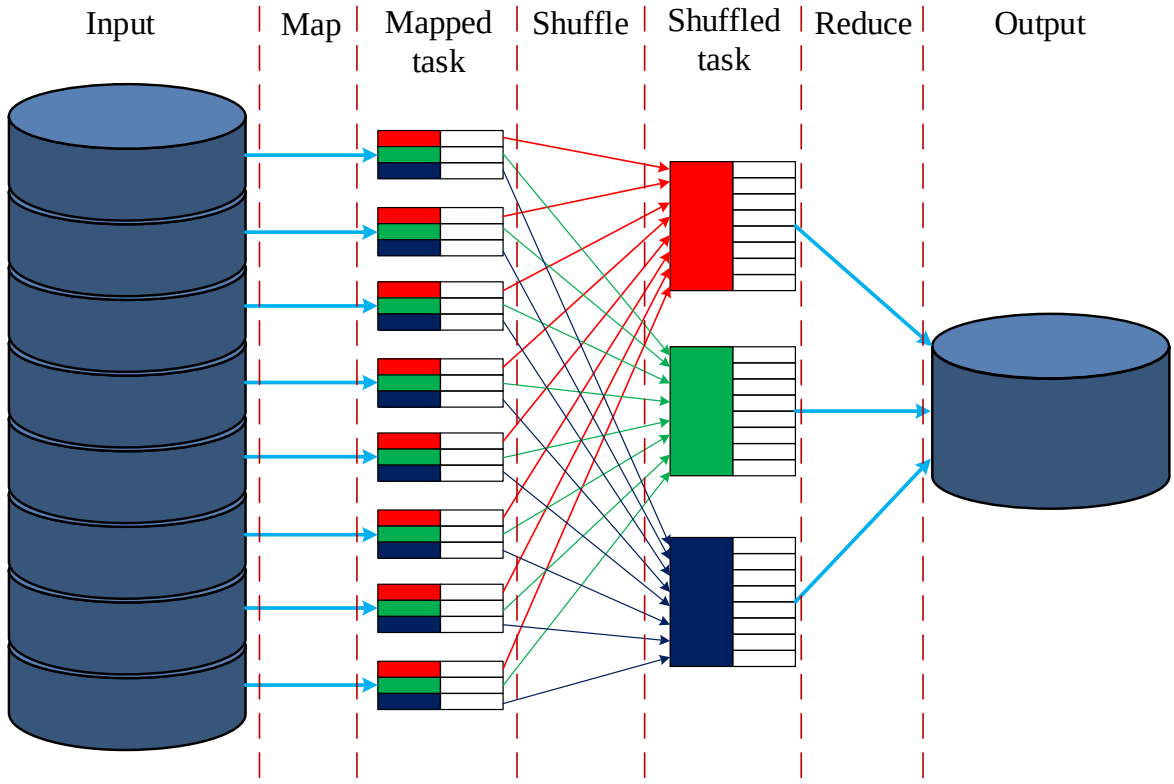

Figure 2.10: A schematic of the MapReduce model [71].

2.5.2 SGCM for Distributed Computing

Complex smart grid applications involve a large number of smart computing devices in data acquisition and processing, monitoring, control, and intelligent computing, and have high requirements on performance, reliability, and security. Due to the constraints of cost and distributed computing resources, a distributed approach is used in the SGCM system, which provides a platform for solving distributed optimization problems, particularly, problems formulated by a MapReduce model or more complicated work-flow model. MapReduce usually deals with a large number of computers (i.e., nodes), usually referred to as a "cluster" or a "grid"; if the nodes are in similar hardware, they are referred to as a cluster, and if the hardware is shared, it is called a grid. As shown in Figure 2.10, the following are the two main steps of the MapReduce model [71]:

- *Map*: The master-node divides the input into smaller sub-problems and distributes them between the nodes. The worker-nodes process the sub-problems and return the solutions to the master-node. If the system has a tree structure, each worker-node acts as a new master-node for its sub-branches.

- *Reduce*: The master-node hierarchically collects the results from the entire set of worker-nodes, combines them in an output format, and releases the results.

Sometimes, there is a "Shuffle" step mid-stage between the Map and Reduce steps, wherein the output of Map operation is sorted in parallel or exchanged between the nodes, in order to prepare the data for a Reduce step. In the Map step, each node operation is independent of the others; hence, the entire computing nodes can run in parallel, and the distributed operation reduces the computational burden. Likewise, in the Reduce step, all the nodes resulting from the map step are presented in one reducer node (i.e., a master-node), simultaneously.

Compared to sequential algorithms, which are more efficient with smaller data-sets, the MapReduce algorithm can handle larger ones. When Google developed the MapReduce algorithm for the first time [134], the purpose was undoubtedly to develop an effective program for significantly large data-sets. The parallelism, and its system-recovery reschedule can reduce the risk of partial system failure.

In the distributed computing approach, there are different overheads, such as communication overhead time, fault overhead time, and bandwidth overhead. The communication overhead time is the time taken to transfer data between the master-node and worker-nodes or amongst worker-nodes; the larger the size of data needed to be transferred, the longer the communication overhead time of the program. Also, when the number of worker-nodes increases, the limit on the data transfer bandwidth should be considered. For example, if a series of data from different worker-nodes arrives simultaneously at the communication channel towards the master-node, a sequential data transfer, which requires longer run-times, is configured in the SGCM system to satisfy the bandwidth constraint. In addition, different faults may take place, such as failure of SGCM nodes, which are addressed by assigning the task to the alternative nodes or re-running the task on the same nodes; this improves the reliability of the system, but increases run-times.

The computational burden and associated run-times are very important for real-time applications in distribution systems. In order to implement the proposed optimization model for real-time applications, a MapReduce model on the SGCM system [73,91] is used in the present work.

2.6 Distribution System Component Models

Common distribution system components are series components such as conductors/cables, transformers, switches, LTCs, and shunt components such as loads, fixed capacitors, SCs, and DG units. In this section, the three-phase models of these components used in this thesis are presented in detail in the context of distribution system power flows, based on [88].

2.6.1 Series Components

These are modeled using ABCD parameters, relate the sending-end and receiving-end voltages and currents, as follows:

$$\begin{bmatrix} V_{s,p,l} \\ I_{s,p,l} \end{bmatrix} = \begin{bmatrix} A_l & B_l \\ C_l & D_l \end{bmatrix} \cdot \begin{bmatrix} V_{r,p,l} \\ I_{r,p,l} \end{bmatrix} \qquad \forall\, l \tag{2.6}$$

where A_l, B_l, C_l, and D_l are 3×3 matrices. The following are the models of the main series elements in distribution systems:

- *Conductors/Cables*: These elements are modeled as π-equivalent circuits, with the following ABCD parameters:

$$A_{wr} = D_{wr} = U + \frac{1}{2}\, Z_{wr}\, Y_{wr} \qquad \forall\, wr \tag{2.7a}$$

$$B_{wr} = Z_{wr} \qquad \forall\, wr \tag{2.7b}$$

$$C_{wr} = Y_{wr} + \frac{1}{4}\, Y_{wr}\, Z_{wr}\, Y_{wr} \qquad \forall\, wr \tag{2.7c}$$

  where Z_{wr} and Y_{wr} are 3×3 matrices and U is a 3×3 identity matrix. The diagonal elements of these two matrices are the self impedance and shunt admittance of each phase, respectively, and the off-diagonal elements are the mutual ones. If the conductors/cables are single-phase or two-phase, the matrices have self and mutual impedance and admittance corresponding only to the available phases, and the elements corresponding to unused phases are zero.

- *Switches*: These elements are modeled as zero-impedance components, as follows:

$$A_{sw} = D_{sw} = U \qquad \forall\, sw \tag{2.8a}$$
$$B_{sw} = C_{sw} = 0 \qquad \forall\, sw \tag{2.8b}$$

- *Transformers*: The ABCD parameters in this case depend on the type of connection (i.e., wye or delta). The following are the ABCD parameters for five common transformer connections in distribution systems:

  – Delta/wye-grounded step-down connection with 30° negative angular phase shift:

$$A_{tr1} = \frac{-N}{3}\begin{bmatrix} 0 & 2 & 1 \\ 1 & 0 & 2 \\ 2 & 1 & 0 \end{bmatrix} \qquad \forall\, tr1 \tag{2.9a}$$
$$B_{tr1} = A_{tr1} Z_{tr} \qquad \forall\, tr1 \tag{2.9b}$$
$$C_{tr1} = 0 \qquad \forall\, tr1 \tag{2.9c}$$
$$D_{tr1} = \frac{1}{N}\begin{bmatrix} 1 & -1 & 0 \\ 0 & 1 & -1 \\ -1 & 0 & 1 \end{bmatrix} \qquad \forall\, tr1 \tag{2.9d}$$

  where N is transformer turn ratio and Z_{tr} is a 3×3 diagonal matrix in which the diagonal elements are the impedance of each phase referred to the secondary side.

  – Wye-ungrounded/delta step-down connection with 30° negative angular displacement:

$$A_{tr2} = N\begin{bmatrix} 1 & -1 & 0 \\ 0 & 1 & -1 \\ -1 & 0 & 1 \end{bmatrix} \qquad \forall\, tr2 \tag{2.10a}$$
$$B_{tr2} = \frac{N}{3} Z_{tr}\begin{bmatrix} 1 & -1 & 0 \\ 1 & 2 & 0 \\ -2 & -1 & 0 \end{bmatrix} \qquad \forall\, tr2 \tag{2.10b}$$
$$C_{tr2} = 0 \qquad \forall\, tr2 \tag{2.10c}$$

$$D_{tr2} = \frac{1}{3\ N} \begin{bmatrix} 1 & -1 & 0 \\ 1 & 2 & 0 \\ -2 & -1 & 0 \end{bmatrix} \qquad \forall\, tr2 \tag{2.10d}$$

– Wye-grounded/wye-grounded connection:

$$A_{tr3} = N\ U \qquad \forall\, tr3 \tag{2.11a}$$
$$B_{tr3} = N\ Z_{tr} \qquad \forall\, tr3 \tag{2.11b}$$
$$C_{tr3} = 0 \qquad \forall\, tr3 \tag{2.11c}$$
$$D_{tr3} = \frac{1}{N}\ U \qquad \forall\, tr3 \tag{2.11d}$$

Single phase transformers are considered in this category, with the A, B, and D matrices having only the element corresponding to the phase in which the transformer is connected.

– Delta/delta connection:

$$A_{tr4} = \frac{N}{3} \begin{bmatrix} 2 & -1 & -1 \\ -1 & 2 & -1 \\ -1 & -1 & 2 \end{bmatrix} \qquad \forall\, tr4 \tag{2.12a}$$

$$B_{tr4} = \frac{N}{3}\ \frac{1}{Z_{tr_{ab}} + Z_{tr_{bc}} + Z_{tr_{ca}}} \times \begin{bmatrix} 2\ Z_{tr_{ab}}\ Z_{tr_{ca}} + Z_{tr_{bc}}\ Z_{tr_{ca}} & -Z_{tr_{ab}}\ Z_{tr_{bc}} + Z_{tr_{bc}}\ Z_{tr_{ca}} & 0 \\ -Z_{tr_{ab}}\ Z_{tr_{ca}} + Z_{tr_{ba}}\ Z_{tr_{ca}} & 2\ Z_{tr_{ab}}\ Z_{tr_{bc}} + Z_{tr_{bc}}\ Z_{tr_{ca}} & 0 \\ -Z_{tr_{ab}}\ Z_{tr_{ca}} - 2\ Z_{tr_{bc}}\ Z_{tr_{ca}} & -Z_{tr_{ab}}\ Z_{tr_{bc}} - 2\ Z_{tr_{bc}}\ Z_{tr_{ca}} & 0 \end{bmatrix} \forall\, tr4 \tag{2.12b}$$

$$C_{tr4} = 0 \qquad \forall\, tr4 \tag{2.12c}$$
$$D_{tr4} = \frac{1}{N}\ U \qquad \forall\, tr4 \tag{2.12d}$$

where $Z_{tr_{ab}}$, $Z_{tr_{bc}}$, and $Z_{tr_{ca}}$ are the diagonal elements of Z_{tr}.

– Open-wye/open-delta connection:

$$A_{tr5} = N \begin{bmatrix} 1 & -1 & 0 \\ 0 & 1 & -1 \\ 0 & 0 & 0 \end{bmatrix} \qquad \forall\, tr5 \tag{2.13a}$$

$$B_{tr5} = N \begin{bmatrix} Z_{tr_{ab}} & 0 & 0 \\ 0 & 0 & -Z_{tr_{bc}} \\ 0 & 0 & 0 \end{bmatrix} \qquad \forall\, tr5 \tag{2.13b}$$

$$C_{tr5} = 0 \qquad \forall\, tr5 \tag{2.13c}$$

$$D_{tr5} = \frac{1}{N} \begin{bmatrix} 1 & 0 & 0 \\ 0 & 0 & -1 \\ 0 & 0 & 0 \end{bmatrix} \qquad \forall\, tr5 \tag{2.13d}$$

- *LTCs*: The ABCD parameters in LTCs depend on the setting of tap positions as follows:

$$A_{fc} = \begin{bmatrix} 1 + \Delta T_{fc} TAP_{a,fc} & 0 & 0 \\ 0 & 1 + \Delta T_{fc} TAP_{b,fc} & 0 \\ 0 & 0 & 1 + \Delta T_{fc} TAP_{c,fc} \end{bmatrix} \forall\, fc \tag{2.14a}$$

$$B_{fc} = C_{fc} = 0 \qquad \forall\, fc \tag{2.14b}$$

$$D_{fc} = A_{fc}^{-1} \qquad \forall\, fc \tag{2.14c}$$

where ΔT_{fc} is per-unit voltage change for each tap changer position; $TAP_{a,fc}$, $TAP_{b,fc}$, and $TAP_{c,fc}$ represent fixed integer values in the range $\overline{TAP}_{p,fc}$ to $\underline{TAP}_{p,fc}$. For three-phase group-controlled tap changers, all taps are the same; thus:

$$TAP_{a,fc} = TAP_{b,fc} = TAP_{c,fc} \qquad \forall\, fc \tag{2.15}$$

TAP is considered as a fixed integer parameter in the DLF model, and hence is treated as an integer variable *tap* in the DOPF model.

2.6.2 Shunt Components

These are loads, fixed capacitors, SCs, and DG units, and are modeled for each phase in order to represent unbalanced three-phase loads. A polynomial ZIP load model is used for loads, while capacitors are considered as constant impedance loads, and DG units are treated as PQ models with constant active and reactive injected powers, since these are sufficient for steady-state analysis. Loads can be divided into two main categories, wye-connected and delta-connected, as follows [34, 88]:

- Wye-connected loads and capacitors:

  1. Constant power loads:

$$V_{n,p}\; I^{*}_{yp,n,p} = P_{yp,n,p} + j\; Q_{yp,n,p} \qquad \forall\, n, p \tag{2.16}$$

  2. Constant impedance loads:

$$Z_{yz,n,p} = \frac{V^{sp\,2}_{n,p}}{P_{yz,n,p} - j\; Q_{yz,n,p}} \qquad \forall\, n, p \tag{2.17a}$$

$$V_{n,p} = Z_{yz,n,p}\, I_{yz,n,p} \qquad \forall\, n, p \tag{2.17b}$$

  3. Constant current loads:

$$|I^{sp}_{yi,n,p}| = \left| \tfrac{P_{yi,n,p} + j\; Q_{yi,n,p}}{V^{sp}_{n,p}} \right| \qquad \forall\, n, p \tag{2.18a}$$

$$\theta^{sp}_{yi,n,p} = \tan^{-1}\left(\tfrac{Q_{yi,n,p}}{P_{yi,n,p}}\right) \qquad \forall\, n, p \tag{2.18b}$$

$$|I_{yi,n,p}|\; e^{j\;(\measuredangle V_{n,p} - \measuredangle I_{yi,n,p})} = |I^{sp}_{yi,n,p}|\; e^{j\;\theta^{sp}_{yi,n,p}} \qquad \forall\, n, p \tag{2.18c}$$

  4. Fixed capacitors:

$$X_{yc,n,p} = \frac{V^{sp\,2}_{n,p}}{Q_{yc,n,p}} \qquad \forall\, n, p \tag{2.19a}$$

$$V_{n,p} = j\; X_{yc,n,p}\, I_{yc,n,p} \qquad \forall\, n, p \tag{2.19b}$$

5. Capacitor banks with SCs:

$$X_{ycc,n,p} = \frac{V_{n,p}^{sp\,2}}{CAP_{ycc,n,p}\,\Delta Q_{ycc,n,p}} \qquad \forall\, n,p \tag{2.20a}$$

$$V_{n,p} = j\; X_{ycc,n,p}\, I_{ycc,n,p} \qquad \forall\, n,p \tag{2.20b}$$

where the parameter $CAP_{ycc,n,p}$ is a non-negative integer value, which is less than C^{max} and $\Delta Q_{ycc,n,p}$ represents the size of each capacitor block in capacitor banks. Capacitor banks with SCs are considered as fixed capacitors here; however, for the DOPF model, the parameter CAP is treated as an integer variable *cap* to find the optimal number of capacitor blocks switched on.

- Delta-connected loads and capacitors: To find phase-to-phase voltages and currents, two transformation matrices from phase variables to phase-to-phase variables are introduced as follows:

$$\begin{bmatrix} V_{n,ab} \\ V_{n,bc} \\ V_{n,ca} \end{bmatrix} = \begin{bmatrix} 1 & -1 & 0 \\ 0 & 1 & -1 \\ -1 & 0 & 1 \end{bmatrix} \begin{bmatrix} V_{n,a} \\ V_{n,b} \\ V_{n,c} \end{bmatrix} \qquad \forall\, n \tag{2.21a}$$

$$\begin{bmatrix} I_{dl,n,a} \\ I_{dl,n,b} \\ I_{dl,n,c} \end{bmatrix} = \begin{bmatrix} -1 & 1 & 0 \\ 0 & -1 & 1 \\ 1 & 0 & -1 \end{bmatrix} \begin{bmatrix} I_{dl,n,ca} \\ I_{dl,n,ab} \\ I_{dl,n,bc} \end{bmatrix} \qquad \forall\, dl,n \tag{2.21b}$$

Then, similar to (2.16)-(2.20b), the delta-connected loads and capacitors can be described, as follows:

1. Constant power loads:

$$V_{n,pp}\; I_{dp,n,pp}^{*} = P_{dp,n,pp} + j\; Q_{dp,n,pp} \qquad \forall\, n,pp \tag{2.22}$$

2. Constant impedance loads:

$$Z_{dz,n,pp} = \frac{V_{n,pp}^{sp\;\;2}}{P_{dz,n,pp} - j\; Q_{dz,n,pp}} \qquad \forall\, n,pp \tag{2.23a}$$

$$V_{n,pp} = Z_{dz,n,pp}\, I_{dz,n,pp} \qquad \forall\, n,pp \tag{2.23b}$$

3. Constant current loads:

$$|I^{sp}_{di,n,pp}| = \left|\frac{P_{di,n,pp}+j\,Q_{di,n,pp}}{V^{sp}_{n,pp}}\right| \qquad \forall\, n, pp \tag{2.24a}$$

$$\theta^{sp}_{di,n,pp} = \tan^{-1}\left(\frac{Q_{di,n,pp}}{P_{di,n,pp}}\right) \qquad \forall\, n, pp \tag{2.24b}$$

$$|I_{di,n,pp}|\; e^{j\;(\measuredangle V_{n,pp} - \measuredangle I_{di,n,pp})} = |I^{sp}_{di,n,pp}|\; e^{j\;\theta^{sp}_{di,n,pp}} \qquad \forall\, n, pp \tag{2.24c}$$

4. Fixed capacitors:

$$X_{dc,n,pp} = \frac{V^{sp\;\;2}_{n,pp}}{Q_{dc,n,pp}} \qquad \forall\, n, pp \tag{2.25a}$$

$$V_{n,pp} = j\; X_{dc,n,pp}\, I_{dc,n,pp} \qquad \forall\, n, pp \tag{2.25b}$$

5. Capacitor banks with SCs:

$$X_{dcc,n,pp} = \frac{V^{sp\;\;2}_{n,pp}}{CAP_{dcc,n,pp}\,\Delta Q_{dcc,n,pp}} \qquad \forall\, n, pp \tag{2.26a}$$

$$V_{n,pp} = j\; X_{dcc,n,pp}\, I_{dcc,n,pp} \qquad \forall\, n, pp \tag{2.26b}$$

Like the wye-connected loads, delta capacitor banks with SCs are considered as fixed capacitors in the DLF.

- Network equations: Kirchhoff's Current Law (KCL) is applied to define the line current balance at each node and phase, as follows:

$$\sum_{lr} I_{r,p,l} = \sum_{ls} I_{s,p,l} + \sum_{yl} I_{yl,n,p} + \sum_{dl} I_{dl,n,p} \qquad \forall\, n, p \tag{2.27}$$

Similarly, the voltages across the elements connected at each node and phase are considered to be equal, i.e.:

$$V_{r,p,lr} = V_{s,p,ls} = V_{n,p} \qquad \forall\, n, p, l \tag{2.28}$$

2.7 Summary

This chapter reviewed the main background topics of this work. A brief review of DSA, DMS, and centralized VVC problems was presented, and load modeling and load manage-

ment programs in the context of DSM and DR were discussed. This was followed by a discussion of the EHMS micro-hubs and PS+ loads, and a brief review of different mathematical programming models and solution approaches was presented. The SGCM system was also introduced, followed by an overview of the SGCM architecture and its application to distributed computing approaches. Finally, mathematical models of distribution system components used in the DLF model were presented.

Chapter 3

Distributed Computing Architecture for Optimal Control of Distribution Feeders with EHMS Micro-Hub Smart Loads

3.1 Introduction

In this chapter, the DOPF with an NN model of EHMS micro-hub smart loads and its implementation using a distributed computing architecture are presented and discussed. Thus, the algorithm for solving an unbalanced three-phase DLF model used in the DOPF is first discussed in Section 3.2; two distribution feeders, namely, the IEEE 13-node test feeder and a practical test feeder are employed to test and validate the DLF model. In Section 3.3, the implementation of the GA-based approach to solve the DOPF model is explained. This is followed by a discussion on solving the DLF problem using the OpenDSS simulator in Section 3.4. Finally, Section 3.5 presents the unbalanced three-phase DOPF model with EHMS micro-hub loads, and the results obtained from different realistic case studies and scenarios are discussed.

3.2 Distribution Load Flow

The DLF mathematical model discussed in Section 2.6 is solved using the `fsolve` routine, which is based on the Levenberg-Marquardt Algorithm (LMA) [135] in MATLAB® [136]. In order to achieve a faster convergence, the Jacobian matrix is pre-defined in `fsolve`. The procedure is iterative and needs to be initialized, which is done with a flat start; thus, the voltage magnitudes for all the nodes in each phase are set to 1.0 p.u. with default values for voltage angles depending on the transformer connection (e.g., 0° or 30°), and all line currents are set to zero. The LTC taps are integer parameters with fixed values in the DLF; similarly, the SCs are fixed capacitors with fixed values.

3.2.1 Distribution Load Flow Validation

To validate the DLF model, the results for the IEEE 13-node test feeder (Figure 3.1) are found to closely match those provided in [34] and [137]. Table 3.1 shows a comparison of the results obtained using the MATLAB® platform with those reported in [34] obtained using GAMS, and those reported in [137], with the LTC tap positions being fixed to 10, 8, and 11 for phases a, b, and c, respectively, in all cases. Observe a maximum error of 0.3% in phase a voltage angle at Node 634, showing that the results closely match those in [34] and [137].

3.2.2 Practical Distribution Feeder

A real unbalanced distribution feeder from [138] is used for the studies presented in this thesis. The system one-line diagram is shown in Figure 3.2. The feeder has 41 nodes, one single-phase transformer, 3 three-phase transformers equipped with LTCs, and 16 load nodes, which are modeled as ZIP loads with 60% constant impedance loads, 30% constant current loads, and 10% constant power loads. Table 3.2 shows the voltages at the substation and at all load buses for the "nominal" load condition and the following three-phase group-controlled LTC positions: 7 at line 15-16, 12 at line 7-8, and 3 at line 40-41; all the LTCs are 32-steps (i.e., -16 to 16).

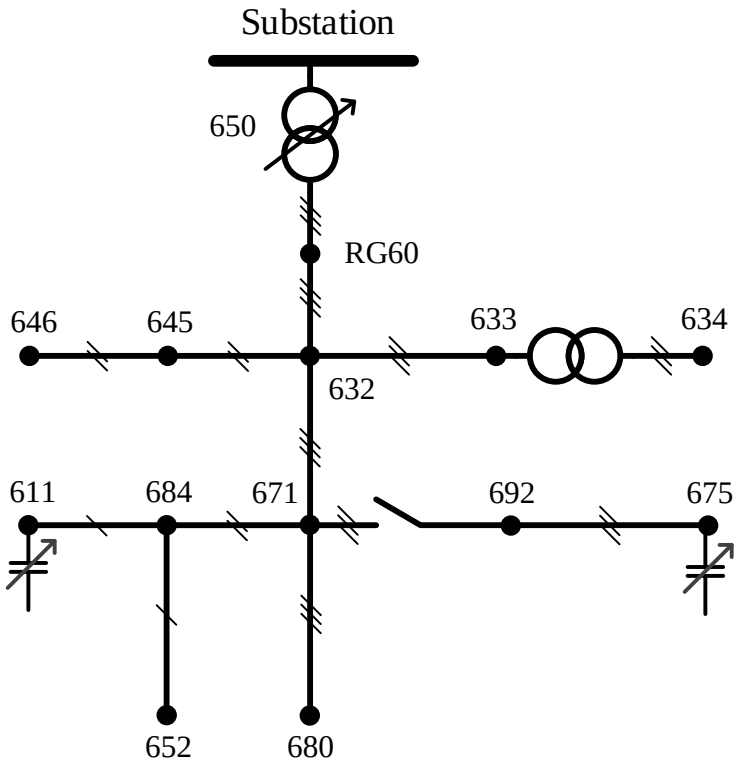

Figure 3.1: IEEE 13-node test feeder [137].

3.3 GA-Based Solution of DOPF

3.3.1 Centralized Computing Approach

The output of the DOPF is an optimal set of LTC tap positions and number of capacitor blocks switched on to supply the given loads. For this reason, TAP, which was a fixed parameter in the DLF model, is considered to be an integer variable, called *tap*; and CAP, which was a fixed parameter in the DLF model, is considered to be a non-negative integer variable, called *cap*. The different elements of the GA implementation are the following [128, 139]:

- Objective function (F): The following function, which is the feeder energy losses, is

Table 3.1: Comparison of DLF results for IEEE 13-node test feeder

Node	Phase	MATLAB platform		GAMS platform [34]		IEEE report [137]	
		Voltage [p.u.]	Angle [deg]	Voltage [p.u.]	Angle [deg]	Voltage [p.u.]	Angle [deg]
650	a	1.0000	0.00	1.0000	0.00	1.0000	0.00
	b	1.0000	-120.00	1.0000	-120.00	1.0000	-120.00
	c	1.0000	120.00	1.0000	120.00	1.0000	120.00
RG60	a	1.0625	0.00	1.0625	0.00	1.0625	0.00
	b	1.0500	-120.00	1.0500	-120.00	1.0500	-120.00
	c	1.0687	120.00	1.0687	120.00	1.0687	120.00
632	a	1.0210	-2.49	1.0210	-2.49	1.0210	-2.49
	b	1.0420	-121.72	1.0420	-121.72	1.0420	-121.72
	c	1.0174	117.83	1.0174	117.83	1.0174	117.83
633	a	1.0179	-2.56	1.0179	-2.56	1.0180	-2.56
	b	1.0401	-121.77	1.0401	-121.77	1.0401	-121.77
	c	1.0148	117.82	1.0148	117.82	1.0148	117.82
634	a	0.9932	-3.24	0.9932	-3.24	0.9940	-3.23
	b	1.0210	-122.22	1.0210	-122.22	1.0218	-122.22
	c	0.9952	117.34	0.9952	117.34	0.9960	117.34
645	b	1.0328	-121.90	1.0328	-121.90	1.0329	-121.90
	c	1.0154	117.85	1.0154	117.85	1.0155	117.86
646	b	1.0311	-121.98	1.0311	-121.98	1.0311	-121.98
	c	1.0134	117.90	1.0134	117.90	1.0134	117.90
671	a	0.9899	-5.30	0.9899	-5.30	0.9900	-5.30
	b	1.0529	-122.35	1.0529	-122.35	1.0529	-122.34
	c	0.9778	116.02	0.9778	116.02	0.9778	116.02
680	a	0.9899	-5.30	0.9899	-5.30	0.9900	-5.30
	b	1.0529	-122.35	1.0529	-122.35	1.0529	-122.34
	c	0.9778	116.02	0.9778	116.02	0.9778	116.02
684	a	0.9880	-5.33	0.9879	-5.33	0.9881	-5.32
	c	0.9758	115.92	0.9758	115.92	0.9758	115.92
611	c	0.9738	115.77	0.9738	115.77	0.9738	115.78
652	a	0.9824	-5.25	0.9824	-5.25	0.9825	-5.25
692	a	0.9899	-5.30	0.9899	-5.30	0.9900	-5.31
	b	1.0529	-122.35	1.0529	-122.35	1.0529	-122.34
	c	0.9778	116.02	0.9778	116.02	0.9777	116.02
675	a	0.9834	-5.55	0.9834	-5.55	0.9835	-5.56
	b	1.0553	-122.52	1.0553	-122.52	1.0553	-122.52
	c	0.9759	116.03	0.9759	116.03	0.9758	116.03

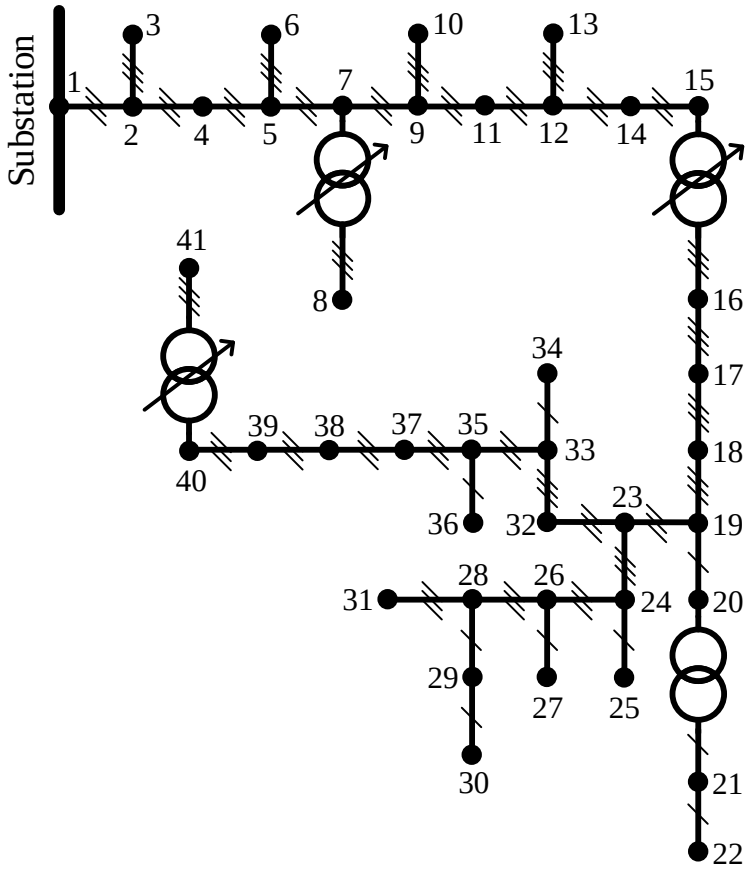

Figure 3.2: Practical distribution feeder [138].

minimized in the DOPF model:

$$F = \ E_{loss} = \sum_{h} \sum_{p} \sum_{n} Re(V_{s_n,p,h} I^*_{s_n,p,h} - V_{r_n,p,h} I^*_{r_n,p,h}) \tag{3.1}$$

- Constraints: The following feeder operating constraints are considered, based on the DLF model:

$$P^g_{n,p,h} - P_{n,p,h} = Re\{V_{n,p,h} I^*_{n,p,h}\} \qquad \forall\, n, p, h \tag{3.2a}$$

Table 3.2: DLF results for the practical distribution feeder

Node	Phase	Voltage [p.u.]	Angle [deg]	Node	Phase	Voltage [p.u.]	Angle [deg]
1	a	1.0000	0.00	23	a	1.0712	-2.76
	b	1.0000	-120.00		b	1.0646	-122.99
	c	1.0000	120.00		c	1.0595	116.69
3	a	0.9681	-1.89	25	a		
	b	1.0529	-122.35		b	1.0615	-123.12
	c	0.9778	116.02		c		
4	a	0.9659	-2.03	27	a	1.0692	-2.86
	b	0.9630	-122.14		b		
	c	0.9591	117.68		c		
6	a	0.9645	-2.11	30	a		
	b	0.9616	-122.22		b		
	c	0.9575	117.59		c	1.0547	116.49
8	a	0.9523	-39.51	31	a	1.0691	-2.90
	b	0.9729	-158.40		b	1.0616	-123.06
	c	0.9361	78.82		c	1.0547	116.49
10	a	1.0359	-2.16	34	a		
	b	1.0326	-122.28		b		
	c	1.0281	117.53		c	1.0564	116.57
13	a	1.0347	-2.23	36	a		
	b	1.0313	-122.36		b	1.0625	-123.08
	c	1.0267	117.44		c		
14	a	1.0305	-2.50	37	a	1.0648	-3.03
	b	1.0264	-122.65		b	1.0584	-123.26
	c	1.0214	117.11		c	1.0521	116.40
22	a			41	a	1.0244	-37.59
	b	1.0547	-124.09		b	1.0406	-157.36
	c				c	1.0234	81.84

$$Q^g_{n,p,h} - Q_{n,p,h} = Im\{V_{n,p,h} I^*_{n,p,h}\} \qquad \forall\, n,p,h \tag{3.2b}$$

$$\underline{V} \le |V_{n,p,h}| \le \overline{V} \qquad \forall\, n,p,h \tag{3.2c}$$

$$|I_{lf,p,h}| \le \overline{I}_{lf} \qquad \forall\, p,h \tag{3.2d}$$

$$\underline{TAP}_{p,fc} \le tap_{p,fc,h} \le \overline{TAP}_{p,fc} \qquad \forall\, p,fc,h \tag{3.2e}$$

$$0 \le cap_{n,p,h} \le C^{max}{}_{n,p} \qquad \forall\, n,p,h \tag{3.2f}$$

while $I_{n,p,h}$ in (3.2a) and (3.2b) is described as below:

$$I_{n,p,h} = \sum_{c=1}^{N_N} Y_{nc,p,h} V_{c,p,h} \qquad \forall\, n, p, h \tag{3.3}$$

where (3.2a) and (3.2b) are the active and reactive power flow equations; (3.2c) represents the nodal voltage operating limits; (3.2d) are the feeder current operating limits; (3.2e) represents the LTCs operating limits; and (3.2f) corresponds to the SCs operating limits. Observe that, since the demand varies over the day, the LTCs and SCs would switch frequently in order to maintain voltages within limits; however, maintenance costs of LTCs and SCs would be considerable in this case, and thus, limits on the number of switching operations per day (5 times) and limits on maximum step changing over consecutive hours ($\pm$ 3 steps) for LTCs and SCs are also considered. In order to satisfy all constraints, all solution sets that violate operating limits are discarded in the DOPF model.

- Individual: Any solution set to which the objective function can be applied is referred to as an individual. For example, a feasible set of LTC tap settings and SC switching decisions in each phase and in each hour is an individual for this optimization problem.
- Population: An array of individuals is called a population.
- Generation (G_m): In each iteration, the GA executes the DLF model with the current population to produce a successive population for a new generation. The GA stops when the maximum number of generations (G) is reached.
- Chromosome: This is an array of binary numbers used to represent the integer variables (i.e., LTCs and SCs) in the DOPF model.
- Population size (PS): This term refers to the size of the population. The diversity of population should be sufficient for the PS to appropriately represent a large region of the search space.
- Cross-over (CR) and mutation (MR) rates: These different rates are used to produce the new generation of population. In this work, CR and MR are respectively equal to 0.85 and 0.005, and the cross-over operator used is a one-point technique [139].
- Parent and off-spring (children): In the GA, the next generation, called off-spring, is selected from the current population, called parent.

- Stall generation limit (SV): This criterion is used to stop the GA when the objective value does not change for an SV number of generations.
- Termination time limit (TL): This stopping criterion stops the GA when the time limit TL is reached.
- Elite off-spring selection (EN): The individuals which result in the most desirable values of F in the current population are chosen as elite off-spring for the next population. EN is the number of those elite individuals.

Without loss of generality, the tap operations are assumed here to be the same for all three phases. Likewise, for SCs, the number of capacitor blocks switched on are assumed the same for all three phases.

Figure 3.3 shows the flowchart of the implementation of the DOPF solution using a centralized GA-based approach. After defining the objective function F, the parameter values G, PS, EN, SV, TL, CR, and MR are chosen. For a 24-hour timeframe, the centralized approach runs the DLF model for all individuals that are determined by the GA procedure. The results are ranked by their value of F; based on this rank, a pool of individuals is selected, and the cross-over and mutation operators are applied to generate an off-spring; The first EN best PS fits among parents and off-springs are then selected for the new generation. The stopping criteria of the GA algorithm are the following:

1. *The run-time is longer than the time limit TL*: This criterion is checked at the end of each generation. In order to feed the system with the new optimized controllable values in real-time applications, TL should be less than the time interval of the application (e.g., 1 hour for the DOPF model).
2. *The solution does not change over SV number of iterations*: Here, $SV = G$ in order to continue the GA up to the last generation, but it has been found that $SV = 10$ is enough for the DOPF to reach a solution.
3. G_m *reaches* G: If the first two stopping criteria are not satisfied before the G number of generations, the solution for the last generation is used.

The output of this model provides the optimal 24-hour LTC tap positions and number of capacitor blocks switched on.

By changing the GA parameters G, PS, EN, and SV, the values of F, i.e., energy losses over a 24-hour timeframe, are obtained for the practical unbalanced distribution

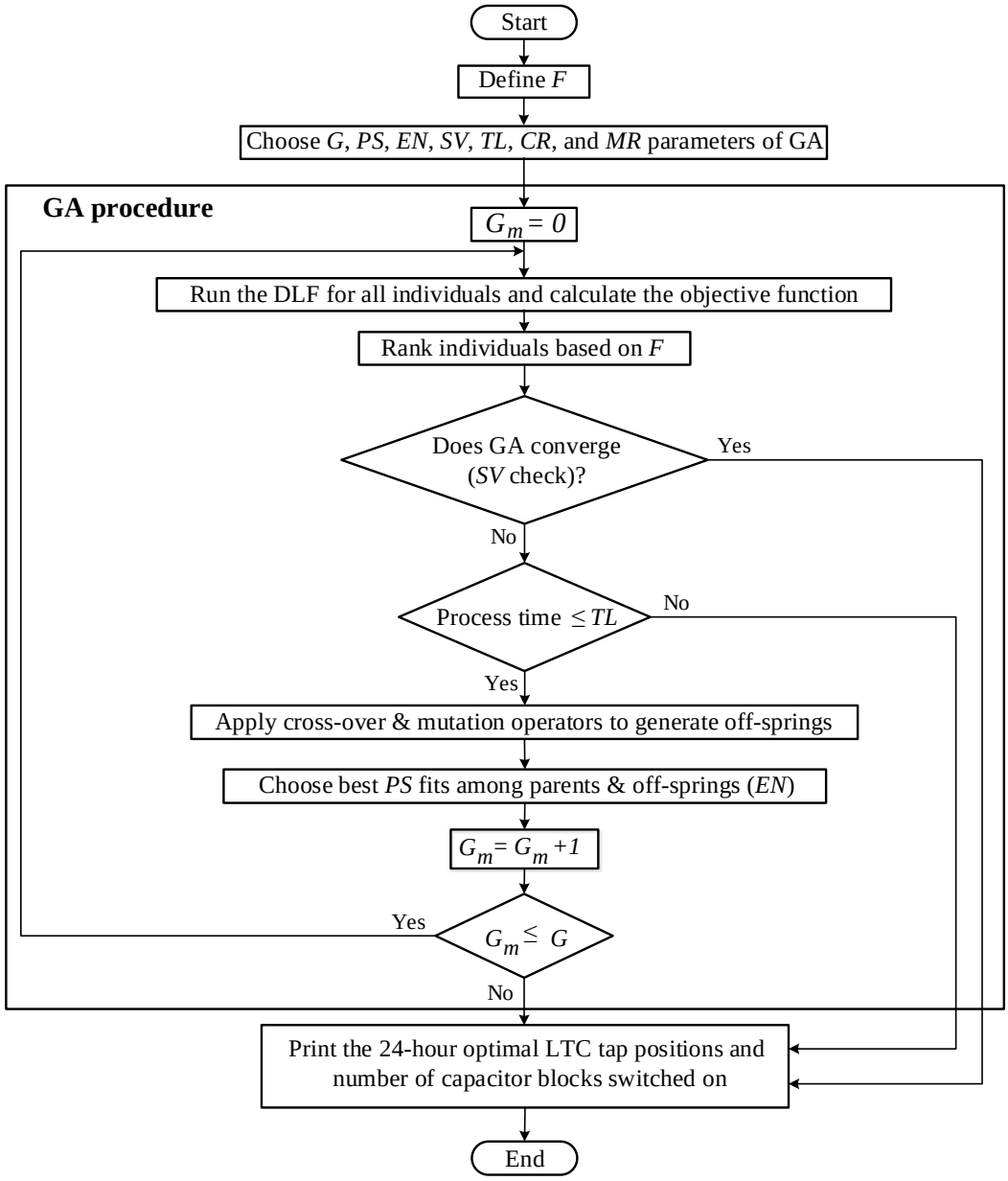

Figure 3.3: Flowchart for the implementation of the proposed DOPF model using a centralized GA-based approach.

Table 3.3: Comparison of DOPF solution with different GA parameters and solution approaches

Case	G	PS	EN	SV	**Solution time**			**Objective function**
					Centralized	Nd **= 12**	Nd **= 24**	**(energy losses [MWh])**
1	40	20	2	10	14h 24m 19s	1h 52m 28s	1h 24m 16s	6.937502
2	40	50	5	10	23h 8m 39s	2h 39m 35s	1h 57m 5s	6.938888
3	50	50	20	50	31h 54m 47s	3h 26m 12s	2h 35m 32s	6.937842
4	100	20	2	20	23h 53m 28s	3h 21m 35s	2h 31m 16s	6.936912
5	100	20	4	20	23h 7m 27s	3h 20m 37s	2h 38m 25s	6.938117
6	100	30	4	20	42h 15m 59s	5h 34m 59s	4h 12m 13s	6.930292
7	200	10	2	200	29h 6m 34s	5h 45m 32s	———	6.948319

feeder of Figure 3.2. Table 3.3 presents the results of the centralized approach for different GA parameters. The model is executed on two servers based on Windows 64-bit operating systems, each with two E5-2650 v2 Intel Xeon 2.60 GHz processors and 48 GB RAM. The closeness of objective function values with different GA parameters shows the robustness of the model, but the solution time varies depending on the GA parameters and solution approach used. In order to achieve better solutions, increasing the value of both generation and population parameters is effective. However, comparison of Cases 2 and 3 shows that increasing the value of SV and EN can also help to find a better solution. Since the DOPF model is an MINLP problem, the computational burden for the centralized approach is significant (the fastest solution time for a 24-hour timeframe is 14h 24m 19s for Case 1).

3.3.2 Proposed Distributed Computing Approach

The DLF model was also implemented using the distributed computing approach mentioned in Section 2.5. Figure 3.4 shows the flowchart for the implementation of the DOPF model with a GA-based solution using the SGCM system. In the SGCM system, for a 24-hour timeframe, the individuals, which are determined by the GA procedure, are appropriately distributed from the master-node among the Nd worker-nodes of the SGCM system. Each worker-node runs the DLF model, and the master-node then combines the results, and ranks them by their value of F. The rest of the procedure is similar to Figure 3.3. By distributing the individuals from the master-node to the worker-nodes, and neglecting small overhead times, the computational time could be divided by the number of worker-nodes, and hence the run-time will be significantly reduced.

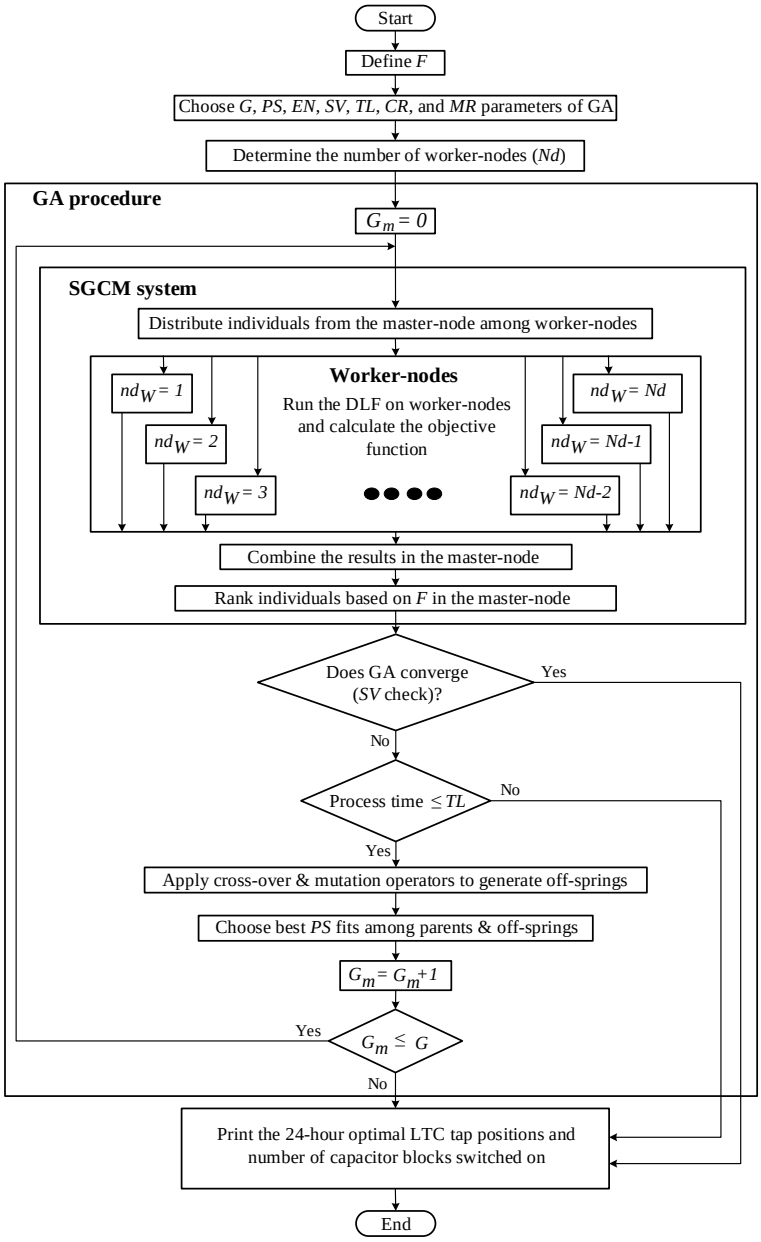

Figure 3.4: Flowchart for the implementation of the proposed DOPF model using a GA-based solution in a distributed computing approach.

The DLF model described in Section 3.2 is implemented in MATLAB®, which allows to generate an executable file that can run on any platform. Thus, there is no need to install MATLAB® on every computer working node, since the DOPF model is envisaged to be executed across different computing nodes of the SGCM system, with the model being a stand-alone executable file independent of any particular computing environment.

To test the DOPF model in the distributed computing approach, it is run on two servers with 12 worker-nodes (i.e., each server has 6 worker-nodes) and with 24 worker-nodes (i.e., each server has 12 worker-nodes). It should be mentioned that if the number of worker-nodes is greater than the number of the population size PS, then there would be idle worker-nodes; for instance, in Cases 1, 4, and 5 with $Nd = 24$ in Table 3.3, four worker-nodes are idle. Also, in Case 7 with $Nd = 12$, two worker-nodes are idle; therefore, it is not necessary to run Case 7 with 24 worker-nodes. It should be added that because of the stall generation SV value, some cases were terminated before reaching the maximum number of generations G; for instance, Case 3 was terminated in 25 generations, Case 4 was terminated in 73 generations, and Case 5 was terminated in 77 generations.

Comparing the solution times in Table 3.3, observe that with 12 worker-nodes in Case 3 takes 3h 26m 12s, against the 31h 54m 47s required in the centralized approach, which means that it takes around 28 hours less to reach the same objective function value; the solution time can be reduced further to 2h 35m 32s in Case 3 with 24 worker-nodes. Case 1 with 24 worker-nodes gives the best solution time with a proper DOPF solution, which shows the effectiveness of the proposed distributed computing approach to solve the unbalanced three-phase DOPF.

Since the computation time for running the DLF model is large; independent of the number of worker-nodes, in order to further reduce the run-time to make the DOPF model suitable for real-time applications, the DLF was solved using a faster and more efficient implementation as discussed next.

3.4 OpenDSS Simulator

In order to reduce the run-time of the DLF model and make it suitable for real-time applications, the open source simulator OpenDSS [72] was used to solve the DLF problem. OpenDSS is able to obtain a single-hour DLF solution for an unbalanced three-phase distribution system within a second, while the time taken to solve the DLF with the `fsolve` MATLAB® solver is 90-120 seconds. Hence, by using OpenDSS together with the distributed computing approach, it is possible to make the DOPF model suitable for real-time applications.

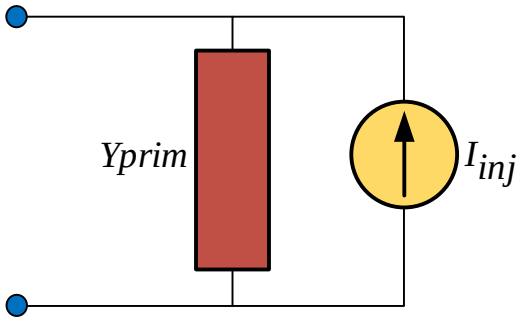

Figure 3.5: Norton equivalent of power conversion elements.

In OpenDSS, generally elements are divided into two different categories: power delivery and power conversion. Power delivery elements usually have two terminals with one or more phases. The function of power delivery elements is to send energy from one terminal to other terminals; examples of these elements are lines and transformers. These elements are defined by their impedance and are represented by the *Yprim* matrices in OpenDSS for each element, as follows:

$$I_{l,p} = Yprim\ V_{n,p} \tag{3.4}$$

Power conversion elements are the other category in the OpenDSS simulator, which convert power from one form of energy to another. Reactors and capacitors are examples of these elements, since they store energy temporarily and then return/absorb it to/from the system as reactive power. Usually power conversion elements just have one terminal and this terminal may include multiple phases. A black-box model is used in OpenDSS to model these elements, which are represented as a simple admittance *Yprim*, or in more complicated models, the injection current is obtained through differential equations. The Norton equivalent of power conversion elements is shown in Figure 3.5. If the element has non-linear characteristic (e.g., special loads and generators), the injection current compensates the non-linear portion of the model. ZIP Loads, as a function of voltage, are modeled as power conversion elements.

Overall, as shown in Figure 3.6, the *Yprim* matrices for power delivery and power conversion elements are fed into the *Ysyst* matrix, which is sparse because of the nature of distribution systems. The *Ysyst* matrix is constant and does not change through simulations in OpenDSS; this efficiently reduces the computational time, especially for long runs.

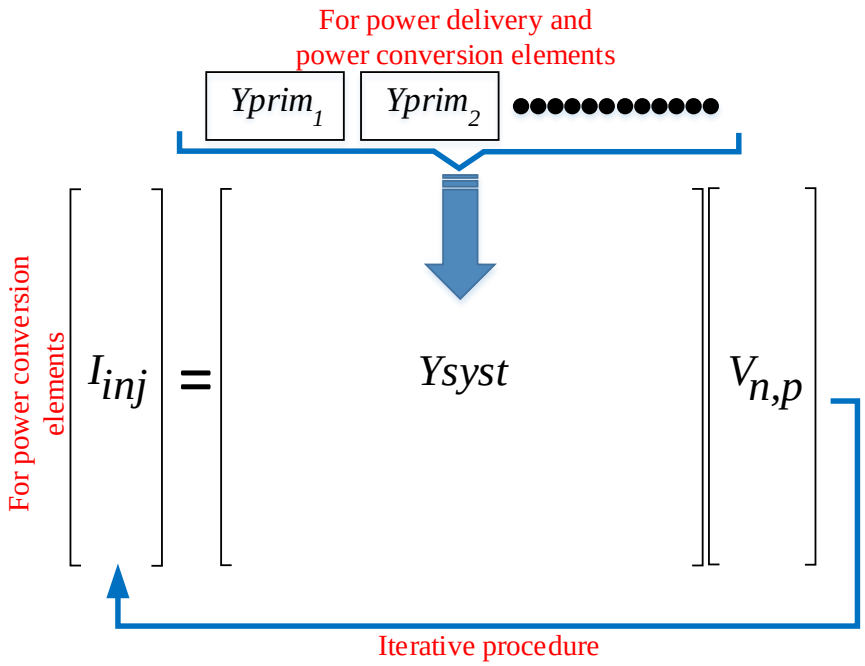

Figure 3.6: Obtaining system admittances and injection currents of power conversion elements in OpenDSS.

To obtain the injection current of power conversion elements, the run starts with an initial guess, with zero load power flow (i.e., all shunt elements are disconnected and just series power delivery elements are considered in the power flow). The obtained voltage and phase angles are used to achieve the injection current for the next iteration of all power conversion elements in the system, which are added into the I_{inj} matrix. When the difference of the voltages in all nodes and all phases converges to typically 0.0001 pu, the iterations are stopped. Since the *Ysyst* matrix is not rebuilt in each iteration, the process of obtaining the results are very quick.

3.5 DOPF Model with EHMS Smart Loads

In the DOPF model so far, the decision variables from the LDC's perspective have been the optimal set of LTC tap positions and the number of capacitor blocks switched on;

hence, in this section demand caps on EHMS micro-hub controllable loads are added to the proposed model, with the objective of minimizing energy losses and/or energy drawn from the substation. Since customers tend to maximize their comfort and convenience, which may lead to high demand peaks, the proposed DOPF model should allow to consider and limit the impact of these controllable customers. Hence, the proposed objective function of the DOPF model for minimization is as follows:

$$F_k = J_k - \alpha_k R \tag{3.5}$$

where the first term represents the feeder energy losses when $k = 1$ (J_1), as described in (3.1), or energy drawn from the substation for $k = 2$ (J_2) as follows:

$$J_1 = E_{loss} \tag{3.6}$$

$$J_2 = E_{drawn} = \sum_h \sum_p Re(V_{s_f,p,h} I^*_{lf,p,h}) \tag{3.7}$$

and the second term:

$$R = \frac{1}{24} \sum_h \sum_p \sum_n \gamma_{n,p,h} \tag{3.8}$$

corresponds to caps on the smart loads' peak demand, which are maximized to maximize the customers' comfort. The parameter α_k allows to control the relative weight of the two conflicting terms in the objective function (3.5).

To study the impact of demand caps on controllable smart loads, the load profile $Ps_{n,p,h}$ for an EHMS micro-hub load, proposed, implemented, and deployed in [12,13], is estimated using an NN with TOU tariff (σ_h), ambient temperature (θ_h), time (h), and peak demand cap ($\gamma_{n,p,h}$) as inputs as follows [140]:

$$Ps_{n,p,h} = f(\sigma_h, \theta_h, h, \gamma_{n,p,h}) \tag{3.9}$$

Without loss of generality, γ is assumed to remain constant over a 24-hour timeframe, hence in (3.8), R represents the sum of all peak demand caps for all controllable loads in all phases and nodes. A fixed power factor is considered for all controllable loads, and the load active power obtained from (3.9) is assumed to correspond to ZIP loads, in order to better represent the various appliances accounted in smart loads. The estimated smart load profile is integrated within the DOPF as a function of the LDCs peak demand cap signal, while the other parameters in (3.9) are assumed known for the day ahead. Thus,

the load profile of each smart load is controlled by the peak demand cap.

In order to obtain the best fitted NN, a NN comprised of a hidden layer with 11 neurons (N_H), and an output layer with one neuron (N_O) was developed in [140], based on the LMA training algorithm, which is provided in the NN MATLAB® toolbox. To obtain the mathematical model for NN-based EHMS controllable loads, power Ps in (3.9), the output from hidden layer neurons can be represented mathematically as follows:

$$H^u_{n,p,h} = \text{tansig}(\omega_{u,1}\ h + \omega_{u,2}\ \theta_h + \omega_{u,3}\ \sigma_h + \omega_{u,4}\ \gamma_{n,p,h} + \delta_u) \tag{3.10}$$

$$\text{tansig}(\tau) = \frac{2}{1+e^{-2\tau}} - 1 \tag{3.11}$$

where the number of inputs N_I for the EHMS load model are four, i.e., h, θ_h, σ_h, and $\gamma_{n,p,h}$. The connection weights between input and hidden layer neurons, i.e., $\omega_{u,i}$ for $u = 1, ..., N_H$ and $i = 1, ..., N_I$, are multiplied with the related inputs, and are then added up together with the bias δ_u of each hidden layer neuron to obtain the output of hidden layer neurons $H^u_{n,p,h}$ in (3.10). The weights and biases for the EHMS loads in this research are those used in [141] having the following values:

$$\omega_{u,i} = \begin{bmatrix} 29.2641 & 8.3822 & -3.9618 & 0.3066 \\ -57.5623 & -0.0478 & -42.5972 & -0.1522 \\ -55.4903 & -0.0400 & -40.8104 & -0.1801 \\ -29.9161 & -6.4604 & 16.6258 & -0.0846 \\ -51.5263 & -0.0658 & -36.7626 & -0.5472 \\ 17.6895 & -0.8765 & -12.2051 & -9.5912 \\ 13.9847 & 0.4149 & -9.2726 & -8.8850 \\ -167.3932 & -0.2311 & 178.3856 & 0.0064 \\ 2.5992 & 0.4391 & -17.9832 & -10.1828 \\ 174.2312 & -0.2591 & -123.1924 & 0.0025 \\ 223.7785 & -0.6084 & -42.0790 & 0.0065 \end{bmatrix} \tag{3.12}$$

$$\delta_u = [-25.3261\ \ 8.6441\ \ 8.4636\ \ 2.7859\ \ 7.7587\ \ 1.1264\ \ -0.9753\ \ 12.5286\ \ -7.2935\ \ 49.6930\ \ -114.8155]^T \tag{3.13}$$

The output of the NN, which is the residential load profile, can be obtained as follows:

$$Ps_{n,p,h} = \text{purelin}((\sum_{u=1}^{N_H} W_{o,u}\, H^u_{n,p,h}) + \Omega_o) \tag{3.14}$$

where the hidden output layer $H^u_{n,p,h}$ with appropriate weights $W_{o,u}$ ($o = 1, ..., N_O$ and $u = 1, ..., N_H$) are summed up in combination with the bias of the output layer neurons Ω_o, to obtain the output from output layer neurons using the purelin function, which is a linear transfer function described in [142]. For the EHMS smart loads considered $N_O = 1$, $W_{o,u}$ and Ω_o are resulting in the following values used in [141]:

$$W_{o,u} = [-0.4365 \quad -6.2111 \quad 7.3630 \quad 0.4832 \quad -1.1307 \quad 0.1022 \quad -.1027 \quad 0.4113 \quad -0.0362 \quad 0.8951 \quad 0.4963] \tag{3.15}$$

$$\Omega_o = -0.9612 \tag{3.16}$$

In the architecture of the proposed feeder and load control presented in Figure 2.6, customers have the ability to receive real-time information from weather stations and market operators, so that their smart load controllers internally optimize their energy consumption and a load profile is obtained. These load profiles are collected by the LDC from the smart loads together with the distribution system status, and used by the LDC control center in real-time to solve the DOPF model. The optimal controls including the peak demand caps obtained from the DOPF solution are fed back to the EHMS micro-hub smart loads to regulate their load, considering the operating feeder constraints (3.2a)-(3.2f) and the following additional peak demand constraint:

$$\gamma_{min_{n,p,h}} \leq \gamma_{n,p,h} \leq \gamma_{max_{n,p,h}} \qquad \forall\, n, p, h \tag{3.17}$$

which reflects the feeder's capacity to deliver power to customers, as well as the customers' minimum feasible consumption, i.e., γ cannot be zero.

OpenDSS, which is used to solve the DLF, and (3.9) are implemented in MATLAB®, which allows to generate an executable file that can be run on a multitude of commonly available platforms. The output of the DOPF model provides the optimal 24-hour LTC tap positions, number of capacitor blocks switched on, and peak demand caps for the EHMS micro-hub loads represented by (3.9).

3.5.1 Results

The real unbalanced distribution feeder with 41 nodes shown in Figure 3.2 is used to test and demonstrate the proposed approach. It is assumed that a portion of the load is controllable through a demand cap. Feeder current limits are not available for this system; hence, (3.2d) is not included.

The proposed distributed computing approach to solve the DOPF model is executed on three physical servers. Two of the servers are based on the Windows 64-bit operating system with two E5-2650 v2 Intel Xeon 2.60 GHz processors and 48 GB RAM with 32 cores, and the third is based on Windows 64-bit operating system with two E5-2670 v3 Intel Xeon 2.30 GHz processors and 128 GB RAM with 48 cores. In all the three servers, the download/upload speed is 95 Mbps.

In order to compare the GA results and solution times, a series of simulations are run, and based on the results, the GA parameters $PS = 24$, $EN = 4$, $SV = G = 100$, $CR = 0.85$, and $MR = 0.005$ for $\alpha_1 = \alpha_2 = 30$ are chosen for this case study. It should be mentioned that the results are fairly close for different set of GA parameters, which demonstrates the robustness and consistency of the DOPF model. The size of data, which is processed in each worker-node, is about 2.46 MB, and the size of the results that should be transferred to the master-node is 8 kB in text format. The size of data processed in the master-node is about 2.56 MB, which is slightly larger than the processed files of each worker-node, and the size of the new set of individuals, which should be transferred to each worker-node is 4 kB in text format. Note that changing the GA parameters such as PS affects the size of the text files, but not significantly. For the DOPF problem with an MINLP model, the size of data is reasonable, i.e., neither small nor too large; in this study, the DOPF is a 24-hour problem with different control variables, including three LTCs (i.e., $3\times24 = 72$ control variables) and peak demand caps for 48 load nodes, for a total of 120 control variables. On the other hand, the large number of state variables for the practical feeder in Figure 3.2 are as follows:

- Voltage magnitudes: (32 nodes $\times$ 3 phases + 9 nodes $\times$ 1 phase) $\times$ 24 hours = 2,520
- Voltage angles: (32 nodes $\times$ 3 phases + 9 nodes $\times$ 1 phase) $\times$ 24 hours = 2,520
- Current magnitudes: (31 lines $\times$ 3 phases + 9 lines $\times$ 1 phase) $\times$ 24 hours = 2,448
- Current angles: (31 lines $\times$ 3 phases + 9 lines $\times$ 1 phase) $\times$ 24 hours = 2,448

Table 3.4: Comparison of F_1, J_1, and R for different numbers of worker-nodes

			Number of generations (G)		
			25	**50**	**100**
Number of worker-nodes (Nd)	**1**	J_1 [kWh]	7892.04	8071.10	7757.61
		R [kWh]	1851.99	1956.57	2046.32
		F_1 [kWh]	-47667.63	-50626.03	-53632.05
	2	J_1 [kWh]	8133.57	8054.96	7905.68
		R [kWh]	1958.79	1971.66	2008.46
		F_1 [kWh]	-50630.16	-51094.78	-52348.06
	5	J_1 [kWh]	8419.75	8011.12	8331.62
		R [kWh]	1887.80	1990.12	2069.62
		F_1 [kWh]	-48214.25	-51692.36	-53757.04
	10	J_1 [kWh]	8172.41	7912.79	8017.24
		R [kWh]	1890.12	1938.29	2069.41
		F_1 [kWh]	-48531.19	-50235.79	-54065.09
	20	J_1 [kWh]	7882.74	8103.66	7881.85
		R [kWh]	1915.08	1990.83	2029.93
		F_1 [kWh]	-49569.72	-51621.09	-53015.99

Hence, the total number of state variables is 9,936. The discrete values of LTC taps can vary between -16 to +16, and the peak demand cap varies between 2.55 and 7.331 kW, with a resolution of 1 W in the GA implementation.

A comparison of the results with different number of worker-nodes and generations, for $k = 1$ and $k = 2$, are presented in Tables 3.4 and 3.5. The closeness of F_k results for different generations with different number of worker-nodes shows that 25 generations are sufficient to arrive at an acceptable solution for the DOPF model. When the number of worker-nodes is low (i.e., 1, 2, or 5), all the worker-nodes are installed and run on one server, whereas for 10 worker-nodes, two servers are used (each server has five worker-nodes), and for 20 worker-nodes three servers are used (two servers with five and one server with ten worker-nodes). It is worth mentioning that there is no limit on the number of worker-nodes on the servers. These servers are identified with their IP addresses, and since each server can handle more than one worker-node, these nodes are identified based on their port numbers; hence, each worker-node has identical node addresses (i.e., a mixture of an IP address and a port number) in the SGCM system. There is access to five open ports on two of the servers and ten unblocked ports on the other one. It is possible to administer the machines in order to have more open ports, and therefore, more worker-nodes on one machine. If there is more than one worker-node installed in a server, the multi-tasking

Table 3.5: Comparison of F_2, J_2, and R for different numbers of worker-nodes

			Number of generations (G)		
			25	**50**	**100**
Number of worker-nodes (Nd)	**1**	J_2 [MWh]	301.76	301.16	300.29
		R [kWh]	1778.10	1771.74	1771.33
		F_2 [MWh]	248.42	248.00	247.15
	2	J_2 [MWh]	305.69	303.84	304.04
		R [kWh]	1645.12	1676.95	1741.88
		F_2 [MWh]	256.34	253.53	251.79
	5	J_2 [MWh]	303.04	301.60	301.85
		R [kWh]	1868.16	1858.93	1942.44
		F_2 [MWh]	247.00	245.84	243.58
	10	J_2 [MWh]	304.17	302.55	302.49
		R [kWh]	1684.36	1785.52	1862.03
		F_2 [MWh]	253.64	248.99	246.63
	20	J_2 [MWh]	302.65	301.00	301.26
		R [kWh]	1657.41	1664.87	1790.17
		F_2 [MWh]	252.93	251.06	247.55

feature of the platforms (i.e., Windows, Linux, and Mac) is responsible for assigning the cores and required physical memories to the worker-nodes in the SGCM system.

In the objective function (3.5), the component R varies between R_{min} and R_{max}, where:

$$R_{min} = \frac{1}{24} \sum_{h} \sum_{p} \sum_{n} \gamma_{min_{n,p,h}} \tag{3.18a}$$

$$R_{max} = \frac{1}{24} \sum_{h} \sum_{p} \sum_{n} \gamma_{max_{n,p,h}} \tag{3.18b}$$

When $\alpha_k = 0$, the objective is essentially to minimize energy loss (J_1) or the energy drawn from the substation (J_2); in either case, the optimal solution yields a low value of γ_k, and the R profile drifts towards R_{min}. Figure 3.7 shows the GA convergence considering energy loss minimization ($k = 1$) for different values of α_1. Observe that for $\alpha_1 = 0$, the value of R drifts towards R_{min} (Figure 3.7(a)), while as α_1 is increased, R increases, as shown in Figure 3.7(b)-3.7(d), with the value of $\gamma_{n,p,h}$ increasing, which means that the peak demand caps for EHMS micro-hub loads increase. In Figure 3.8, note for $\alpha_1 > 5$, the R profile is close to R_{max}, which indicates a high peak demand cap for EHMS micro-hub

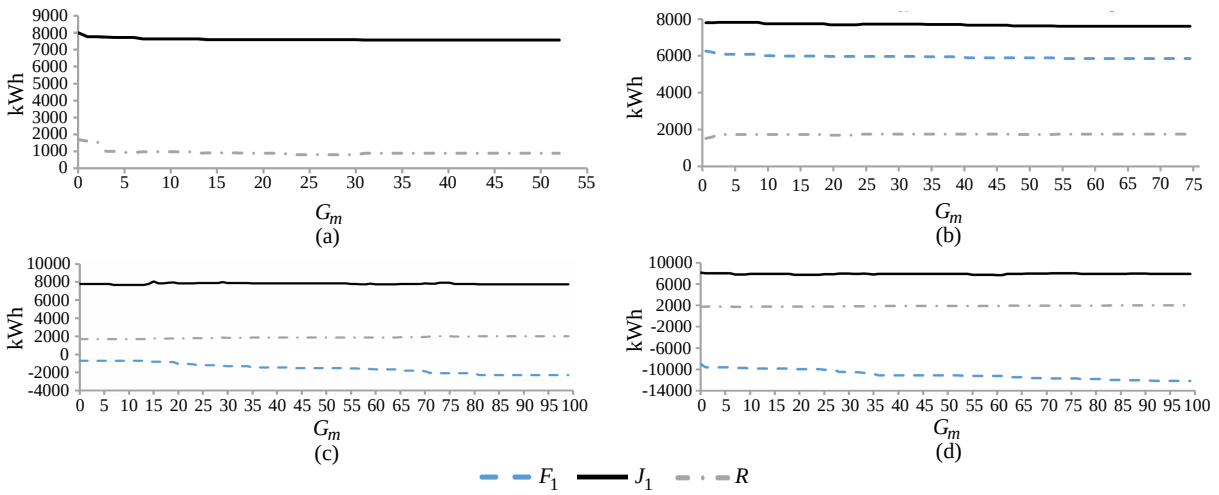

Figure 3.7: GA convergence for minimization of F_1 with: (a) $\alpha_1 = 0$; (b) $\alpha_1 = 1$; (c) $\alpha_1 = 5$; and (d) $\alpha_1 = 10$.

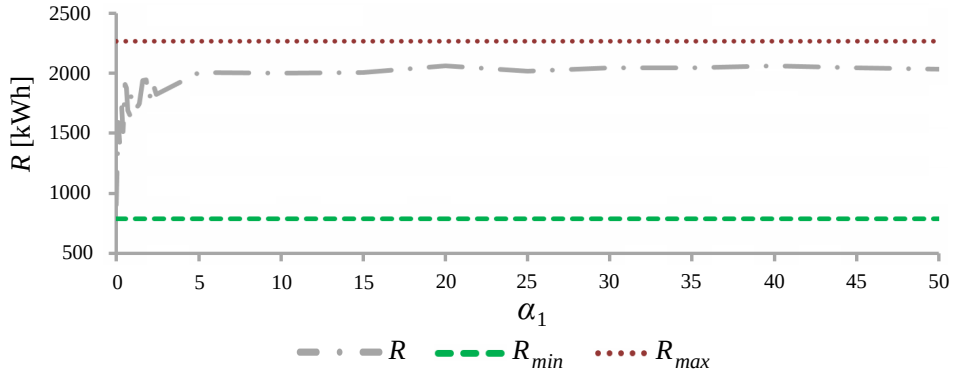

Figure 3.8: Effect of α_1 on R.

loads. On the other hand, in Figure 3.9, the effect of α_1 on J_1 is shown, demonstrating that as α_1 increases, J_1 generally increases; the variations of J_1 are due to the GA convergence characteristics, which yield the changes in the J_1 values observe in Figure 3.9.

Figure 3.10 shows the convergence of the GA considering the energy drawn from the substation ($k = 2$) for different values of α_2. Note that the R profile converges towards R_{min} for $\alpha_2 = 0$, while as α_2 is increased, the peak demand cap increases, effectively allowing more flexibility of the EHMS micro-hub loads. In Figure 3.11, observe that for $\alpha_2 > 200$,

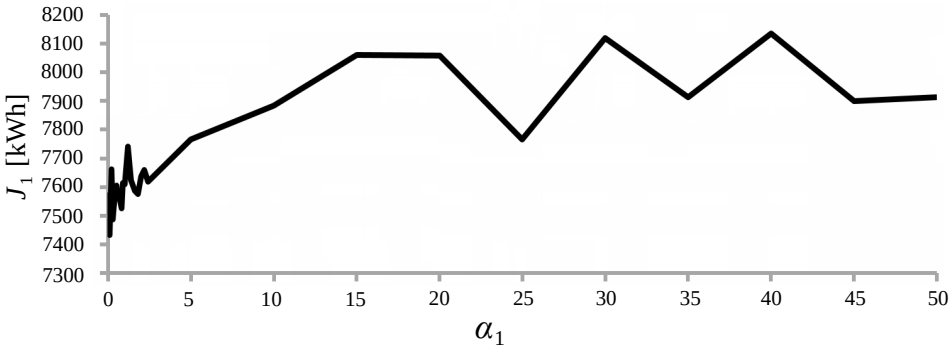

Figure 3.9: Effect of α_1 on J_1.

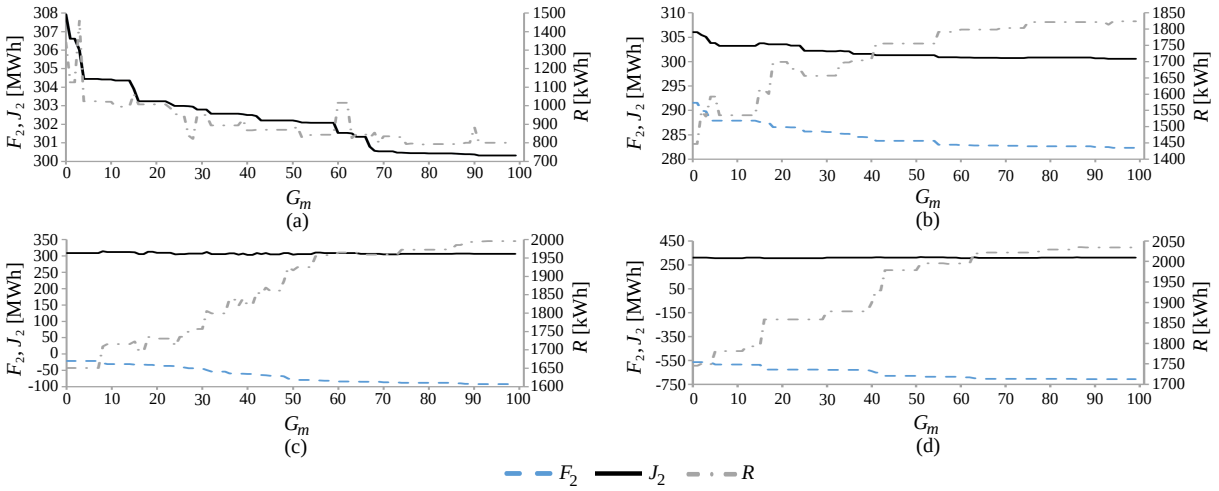

Figure 3.10: GA convergence for minimization of F_2 with: (a) $\alpha_2 = 0$; (b) $\alpha_2 = 10$; (c) $\alpha_2 = 200$; and (d) $\alpha_2 = 500$.

the R profile is close to R_{max}, and when α_2 is increased beyond 200, the contribution of R to F_2 increases, while the one from J_2 decreases, which leads to a general increase of J_2 value (Figure 3.12).

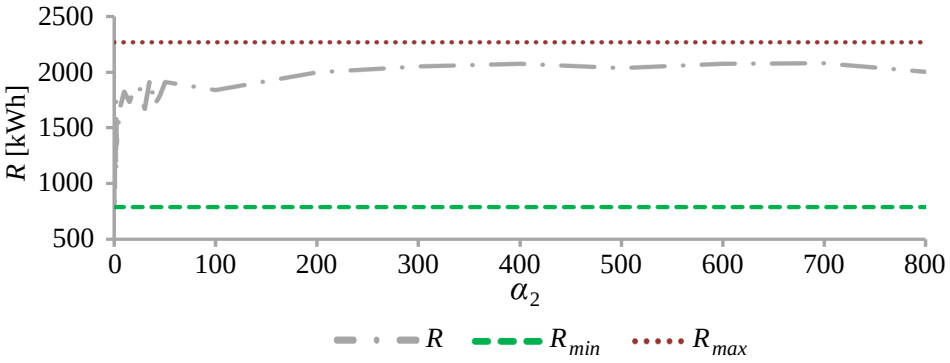

Figure 3.11: Effect of α_2 on R.

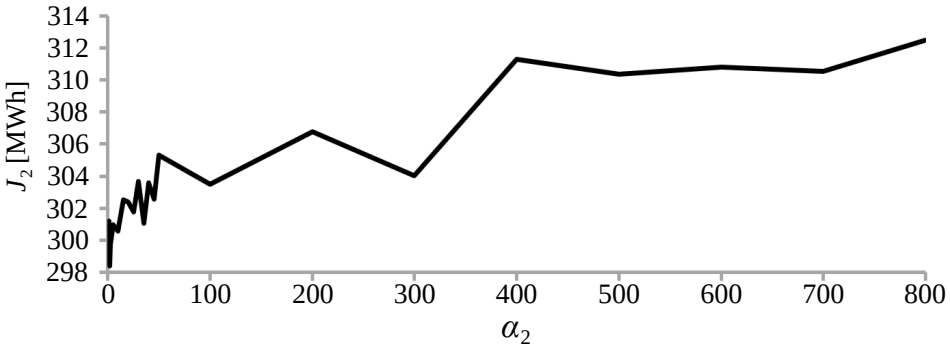

Figure 3.12: Effect of α_2 on J_2.

3.5.2 Impact of the Distributed Computing Platform on Solution Time

Figures 3.13 and 3.14 present the impact of Nd on the solution times with different generation numbers for the GA. Observe that the distributed computing approach has a significant impact on the reduction of solution time, taking about 15 minutes, whereas the centralized approach requires a much larger computation time. Furthermore, these studies also reveal that increasing the number of parallel computers enhances the parallelization of the computation process and decreases the run-time. However, increasing Nd cannot always reduce the run-time; thus, Nd needs to be optimally determined for each case study, which corresponds to a value of $Nd = 10$ for the present study.

The closeness of the objective function values F_1 and F_2 for different generation numbers

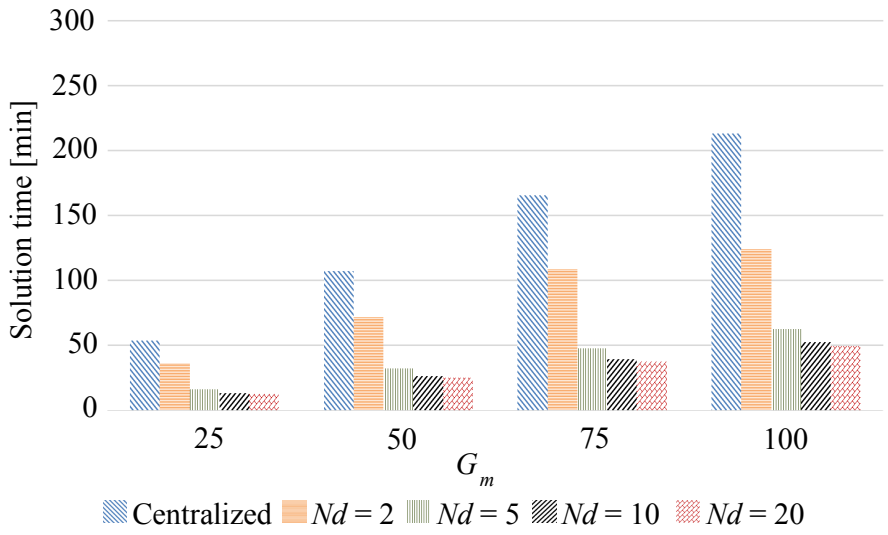

Figure 3.13: Computation times for centralized versus proposed distributed computing approach with F_1, for different Nd values.

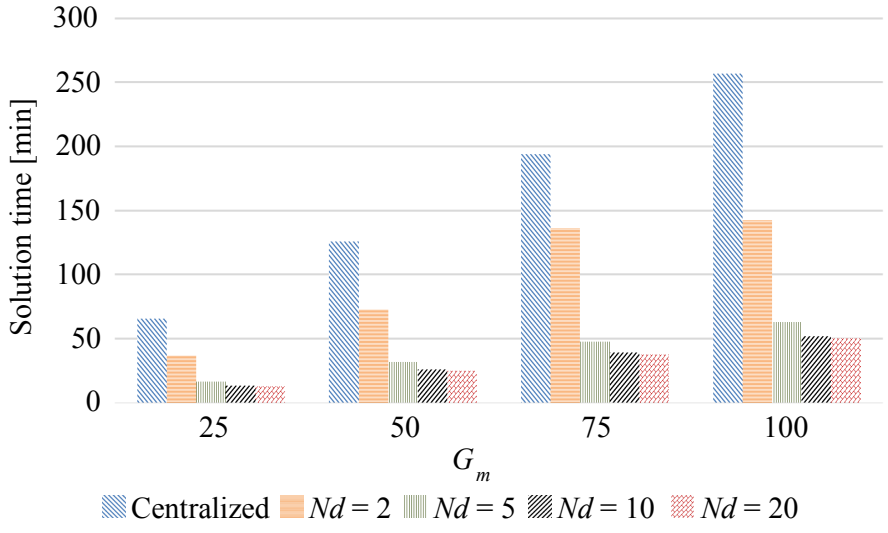

Figure 3.14: Computation times for centralized versus proposed distributed computing approach with F_2, for different Nd values.

demonstrates the robustness of the model, although the solution time varies. Short solution times help with shorter feeder dispatch intervals, which is necessary with controllable loads. In distribution systems, real-time intervals for the application being considered would be about 15 min; hence, with the run-times shown for the proposed approach with Nd=10, as well as appropriate number of GA generations, which is 25 for this case study, it should be possible to yield reasonably optimal solutions of the DOPF model for real-time applications.

3.6 Summary

This chapter presented the algorithm for solving an unbalanced three-phase DLF model; two distribution feeders, namely, the IEEE 13-node test feeder and a practical test feeder were employed to test and validate the DLF model. The implementation of the DOPF model with a GA-based solution in a centralized and decentralized approaches were also explained; the results showed that distributing the individuals amongst worker-nodes reduces the computational burden in comparison with the run-time of the DOPF model in the centralized approach. This was followed by a discussion on executing the DLF model in the OpenDSS simulator, which can considerably reduce the run-time of the DLF model.

The unbalanced three-phase DOPF model in the presence of EHMS micro-hub loads was presented, and the results obtained from different realistic case studies and scenarios were discussed. The studies demonstrate that compared to the centralized approach, the proposed distributed computing architecture yields significantly faster solutions by increasing the number of SGCM worker-nodes, with realistic peak demand caps for controllable smart loads, considering both the LDC's and customers' interests.

Chapter 4

Optimal Demand Response for Distribution Feeders with Existing Smart Loads

4.1 Introduction

In this chapter, the integration of existing smart loads, particularly PS+ loads, into the proposed distributed-computing-based DOPF is presented and discussed. Thus, the modeling of controllable smart loads using an NN technique is discussed in Section 4.2, and its application to existing controllable PS+ loads is demonstrated. The mathematical function of the proposed NN-based PS+ load model and its integration into a DOPF are also discussed in this section, together with the GA and distributed computing approaches used to solve it. In Section 4.3, the results of applying the proposed DOPF model to the practical distribution feeder used throughout the thesis are discussed for different scenarios, and the effect of optimal management of PS+ loads is presented.

4.2 Mathematical Model of PS+ Smart Loads

In order to model the PS+ loads using an NN approaches as in the case of the EHMS loads, a data-set of different load profiles, which include the effect of PCT ON/OFF signals together with various range of temperatures and electricity prices, is needed. Based on the characteristics of the PS+ program, PCTs are activated on average five times per year, up

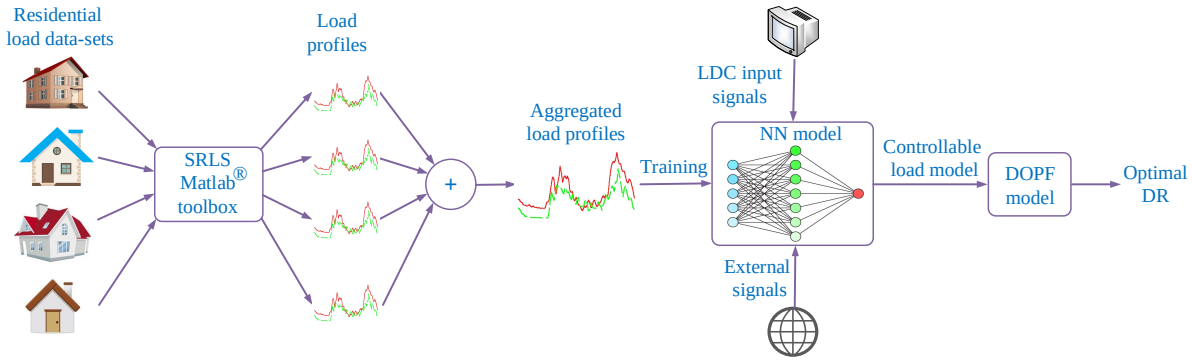

Figure 4.1: Schematic of modeling of controllable smart load and its integration into the DOPF model.

to a maximum of 40 hours. However, because of these limited hours of activation, adequate realistic field data was not available, and hence it is not possible to obtain an adequate NN model of the PS+ loads from the amount of data available. Therefore, in order to generate adequate and realistic data for residential loads, a data-set of energy usage of different appliances and devices of multitude of houses in the EHMS project for all days of July 2013 was simulated using the SRLS [113], and then the effect of PS+ signals were studied by changing the variables like ambient temperature, AC setpoints, and hours of PS+ signal activations.

In general, the load profiles generated by the SRLS may vary widely by a location, customer preferences, and time of usage across households; hence, it is not possible to obtain adequate NN models of each household. Therefore, aggregated load profiles, which are smoother and have less variations, were used to model the load at the feeder level. Based on the the focus of this study at the feeder level, an average profile of the aggregated load profiles of PS+ loads was used. The general procedure followed to obtain the PS+ load NN models for integration into the DOPF model is depicted in Figure 4.1.

For existing PS+ controllable loads, the following residential load profile ($Psl_{n,p,h}$) can be estimated from measurements or simulations, as previously mentioned, as a function of time (h), TOU tariff (σ_h), ambient temperature (θ_h), and binary ON/OFF signals ($\mu_{n,p,h}$) for PCT setpoints of ACs:

$$Psl_{n,p,h} = f(h, \sigma_h, \theta_h, \mu_{n,p,h}) \tag{4.1}$$

where, if the PCT setpoint signal is ON ($\mu = 1$), the PCT setpoints are increased by 2°C

for a limited time within a day, which decreases the run-cycle of ACs, thus, decreasing the demand in all participating residential houses in the PS+ program and hence reducing peak load at the feeder level. Function (4.1) is modeled here using an NN, as explained next.

The average load profile was used for training purposes, obtaining the best fitted NN with a hidden layer with 8 neurons (N_H), and an output layer with one neuron (N_O), based on the Bayesian regularization back-propagation training algorithm provided in the NN MATLAB® toolbox. The maximum allowable number of epochs was set to 1000, and the desired gradient to 10^{-7}; 70% of the load data-set was used for training, 15% for validation, and 15% for testing. The Mean Squared Error (MSE) function was used to check the performance of the NN model, and the input data was randomly divided for training, validation, and testing. The NN output yielded an overall R-squared value of 0.9206 and an MSE value of 0.2392 kW^2.

To obtain the mathematical *Psl* model (4.1) for NN-based PS+ controllable loads, the output from hidden layer neurons can be represented mathematically as follows:

$$H^u_{n,p,h} = \text{tansig}(\omega_{u,1}\ h + \omega_{u,2}\ \theta_h + \omega_{u,3}\ \sigma_h + \omega_{u,4}\ \mu_{n,p,h} + \delta_u) \tag{4.2}$$

where the number of inputs (N_I) for the PS+ load model are 4, i.e., h, θ_h, σ_h, and $\mu_{n,p,h}$. The connection weights between input and hidden layer neurons, i.e., $\omega_{u,i}$ for $u = 1, ..., N_H$ and $i = 1, ..., N_I$, are multiplied with the related inputs, and then are added up together with the bias (δ_u) of each hidden layer neuron to obtain the output of hidden layer neurons ($H^u_{n,p,h}$) in (4.2), using a Tan-Sigmoid transfer function that is defined in (3.11). The weights and biases obtained were:

$$\omega_{u,i} = \begin{bmatrix} -0.2516 & 0.7686 & 0.3734 & 0.7471 \\ -1.7367 & 0.2107 & 0.8732 & 0.2173 \\ -1.5808 & 0.4423 & -0.0448 & 0.0803 \\ 0.1089 & -0.4816 & -0.5954 & -0.2575 \\ -0.8702 & -0.3230 & -1.2442 & -0.0854 \\ 3.0763 & 0.0394 & 0.0003 & 0.0358 \\ 3.0820 & 0.0662 & -0.3579 & -0.1338 \\ -0.2406 & -2.6781 & 0.2834 & 0.0853 \end{bmatrix} \tag{4.3}$$

$$\delta_u = \begin{bmatrix} -0.1383 & 1.5079 & 0.2666 & 0.3245 & -0.1001 & -0.7541 & -1.4913 & 1.1365 \end{bmatrix}^T \tag{4.4}$$

The output of the NN, which is the residential load profile, is obtained as follows:

$$Psl_{n,p,h} = \text{purelin}((\sum_{u=1}^{N_H} W_{o,u}\, H^u_{n,p,h}) + \Omega_o) \tag{4.5}$$

where the hidden output layer $H^u_{n,p,h}$ with appropriate weights $W_{o,u}$ ($o = 1, ..., N_O$ and $u = 1, ..., N_H$) are summed up in combination with the bias of the output layer neurons Ω_o to obtain the output from output layer neurons using the purelin function described in [142]. For Psl, $N_O = 1$, and hence, the $W_{o,u}$ is a row vector, and Ω_o is just a number with the following values:

$$W_{o,u} = \begin{bmatrix} -0.3176 & 1.4993 & -1.3475 & -1.5726 & 1.1348 & -1.0531 & 1.6122 & -0.8345 \end{bmatrix} \tag{4.6}$$

$$\Omega_o = 0.1959 \tag{4.7}$$

Figure 4.2 presents a comparison of the developed NN output and target for the aggregated loads in July 2013. The peak demand MSE is 0.1860 kW^2, which shows the effectiveness of the obtained NN model.

4.2.1 DOPF Model with PS+ Loads

From Chapter 3, the general form of a DOPF with controllable loads can be summarized as follows:

$$\begin{aligned} \min \quad & F = \text{ Objective function} && \text{(4.8a)} \\ \text{s.t.} \quad & \text{Operational and system constraints} && \text{(4.8b)} \\ & \text{Smart load model and constraints} && \text{(4.8c)} \end{aligned}$$

Various objective functions such as minimization of energy loss, minimization of energy drawn from the substation, or minimization of energy cost can be adopted in (4.8a) as discussed next. Operating constraints in (4.8b) include the power flow equations (3.2a)-(3.2b), bus voltage limits (3.2c), feeder current limits (3.2d), and LTC (3.2e) and SC (3.2f) operating limits. Depending on the purpose and model of controllable smart loads represented in (4.8c), the LDC can send signals such as peak demand constraints (e.g., in EHMS micro-hub loads) or temperature setpoints (e.g., in PS+ loads) to these loads.

In order to study the effect of PS+ controllable loads, the average load model developed

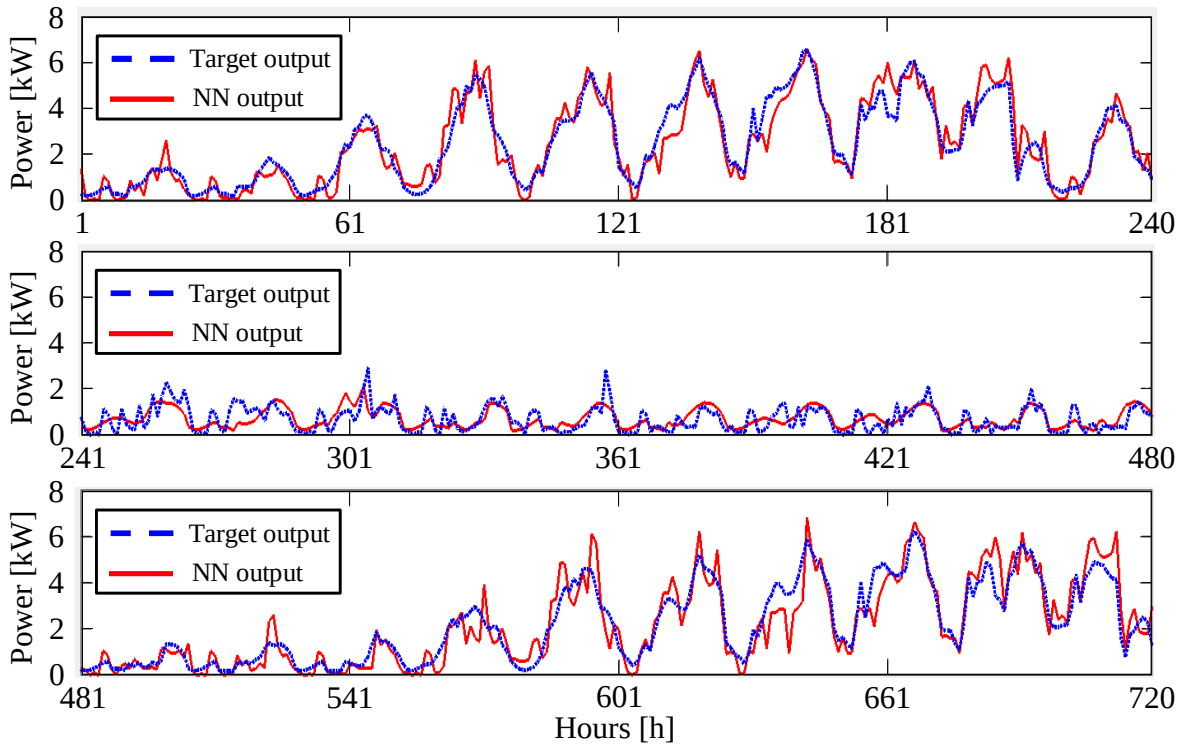

Figure 4.2: Comparison of NN output and target of aggregated PS+ loads for 30 days in July 2013.

using NN for these loads can be integrated into the DOPF model. The DOPF model would then determine the optimal decisions from the LDC's perspective, such as the LTC tap positions and number of capacitor blocks switched on, as well as the optimal ON/OFF signals to PCTs of ACs to reduce the peak load at the feeder level under the PS+ program. In this study, the DOPF is a 24-hour problem with various control variables, including three LTCs and ON/OFF signals of PCTs for 48 load nodes, for a total of 1,224 control variables. In this context, two different DOPF models are proposed here; the first objective function F_3 seeks to minimize the energy losses over the day, as follows:

$$\min \; F_3 = \; E_{loss} \tag{4.9}$$

where E_{loss} is defined in (3.1), with the following constraints to limit the feeder peak load:

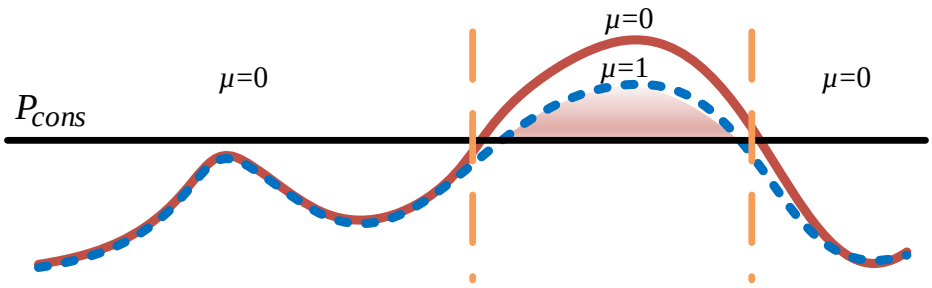

Figure 4.3: ON/OFF decision making during peak load based on the value of P_{cons}.

$$\max(P_{feeder_{p,h}}) \leq P_{lim} \qquad \forall\, p, h \tag{4.10a}$$

$$\sum_{h} \mu_{n,p,h} \leq T_{n,p}^{max} \qquad \forall\, n, p \tag{4.10b}$$

However, the hard constraint (4.10a) may yield infeasible results, as it forces the control variables to reduce the demand below P_{lim}, which might not be feasible depending on the available controllable loads. Hence, a second objective function F_4 can be defined that seeks to keep the load profile close to a target demand P_{cons} as follows:

$$\min \quad F_4 = E_{loss} + \beta S \tag{4.11a}$$

$$\text{s.t.} \quad S = \sum_{h} \sum_{p} |P_{feeder_{p,h}} - P_{cons}| \tag{4.11b}$$

$$\sum_{h} \mu_{n,p,h} \leq T_{n,p}^{max} \quad \forall\, n, p \tag{4.11c}$$

As shown in Figure 4.3, when the feeder power exceeds P_{cons}, PS+ loads will be activated by forcing $\mu_{p,n,h} = 1$, thus, reducing peak demand during the hours when $P_{feeder} > P_{cons}$. Otherwise, $\mu_{p,n,h} = 0$ when $P_{feeder} < P_{cons}$.

The DOPF model is solved using a recursive GA-based model, which runs the DLF of the feeder to obtain the best solution of the control variables, i.e., LTC tap positions, number of capacitor blocks switched on, and ON/OFF signals of PCTs for PS+ loads. As discussed in Section 3.5 for EHMS micro-hub loads, the DLF of the real feeder with

unbalanced three-phase loads is also modeled here using OpenDSS [72]. PS+ controllable loads are modeled with an NN, as previously discussed, and are integrated into OpenDSS as a power demand variable defined by (4.1) as a function of the binary decision variable $\mu_{p,n,h}$.

The flowchart of the DOPF model with PS+ loads is similar to Figure 3.4, but the output in this case also includes the optimal ON/OFF PS+ signals. Hence, the solution of the DOPF model is the 24-hour optimal LTC tap positions, number of capacitor blocks switched on, and ON/OFF signals for PS+ smart loads.

4.3 Results and Discussions

The aforementioned DOPF with an NN model of PS+ loads was applied to the optimal dispatch of the practical unbalanced distribution feeder with 41 nodes, shown in Figure 3.2. In the presented study, 10% of the loads are assumed to be PS+ controllable loads, while the rest of the loads are modeled as ZIP loads. Furthermore and without loss of generality, the maximum ON hours of PS+ loads are increased from a maximum of 4 hours to 13 hours, within a fixed window from 7:00 to 20:00 on weekdays to allow studying the effect of more flexible controllable loads. Also, PS+ loads are assumed to be activated for longer periods of time, since based on the PS+ rules, the average activation is five times per year, up to a maximum of 40 hours, excluding emergencies such as a blackout during summer.

4.3.1 Case 1

The F_3 objective is used in this case with nodal and phase-wise application of PS+ signals. For the DOPF model (4.9)-(4.10b), based on different experiments, P_{lim} was set to 14.5 MW, which is the minimum possible value that can be reached, since solutions with P_{lim} less than 14.5 MW were infeasible. Figure 4.4 shows the effect of PS+ signal on the feeder load profile for three different days. Observe the impact on load profiles when PS+ loads are activated between hours 14:00 and 18:00, showing a reduction in demand during these times, but resulting in moving the peak to later hours in some cases, which can be attributed to HVAC operation.

For different maximum hours of PCT operation from hours 4 to 13, simulations were performed with each phase of each node receiving unique μ signals, i.e., PS+ loads located in different nodes and phases were assumed to have different μ values. The results obtained show that by increasing $T_{p,n}^{max}$, the energy usage gradually decreasing, as shown in

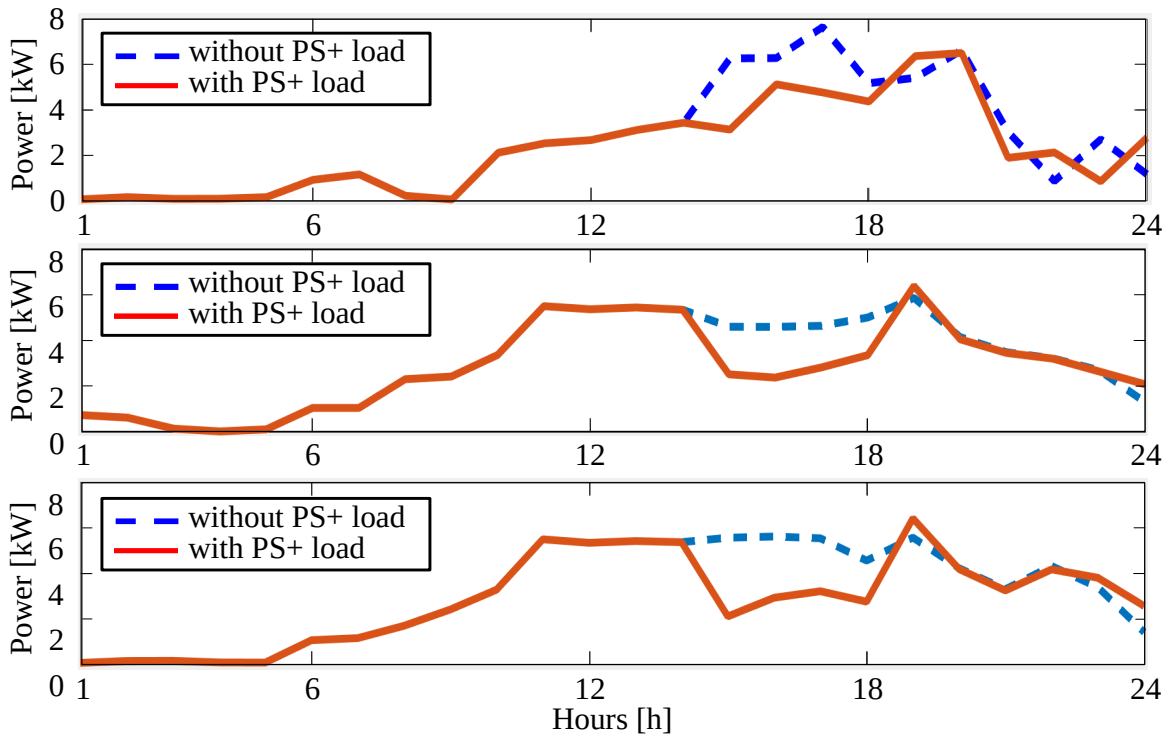

Figure 4.4: Effect of PS+ signal on load profiles for hours 14:00 to 18:00 on three different days in July, 2013.

Figure 4.5; for $T_{p,n}^{max}$ of 4, 10, and 13 hours, the energy savings are 1470.4, 1877.6, and 2048.9 kWh, respectively. Figure 4.6 depicts the μ signals sent to Node 8 for each phase for $T_{p,n}^{max}$ of 4, 10, and 13 hours of PCT control; this node houses 70 PS+ customers in phase a, 60 in phase b, and 80 in phase c. Although the energy consumption decreases by increasing $T_{p,n}^{max}$, the peak load reduction for different hours does not change considerably.

It is worth mentioning that the PCT signals do not work effectively during extreme temperature conditions. Thus, in low temperatures, when the ACs are normally OFF, the PCT signals have no impact on their energy usage. Similarly, during high temperatures, ACs are normally ON, and increasing the setpoint by 2°C does not turn the ACs off, not affecting the energy usage of the system. Hence, this program is not effective during extreme hot summer-days, unless an AC cycling approach is used [143, 144].

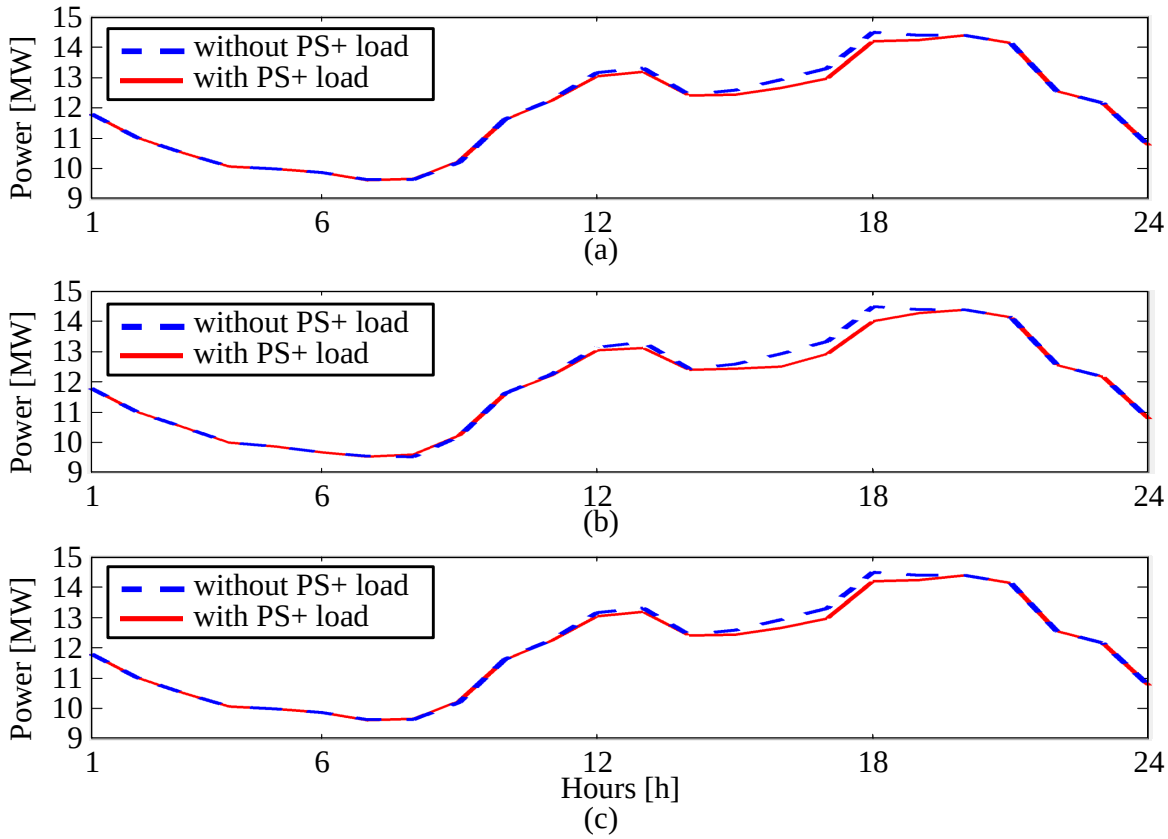

Figure 4.5: Load profiles at the feeder level for $T_{p,n}^{max}$ of (a) 4, (b) 10, and (c) 13 hours, from hours 7:00 to 20:00.

4.3.2 Case 2

Since F_3 seeks to minimize E_{loss}, increasing $T_{p,n}^{max}$ may reduce the energy usage, and consequently reduce E_{loss}; however, peak load reduction may not take place, as shown in Figure 4.5. Hence, the F_4 objective function in (4.11a)-(4.11c) is used in this case to reduce both E_{loss} and peak load, assuming that the same PCT signal is sent to all PS+ controllable loads; the effect of β in (4.11b) for $T^{max} = 4$ h and $P_{cons} = 11.5$ MW is studied here. Since in F_4 the target is to keep the peak load close to P_{cons}, the value of P_{cons} is chosen to be less than the P_{lim} value of 14.5 MW in Case 1 in order to effectively reduce the peak. Table 4.1 shows the effect of different values of β with uniform application of PS+ signals; note that when $\beta = 0$, the peak load reduction achieved is 99.9 kW. Further-

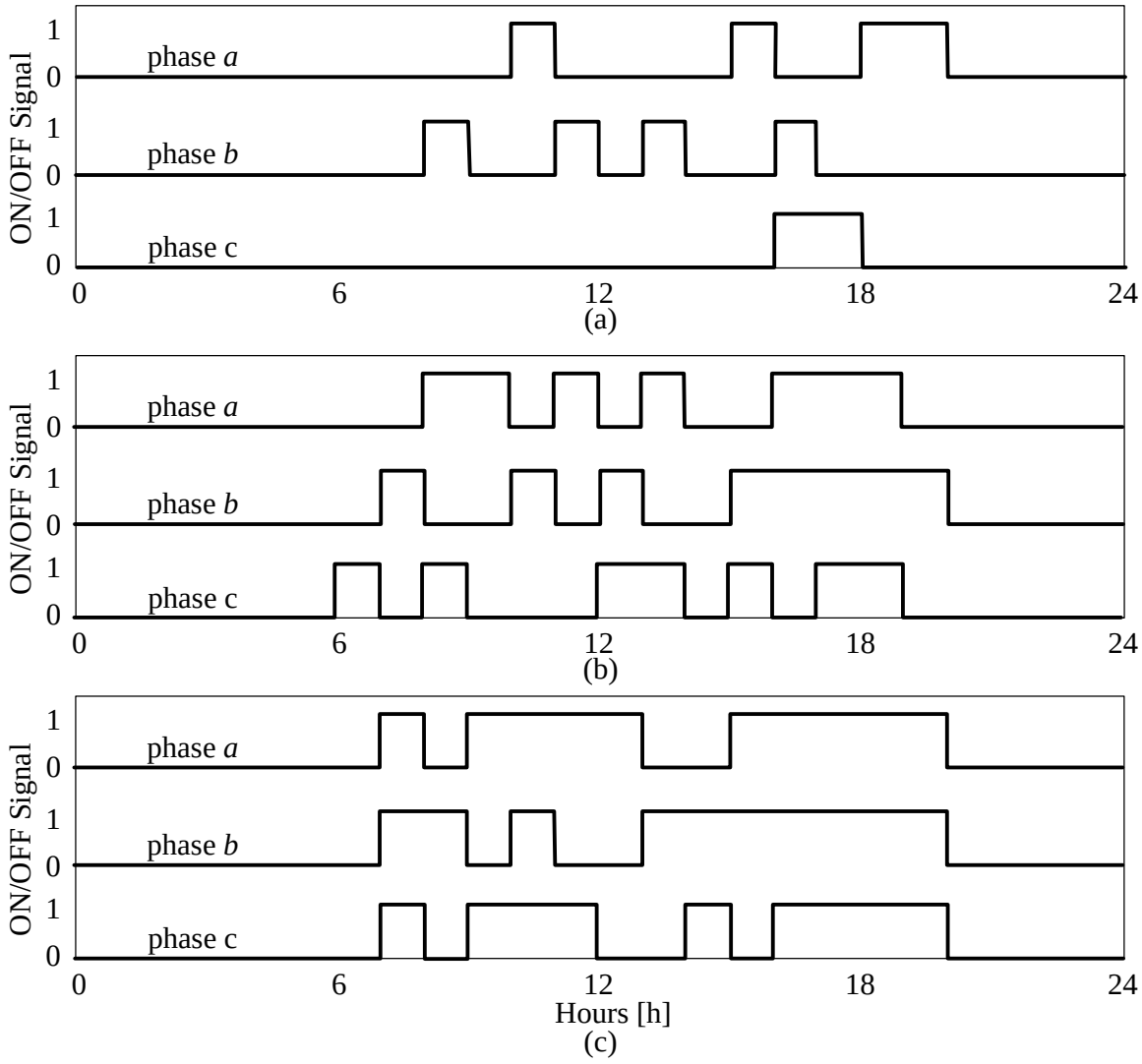

Figure 4.6: Smart load activation signals μ at Node 8 for $T_{p,n}^{max}$ of (a) 4, (b) 10, and (c) 13 hours, from hours 7:00 to 20:00.

more, when β is varied over a wide range, the peak load reduction remains more or less at the same level (95 to 100 kW). Thus, the peak load reduction is almost independent of β. However, note that increasing β increases the saving in energy usage from 1.62 to 2.38 MWh.

Table 4.1: F_4 objective with uniform application of PS+ signals with T^{max} = 4 h and P_{cons} = 11.5 MW

β	Energy usage [MWh]			Peak load [kW]		
	Without PS+ signals	**With PS+ signals**	**Difference**	**Without PS+ signals**	**With PS+ signals**	**Difference**
0	287.61	285.99	1.62 (0.56%)	14575.5	14475.6	99.9 (0.69%)
0.01	287.61	285.99	1.62 (0.56%)	14597.7	14501.7	96.0 (0.66%)
0.02	287.81	286.16	1.65 (0.74%)	14549.5	14449.7	99.8 (0.69%)
0.1	288.09	286.37	1.71 (0.59%)	14597.8	14501.6	96.2 (0.66%)
0.15	287.76	286.01	1.75 (0.61%)	14542.8	14446.5	96.3 (0.66%)
1	287.27	285.09	2.18 (0.76%)	14476.7	14378.2	98.5 (0.68%)
2	287.79	285.40	2.38 (0.83%)	14540.0	14445.4	94.6 (0.65%)

Table 4.2: F_4 objective with uniform application of PS+ signals with β = 1 and P_{cons} = 11.5 MW

PS+ ON signal hours [h]	**Energy usage [MWh]**			**Peak load [kW]**		
	Without PS+ signals	**With PS+ signals**	**Difference**	**Without PS+ signals**	**With PS+ signals**	**Difference**
4	286.67	285.09	1.58 (0.55%)	14476.7	14378.2	98.5 (0.68%)
5	287.36	284.81	2.55 (0.89%)	14506.7	14411.0	95.7 (0.66%)
6	288.13	285.64	2.49 (0.86%)	14509.7	14412.3	97.4 (0.67%)
7	286.31	283.55	2.76 (0.96%)	14440.6	14342.7	97.9 (0.68%)
8	287.19	284.52	2.67 (0.93%)	14476.7	14378.2	98.5 (0.68%)
9	288.07	285.66	2.42 (0.84%)	14448.3	14342.8	105.5 (0.73%)
10	288.29	286.15	2.15 (0.75%)	14476.7	14137.4	339.3 (2.34%)
11	287.94	284.61	3.34 (1.16%)	14509.7	14171.1	338.6 (2.33%)
12	286.92	283.55	3.37 (1.17%)	14476.7	14137.4	339.3 (2.34%)
13	287.08	284.05	3.03 (1.06%)	14509.7	14171.1	338.6 (2.33%)

The impact of hours of PS+ operation on the energy usage and the peak loads are presented in Table 4.2 for β = 1 and P_{cons} = 11.5 MW, for T^{max} = 4-13 hours of PCT operation. Observe that for T^{max} = 4-9 hours of PCT operation, the peak loads are not considerably reduced, while for T^{max} = 10-13 hours, peak loads are efficiently decreased (up to 3.5 times further decrease in peak load). By increasing the maximum hours of ON signals, the DOPF model tends to activate the PCT for more hours, and hence the chance of reducing the peak load increases. The reduction of energy usage with T^{max} = 4 h is

Table 4.3: F_4 objective with nodal and phase-wise application of PS+ signals with T^{max} = 4 h and P_{cons} = 11.5 MW

β	Energy usage [MWh]			Peak load [kW]		
	Without PS+ signals	**With PS+ signals**	**Difference**	**Without PS+ signals**	**With PS+ signals**	**Difference**
0	287.06	286.09	0.97 (0.34%)	14509.7	14404.8	104.9 (0.72%)
0.01	287.34	286.36	0.97 (0.34%)	14509.7	14374.6	135.1 (0.93%)
0.02	287.40	286.25	1.15 (0.40%)	14476.7	14340.0	136.7 (0.94%)
0.1	288.51	287.34	1.17 (0.41%)	14473.6	14326.6	147.0 (1.02%)
0.15	288.66	287.45	1.20 (0.42%)	14509.7	14352.6	157.1 (1.08%)
1	289.20	287.99	1.21 (0.42%)	14509.7	14309.5	200.2 (1.38%)
2	289.12	287.85	1.28 (0.44%)	14502.8	14301.3	201.5 (1.39%)

1.58 MWh, while this reduction is 3.03 MWh with T^{max} = 13 h. Hence, offering further incentives to customers to opt for a higher value of T^{max} should be considered.

4.3.3 Case 3

In this case, the effect of sending different PCT signals to the PS+ controllable loads in each phase and node of the distribution system, instead of sending the same PCT signal to all controllable loads, is studied for the F_4 objective function; the results are presented in Table 4.3. Comparing this table to Table 4.1 shows that different signals yield more reduction in peak load, but the energy usage increases. In this case, loads with higher peak load in each phase are activated, and hence the overall peak load is reduced more effectively than in the case of a uniform PS+ signal (Case 2); for instance, with $\beta = 2$ the peak load reduction in Case 3 is almost double that in Case 2. However, different signals reduces the savings in energy; for example, for $\beta = 2$, the saving in the energy usage is 2.38 MWh in Case 2, whereas this value is 1.28 MWh in the present case. Hence, based on the need of the system and also the DR program, LDCs need to consider what method is more suitable for them.

4.4 Summary

This chapter has proposed NN-based models of existing PS+ controllable loads demonstrating its application and integration into the DOPF, together with the GA and distributed

computing approaches to solve it. Thereafter, based on a distributed computing approach, a DOPF model using a GA-based solution technique was used to determine the optimal setpoints for LTCs, SCs, and PS+ ON/OFF signals in a realistic distribution feeder.

The studies carried out on the practical feeder demonstrate that different scenarios with single and multiple PCT ON/OFF signals for controllable loads can impact the load profiles, reduce peak loads, and decrease the energy usage. Based on the presented results, using a single ON/OFF signal for all controllable loads together with longer signal schedules can effectively reduce both peak loads and energy consumption of a distribution system at the feeder level, depending on the proportion of controllable loads in the system.

Chapter 5

Conclusions

5.1 Summary

The research conducted in this thesis concentrates on the minimization of energy consumption and peak load reduction in smart distribution systems, proposing a mathematical model of an unbalanced three-phase DOPF model with a GA-based solution approach at the feeder level, including different kinds of smart loads and other components of distribution systems, and solved using a distributed computing approach. The motivations and main research objectives for the research were identified based on a critical review of the existing literature presented in Chapter 1.

In Chapter 2, the main background topics relevant to the research on optimal feeder operation with smart loads were reviewed. A brief overview of DSA, DMS, and centralized VVC problems was presented. Load modeling and load management programs in the context of DSM and DR were discussed, followed by a discussion of the EHMS micro-hubs and PS+ smart loads. Furthermore, a brief review of different mathematical programming models and solution approaches was made, and the SGCM system, which is a parallel distributed system for real-time applications based on the MapReduce model, was introduced; this was followed by an overview of the SGCM architecture and its application to distributed computing approaches. Finally, mathematical models of distribution system components were presented.

In Chapter 3, an unbalanced three-phase DOPF model with EHMS micro-hub smart loads in centralized and distributed computing approaches was presented. Hence, an unbalanced three-phase DLF model was first discussed, using two distribution feeders, namely,

the IEEE 13-node test feeder and a practical test feeder, to test and validate the DLF model. The implementation of DOPF model based on the proposed DLF model, with a GA-based solution using centralized and decentralized approaches, was then presented, with the results showing that the parallel computing approach could reduce the run-time of the DOPF model significantly in comparison with the centralized approach. This was followed by a discussion on solving the DLF model using OpenDSS to considerably reduce the run-time. Finally, the unbalanced three-phase DOPF model including of EHMS micro-hub smart loads was presented, and the results obtained from different realistic case studies and scenarios were discussed. The studies demonstrated that compared to the centralized approach, the proposed distributed computing architecture yielded significantly faster solutions by increasing the number of SGCM worker-nodes, with realistic peak demand caps for controllable smart loads, considering both LDC's and customers' interests.

In Chapter 4, an NN model of existing PS+ smart loads was developed and integrated into the DOPF model to optimally control tap changers and switched capacitors, as well as sent signals to programmable thermostats of ACs in residential buildings, associated with the PS+ program. Based on a distributed computing approach, a GA-based solution technique was used to solve the DOPF model and hence determine the optimal setpoints for LTCs, SCs, and PS+ ON/OFF signals. Different scenarios with single and multiple PCT ON/OFF signals for controllable loads were studied, which showed the controllable loads' impact on the load profiles, reducing the peak load, and reducing the energy usage. Based on the presented results, using a single ON/OFF signal for all controllable loads, together with longer signal schedules, could effectively reduce both peak loads and energy consumption of a distribution system at the feeder level, depending on the proportion of controllable loads in the system.

5.2 Contributions

The main contributions of the research presented in this thesis are as follows:

- Implemented a power flow model of an unbalanced three-phase distribution system, referred to as a DLF, including controllable smart loads modeled using NNs and other components of distribution systems. The DLF model needs to be a stand-alone executable program that can be used on different platforms (i.e., the Windows, Linux, and Mac), for its implementation in the proposed distributed computing approach.
- Developed NN-based models of EHMS micro-hub and PS+ controllable loads, and

integrated them into the DLF model, to realize appropriate DOPF models with the objectives of minimizing energy loss and peak demand over a desired horizon.

- Developed a GA-based solution approach for the DOPF model to find optimal switching of control devices such as LTCs, SCs, peak demand caps on EHMS micro-hub loads, and thermostat signals on PS+ loads, and developed a MapReduce model, using a distributed computing approach in order to reduce the computational time of the GA-based model to make it suitable for real-time applications.

- Tested the developed DOPF model on a practical test feeder to demonstrate and validate the proposed method for practical applications.

The main contents and contributions of Chapter 3 have been published in the IEEE Transactions on Smart Grid [91]. The main contents of Chapter 4 have been submitted for possible publication in the IEEE Transactions on Smart Grid [145], and is currently under review. Also, work is being carried out on another application of the SGCM system for reducing the run-time of large-scale dynamic OPF problems.

5.3 Future Work

Based on the research presented in this thesis, the following are some possible directions for future research:

- The proposed DOPF model used a recursive GA-based method to find the optimal solution. Other EAs such as PSO and Ant Colony algorithms can be studied instead of GA to find which EA is best fit for this MINLP DOPF model.

- The proposed SGCM system uses the multi-tasking feature of the computing platforms for assigning the cores and required memory to the worker-nodes. The next direction of development of the SGCM system is to fully parallelize the SGCM system, which should be responsible for allocating the cores and memory to the worker-nodes. This parallel feature can reduce the run-time and decrease the number of errors/failures in parallel computing approaches.

- The impacts of DG sources and PEV customers on the control and operation of distribution feeders need further research.

References

[1] "International Energy Outlook 2013," *U. S. Energy Information Administration*, July 2013, [online]. Available: http://www.eia.gov/forecasts/archive/ieo13/pdf/0484(2013).pdf.

[2] "Long-Term Energy Plan 2013," *Independent Electricity System Operator (IESO)*, 2013, [online]. Available: http://www.powerauthority.on.ca/power-planning/long-term-energy-plan-2013.

[3] "International Energy Outlook 2014," *U. S. Energy Information Administration*, Sept. 2014, [online]. Available: http://www.eia.gov/forecasts/ieo/pdf/0484(2014).pdf.

[4] "Clean Energy in Ontario," *Ontario Ministry of Energy*, [online]. Available: http://www.energy.gov.on.ca/en/clean-energy-in-ontario/.

[5] A. Ipakchi and F. Albuyeh, "Grid of the future," *IEEE Power and Energy Magazine*, vol. 7, no. 2, pp. 52 – 62, Mar. 2009.

[6] H. Farhangi, "The path of the smart grid," *IEEE Power and Energy Magazine*, vol. 8, no. 1, pp. 18 – 28, Jan. 2010.

[7] F. Goodman and M. McGranaghan, "EPRI research plan for advanced distribution automation," in *Proc. 2005 IEEE Power Engineering Society General Meeting*, vol. 3, June 2005, p. 2620.

[8] "Enabling Tomorrow's Electricity System," *Ontario Smart Grid Forum*, Feb. 2009, [online]. Available: http://www.ieso.ca/imoweb/pubs/smart_grid/Smart_Grid_Forum-Report.PDF.

[9] "Modernizing Ontario's Electricity System: Next Steps," *Ontario Smart Grid Forum*, May 2011, [online]. Available: http://www.ieso.ca/imoweb/pubs/smart_grid/Smart_Grid_Forum-Report-May_2011.pdf.

[10] "Ontario Smart Grid Progress Assessment: A Vignette," *Ontario Smart Grid Forum*, Aug. 2013, [online]. Available: http://www.ieso.ca/documents/smart_grid/Smart_Grid_Progress_Assessment_Vignette.pdf.

[11] "Smart Grid-Related Innovation: The Emerging Debate," *Ontario Smart Grid Forum*, July 2015, [online]. Available: http://www.ieso.ca/Documents/smart_grid/Smart-Grid-Forum-Report-July_2015.pdf.

[12] M. C. Bozchalui, S. A. Hashmi, H. Hassen, C. A. Canizares, and K. Bhattacharya, "Optimal Operation of Residential Energy Hubs in Smart Grids," *IEEE Trans. Smart Grid*, vol. 3, no. 4, pp. 1755 – 1766, Dec. 2012.

[13] M. C. Bozchalui, "Optimal Operation of Energy Hubs in the Context of Smart Grids," Ph.D. dissertation, Department of Electrical and Computer Engineering, University of Waterloo, 2011.

[14] "Directives from Minister of Energy," *Independent Electricity System Operator (IESO)*, 2015, [online]. Available: http://www.powerauthority.on.ca/about-us/directives-opa-minister-energy-and-infrastructure.

[15] A. Pahwa, D. Staszesky, N. D. R. Sarma, G. Simard, C. Williams, D. Nordell, M. McGranaghan, and S. Mak, "Distribution Automation Tutorial," *2007 IEEE Power Engineering Society General Meeting*, June 2007.

[16] V. Vyatkin, "IEC 61499 as Enabler of Distributed and Intelligent Automation: State-of-the-Art Review," *IEEE Trans. Ind. Informat.*, vol. 7, no. 4, pp. 768 – 781, Nov. 2011.

[17] N. Singh, E. Kliokys, H. Feldmann, R. Kussel, R. Chrustowski, and C. Joborowicz, "Power system modelling and analysis in a mixed energy management and distribution management system," *IEEE Trans. Power Syst.*, vol. 13, no. 3, pp. 1143 – 1149, Aug. 1998.

[18] I. Roytelman and V. Ganesan, "Coordinated local and centralized control in distribution management systems," *IEEE Trans. Power Del.*, vol. 15, no. 2, pp. 718 – 724, Apr. 2000.

[19] K. R. C. Mamandur and R. D. Chenoweth, "Optimal Control of Reactive Power flow for Improvements in Voltage Profiles and for Real Power Loss Minimization," *IEEE Trans. Power App. Syst.*, vol. PAS-100, no. 7, pp. 3185 – 3194, July 1981.

[20] Y.-Y. Hsu and F.-C. Lu, "A combined artificial neural network-fuzzy dynamic programming approach to reactive power/voltage control in a distribution substation," *IEEE Trans. Power Syst.*, vol. 13, no. 4, pp. 1265 – 1271, Nov. 1998.

[21] J. Kearly, A. Y. Chikhani, R. Hackam, M. M. A. Salama, and V. H. Quintana, "Microprocessor controlled reactive power compensator for loss reduction in radial distribution feeders," *IEEE Trans. Power Del.*, vol. 6, no. 4, pp. 1848 – 1855, Oct. 1991.

[22] R. Baldick and F. F. Wu, "Efficient integer optimization algorithms for optimal coordination of capacitors and regulators," *IEEE Trans. Power Syst.*, vol. 5, no. 3, pp. 805 – 812, Aug. 1990.

[23] M. M. A. Salama, N. Manojlovic, V. H. Quintana, and A. Y. Chikhani, "Real-time optimal reactive power control for distribution networks," *Int. Journal Elect. Power Energy Syst.*, vol. 18, no. 3, pp. 185 – 193, Mar. 1996.

[24] F. A. Rahiman, H. H. Zeineldin, V. Khadkikar, S. W. Kennedy, and V. R. Pandi, "Demand Response Mismatch (DRM): Concept, Impact Analysis, and Solution," *IEEE Trans. Smart Grid*, vol. 5, no. 4, pp. 1734 – 1743, July 2014.

[25] V. Borozan, M. E. Baran, and D. Novosel, "Integrated volt/VAr control in distribution systems," in *Proc. 2001 IEEE Power Engineering Society Winter Meeting*, vol. 3, Jan. 2001, pp. 1485 – 1490.

[26] J. J. Grainger and S. Civanlar, "Volt/Var Control on Distribution Systems with Lateral Branches Using Shunt Capacitors and Voltage Regulators Part I: The Overall Problem," *IEEE Trans. Power App. Syst.*, vol. PAS-104, no. 11, pp. 3278 – 3283, Nov. 1985.

[27] S. Touré, R. Caire, Y. Bésanger, S. Grenard, and A. Forissier, "Benders' decomposition for voltage profile management of distribution network with distributed generators," in *Proc. 2013 IEEE Grenoble PowerTech (POWERTECH)*, June 2013, pp. 1 – 6.

[28] A. T. Saric and A. M. Stankovic, "A robust algorithm for Volt/Var control," in *Proc. 2009 PSCE IEEE/PES Power Systems Conf. and Expo.*, Mar. 2009, pp. 1 – 8.

[29] I. Roytelman, B. K. Wee, and R. L. Lugtu, "Volt/var control algorithm for modern distribution management system," *IEEE Trans. Power Syst.*, vol. 10, no. 3, pp. 1454 – 1460, Aug. 1995.

[30] M. Biserica, Y. Besanger, R. Caire, O. Chilard, and P. Deschamps, "Neural Networks to Improve Distribution State Estimation–Volt Var Control Performances," *IEEE Trans. Smart Grid*, vol. 3, no. 3, pp. 1137 – 1144, Sept. 2012.

[31] A. Mohapatra, P. R. Bijwe, and B. K. Panigrahi, "An Efficient Hybrid Approach for Volt/Var Control in Distribution Systems," *IEEE Trans. Power Del.*, vol. 29, no. 4, pp. 1780 – 1788, Aug. 2014.

[32] M. Liu, S. K. Tso, and Y. Cheng, "An extended nonlinear primal-dual interior-point algorithm for reactive-power optimization of large-scale power systems with discrete control variables," *IEEE Trans. Power Syst.*, vol. 17, no. 4, pp. 982 – 991, Nov. 2002.

[33] M. B. Liu, C. A. Canizares, and W. Huang, "Reactive Power and Voltage Control in Distribution Systems With Limited Switching Operations," *IEEE Trans. Power Syst.*, vol. 24, no. 2, pp. 889 – 899, May 2009.

[34] S. Paudyal, "Optimal Energy Management of Distribution Systems and Industrial Energy Hubs in Smart Grids," Ph.D. dissertation, Department of Electrical and Computer Engineering, University of Waterloo, 2012.

[35] S. Paudyal, C. A. Canizares, and K. Bhattacharya, "Optimal Operation of Distribution Feeders in Smart Grids," *IEEE Trans. Ind. Electron.*, vol. 58, no. 10, pp. 4495 – 4503, Oct. 2011.

[36] S. Paudyal, C. A. Cañizares, and K. Bhattacharya, "Three-phase distribution OPF in smart grids: Optimality versus computational burden," in *Proc. 2011 2nd IEEE PES Int. Conf. and Exhib. Innovative Smart Grid Technologies (ISGT Europe)*, Dec. 2011, pp. 1 – 7.

[37] A. P. Sanghvi, "Flexible strategies for load/demand management using dynamic pricing," *IEEE Trans. Power Syst.*, vol. 4, no. 1, pp. 83 – 93, Feb. 1989.

[38] "Demand Side Integration," CIGRE Working Group, Tech. Rep. C6.09, Aug. 2011.

[39] P. Palensky and D. Dietrich, "Demand Side Management: Demand Response, Intelligent Energy Systems, and Smart Loads," *IEEE Trans. Ind. Informat.*, vol. 7, no. 3, pp. 381 – 388, Aug. 2011.

[40] I. Lampropoulos, W. L. Kling, P. F. Ribeiro, and J. van den Berg, "History of demand side management and classification of demand response control schemes," in *Proc. 2013 IEEE Power Energy Society General Meeting (PES)*, July 2013, pp. 1 – 5.

[41] S. A. Pourmousavi and M. H. Nehrir, "Real-Time Central Demand Response for Primary Frequency Regulation in Microgrids," *IEEE Trans. Smart Grid*, vol. 3, no. 4, pp. 1988 – 1996, Dec. 2012.

[42] M. Bayat, K. Sheshyekani, and A. Rezazadeh, "A Unified Framework for Participation of Responsive End-User Devices in Voltage and Frequency Control of the Smart Grid," *IEEE Trans. Power Syst.*, vol. 30, no. 3, pp. 1369 – 1379, May 2015.

[43] T. J. Krupa and H. Asgeirsson, "The Effects of Reduced Voltage on Distribution Circuit Loads," *IEEE Trans. Power Syst.*, vol. 2, no. 4, pp. 1013 – 1018, Nov. 1987.

[44] B. W. Kennedy and R. H. Fletcher, "Conservation voltage reduction (CVR) at Snohomish County PUD," *IEEE Trans. Power Syst.*, vol. 6, no. 3, pp. 986 – 998, Aug. 1991.

[45] J. P. A. Sandraz, R. Macwan, M. Diaz-Aguiló, J. McClelland, F. de León, D. Czarkowski, and C. Comack, "Energy and Economic Impacts of the Application of CVR in Heavily Meshed Secondary Distribution Networks," *IEEE Trans. Power Del.*, vol. 29, no. 4, pp. 1692 – 1700, Aug. 2014.

[46] Z. Wang and J. Wang, "Review on Implementation and Assessment of Conservation Voltage Reduction," *IEEE Trans. Power Syst.*, vol. 29, no. 3, pp. 1306 – 1315, May 2014.

[47] IEEE Working Group on Effectiveness of Distribution Protection, "Distribution Line Protection Practices: Industry Survey Analysis," *IEEE Trans. Power App. Syst.*, vol. PAS-102, no. 10, pp. 3279 – 3287, Oct. 1983.

[48] A. Faruqui, P. Hanser, R. Hledik, and J. Palmer, "Assessing Ontario's Regulated Price Plan: A White Paper," The Brattle Group, Tech. Rep., Dec. 2010, [online]. Available: http://www.ontarioenergyboard.ca/oeb/_Documents/EB-2010-0364/Report-Assessing%20Ontarios%20Regulated%20Price%20Plan.pdf.

[49] E. Celebi and J. D. Fuller, "A Model for Efficient Consumer Pricing Schemes in Electricity Markets," *IEEE Trans. Power Syst.*, vol. 22, no. 1, pp. 60 – 67, Feb. 2007.

[50] A. H. Mohsenian-Rad and A. Leon-Garcia, "Optimal Residential Load Control With Price Prediction in Real-Time Electricity Pricing Environments," *IEEE Trans. Smart Grid*, vol. 1, no. 2, pp. 120 – 133, Sept. 2010.

[51] P. Samadi, H. Mohsenian-Rad, V. W. S. Wong, and R. Schober, "Real-Time Pricing for Demand Response Based on Stochastic Approximation," *IEEE Trans. Power Syst.*, vol. 5, no. 2, pp. 789 – 798, Mar. 2014.

[52] C. Vivekananthan, Y. Mishra, and F. Li, "Real-Time Price Based Home Energy Management Scheduler," *IEEE Trans. Power Syst.*, vol. 30, no. 4, pp. 2149 – 2159, July 2015.

[53] Z. Chen, L. Wu, and Y. Fu, "Real-Time Price-Based Demand Response Management for Residential Appliances via Stochastic Optimization and Robust Optimization," *IEEE Trans. Smart Grid*, vol. 3, no. 4, pp. 1822 – 1831, Dec. 2012.

[54] M. P. F. Hommelberg, C. J. Warmer, I. G. Kamphuis, J. K. Kok, and G. J. Schaeffer, "Distributed Control Concepts using Multi-Agent technology and Automatic Markets: An indispensable feature of smart power grids," in *Proc. 2007 IEEE Power Engineering Society General Meeting*, June 2007, pp. 1 – 7.

[55] C. Y. Tee and J. B. Cardell, "Market Integration of Distributed Resources Through Coordinated Frequency and Price Droop," *IEEE Trans. Smart Grid*, vol. 5, no. 4, pp. 1556 – 1565, July 2014.

[56] C. Chen, J. Wang, Y. Heo, and S. Kishore, "MPC-Based Appliance Scheduling for Residential Building Energy Management Controller," *IEEE Trans. Smart Grid*, vol. 4, no. 3, pp. 1401 – 1410, Sept. 2013.

[57] C. Wang, Y. Zhou, J. Wu, J. Wang, Y. Zhang, and D. Wang, "Robust-Index Method for Household Load Scheduling Considering Uncertainties of Customer Behavior," *IEEE Trans. Smart Grid*, vol. 6, no. 4, pp. 1806 – 1818, July 2015.

[58] Y. Zong, L. Mihet-Popa, D. Kullmann, A. Thavlov, O. Gehrke, and H. W. Bindner, "Model Predictive Controller for Active Demand Side Management with PV self-consumption in an intelligent building," in *Proc. 2012 3rd IEEE PES Int. Conf. and Exhib. Innovative Smart Grid Technologies (ISGT Europe)*, Oct. 2012, pp. 1 – 8.

[59] J. Li, Z. Wu, S. Zhou, H. Fu, and X. P. Zhang, "Aggregator service for PV and battery energy storage systems of residential building," *CSEE Journal of Power and Energy Systems*, vol. 1, no. 4, pp. 3 – 11, Dec. 2015.

[60] I. Lampropoulos, N. Baghină, W. L. Kling, and P. F. Ribeiro, "A Predictive Control Scheme for Real-Time Demand Response Applications," *IEEE Trans. Smart Grid*, vol. 4, no. 4, pp. 2049 – 2060, Dec. 2013.

[61] E. Mohagheghi, A. Gabash, and P. Li, "Real-time optimal power flow under wind energy penetration-Part I: Approach," in *Proc. 2016 IEEE 16th Int. Conf. Environment and Electrical Engineering (EEEIC)*, June 2016, pp. 1 – 6.

[62] J. A. Martinez and G. Guerra, "A Parallel Monte Carlo Method for Optimum Allocation of Distributed Generation," *IEEE Trans. Power Syst.*, vol. 29, no. 6, pp. 2926 – 2933, Nov. 2014.

[63] B. R. Sathyanarayana and G. T. Heydt, "Sensitivity-Based Pricing and Optimal Storage Utilization in Distribution Systems," *IEEE Trans. Power Del.*, vol. 28, no. 2, pp. 1073 – 1082, Apr. 2013.

[64] W. K. Tao, C. Cavellucci, and C. Lyra, "Parallel intelligent search for loss minimization in distribution systems," in *Proc. 1999 IEEE Transmission and Distribution Conf.*, vol. 1, Apr. 1999, pp. 218 – 222.

[65] A. R. Malekpour, A. Pahwa, A. Malekpour, and B. Natarajan, "Hierarchical Architecture for Integration of Rooftop PV in Smart Distribution Systems," *IEEE Trans. Smart Grid*, vol. PP, no. 99, pp. 1 – 11, Sept. 2016.

[66] K. Y. Liu, W. Sheng, X. Meng, and Y. Liu, "Decentralized voltage optimization and coordinated method in smart distribution grid," in *Proc. 2015 IEEE Power Energy Society General Meeting*, July 2015, pp. 1 – 5.

[67] H. Fan and Y.-A. Chen, "System and method for providing p2p based reconfigurable computing and structured data distribution," Patent, July 2013, WO Patent App. PCT/CA2012/000,912, [online]. Available: http://www.google.com/patents/WO2013102253A1?cl=en.

[68] K. Shvachko, H. Kuang, S. Radia, and R. Chansler, "The Hadoop Distributed File System," in *Proc. 2010 IEEE 26th Symp. Mass Storage Systems and Technologies (MSST)*, May 2010, pp. 1 – 10.

[69] M. Khan, Y. Jin, M. Li, Y. Xiang, and C. Jiang, "Hadoop Performance Modeling for Job Estimation and Resource Provisioning," *IEEE Trans. Parallel Distrib. Syst.*, vol. 27, no. 2, pp. 441 – 454, Feb. 2016.

[70] Z. Ren, J. Wan, W. Shi, X. Xu, and M. Zhou, "Workload Analysis, Implications, and Optimization on a Production Hadoop Cluster: A Case Study on Taobao," *IEEE Trans. Serv. Comput.*, vol. 7, no. 2, pp. 307 – 321, Apr. 2014.

[71] J. Dean and S. Ghemawat, "MapReduce: Simplified Data Processing on Large Clusters," *Communications of the ACM*, vol. 51, no. 1, pp. 107 – 113, Jan. 2008, [online]. Available: = http://doi.acm.org/10.1145/1327452.1327492.

[72] "Smart Grid Resource Center," *EPRI: Electric Power Research Institute*, [online]. Available: http://smartgrid.epri.com/SimulationTool.aspx.

[73] "Smart Grid Fund," *Ontario Ministry of Energy*, [online]. Available: http://www.energy.gov.on.ca/en/smart-grid-fund/.

[74] S. Price and M. McGranaghan, "Value of Distribution Automation Application," *California Energy Commission, Public Interest Energy Research (PIER) Program*, Apr. 2007, [online]. Available: http://www.energy.ca.gov/2007publications/CEC-500-2007-028/CEC-500-2007-028.PDF.

[75] J. B. Bunch, "Guidelines for Evaluating Distribution Automation," EPRI, Tech. Rep. EPRI EL-3728, Nov. 1984.

[76] V. Madani, R. Das, F. Aminifar, J. McDonald, S. S. Venkata, D. Novosel, A. Bose, and M. Shahidehpour, "Distribution Automation Strategies Challenges and Opportunities in a Changing Landscape," *IEEE Trans. Smart Grid*, vol. 6, no. 4, pp. 2157 – 2165, July 2015.

[77] R. Das, V. Madani, F. Aminifar, J. McDonald, S. S. Venkata, D. Novosel, A. Bose, and M. Shahidehpour, "Distribution Automation Strategies: Evolution of Technologies and the Business Case," *IEEE Trans. Smart Grid*, vol. 6, no. 4, pp. 2166 – 2175, July 2015.

[78] M. Dixon, "Autodaptive volt/VAr management system," in *Proc. 2001 Rural Electric Power Conf.*, May 2001, pp. D4/1 – D4/8.

[79] C.-h. Lien, Y.-w. Bai, and M.-b. Lin, "Remote-Controllable Power Outlet System for Home Power Management," *IEEE Trans. Consum. Electron.*, vol. 53, no. 4, pp. 1634 – 1641, Nov. 2007.

[80] M. A. A. Pedrasa, T. D. Spooner, and I. F. MacGill, "Coordinated Scheduling of Residential Distributed Energy Resources to Optimize Smart Home Energy Services," *IEEE Trans. Smart Grid*, vol. 1, no. 2, pp. 134 – 143, Sept. 2010.

[81] G. A. McNaughton and R. Saint, "Enterprise integration implications for home-area network technologies," in *Proc. 2010 Innovative Smart Grid Technologies (ISGT)*, Jan. 2010, pp. 1 – 5.

[82] M. Fan, Z. Zhang, and C. E. Lin, "Discrete VAR optimization in a distribution system using mixed-integer programming with an expert system," *Electric Power Systems Research*, vol. 27, no. 3, pp. 191 – 201, Aug. 1993.

[83] R.-H. Liang and C.-K. Cheng, "Dispatch of main transformer ULTC and capacitors in a distribution system," *IEEE Trans. Power Del.*, vol. 16, no. 4, pp. 625 – 630, Oct. 2001.

[84] M. E. Elkhatib, R. El-Shatshat, and M. M. A. Salama, "Novel Coordinated Voltage Control for Smart Distribution Networks With DG," *IEEE Trans. Smart Grid*, vol. 2, no. 4, pp. 598 – 605, Dec. 2011.

[85] R. A. Jabr and I. Džafić, "Sensitivity-Based Discrete Coordinate-Descent for Volt/VAr Control in Distribution Networks," *IEEE Trans. Power Syst.*, vol. PP, no. 99, pp. 1 – 9, Jan. 2016.

[86] I. Sharma, C. A. Cañizares, and K. Bhattacharya, "Residential micro-hub load model using neural network," in *2015 North American Power Symp. (NAPS)*, Oct. 2015, pp. 1 – 6.

[87] Y. Liang, K. S. Tam, and R. Broadwater, "Load Calibration and Model Validation Methodologies for Power Distribution Systems," *IEEE Trans. Power Syst.*, vol. 25, no. 3, pp. 1393 – 1401, Aug. 2010.

[88] W. H. Kersting, *Distribution System Modeling and Analysis*, 3rd ed. Boca Raton: CRC Press, 2012.

[89] IEEE Task Force on Load Representation for Dynamic Performance, "Load representation for dynamic performance analysis [of power systems]," *IEEE Trans. Power Syst.*, vol. 8, no. 2, pp. 472 – 482, May 1993.

[90] A. Mosaddegh, C. A. Cañizares, and K. Bhattacharya, "Distributed computing approach to solve unbalanced three-phase DOPFs," in *Proc. 2015 IEEE Electrical Power and Energy Conf. (EPEC)*, Oct. 2015, pp. 408 – 413.

[91] A. Mosaddegh, C. A. Cañizares, K. Bhattacharya, and H. Fan, "Distributed Computing Architecture for Optimal Control of Distribution Feeders with Smart Loads," *IEEE Trans. Smart Grid*, vol. PP, no. 99, pp. 1 – 10, Sept. 2016.

[92] A. Bokhari, A. Alkan, R. Dogan, M. Diaz-Aguilò, F. de Leòn, D. Czarkowski, Z. Zabar, L. Birenbaum, A. Noel, and R. E. Uosef, "Experimental Determination of the ZIP Coefficients for Modern Residential, Commercial, and Industrial Loads," *IEEE Trans. Power Del.*, vol. 29, no. 3, pp. 1372 – 1381, June 2014.

[93] A. Garces, "A Linear Three-Phase Load Flow for Power Distribution Systems," *IEEE Trans. Power Syst.*, vol. 31, no. 1, pp. 827 – 828, Jan. 2016.

[94] J. Y. Wen, L. Jiang, Q. H. Wu, and S. J. Cheng, "Power system load modeling by learning based on system measurements," *IEEE Trans. Power Del.*, vol. 18, no. 2, pp. 364 – 371, Apr. 2003.

[95] B.-K. Choi, H.-D. Chiang, Y. Li, H. Li, Y.-T. Chen, D.-H. Huang, and M. G. Lauby, "Measurement-based dynamic load models: derivation, comparison, and validation," *IEEE Trans. Power Syst.*, vol. 21, no. 3, pp. 1276 – 1283, Aug. 2006.

[96] S. Son, S. H. Lee, D.-H. Choi, K.-B. Song, J.-D. Park, Y.-H. Kwon, K. Hur, and J.-W. Park, "Improvement of Composite Load Modeling Based on Parameter Sensitivity and Dependency Analyses," *IEEE Trans. Power Syst.*, vol. 29, no. 1, pp. 242 – 250, Jan. 2014.

[97] D. Chen and R. R. Mohler, "Neural-network-based load modeling and its use in voltage stability analysis," *IEEE Trans. Control Syst. Technol.*, vol. 11, no. 4, pp. 460 – 470, July 2003.

[98] P. Regulski, D. S. Vilchis-Rodriguez, S. Djurović, and V. Terzija, "Estimation of Composite Load Model Parameters Using an Improved Particle Swarm Optimization Method," *IEEE Trans. Power Del.*, vol. 30, no. 2, pp. 553 – 560, Apr. 2015.

[99] P. Ju, E. Handschin, and D. Karlsson, "Nonlinear dynamic load modelling: model and parameter estimation," *IEEE Trans. Power Syst.*, vol. 11, no. 4, pp. 1689 – 1697, Nov. 1996.

[100] "Annual Energy Review 2011," U. S. Energy Information Administration, Tech. Rep. DOE/EIA-0384(2011), Sept. 2012, [online]. Available: http://www.eia.gov/totalenergy/data/annual/archive/038411.pdf.

[101] J. H. Eto, "The Past, Present, and Future of U.S. Utility Demand-Side Management Programs," LBNL, University of California, Berkeley, Tech. Rep. LBNL-39931, Sept. 1996, [online]. Available: eetd.lbl.gov/sites/all/files/publications/39931.pdf.

[102] R. M. Delgado, "Demand-side management alternatives," *Proc. IEEE*, vol. 73, no. 10, pp. 1471 – 1488, Oct. 1985.

[103] M. Geidl, G. Koeppel, P. Favre-Perrod, B. Klockl, G. Andersson, and K. Frohlich, "Energy hubs for the future," *IEEE Power Energy Mag.*, vol. 5, no. 1, pp. 24 – 30, Jan. 2007.

[104] A. Ghasemi, M. Hojjat, and M. H. Javidi, "Introducing a new framework for management of future distribution networks using potentials of energy hubs," in *Proc. 2012 2nd Iranian Conf. Smart Grids (ICSG)*, May 2012, pp. 1 – 7.

[105] M. Geidl and G. Andersson, "Optimal Power Flow of Multiple Energy Carriers," *IEEE Trans. Power Syst.*, vol. 22, no. 1, pp. 145 – 155, Feb. 2007.

[106] M. Moeini-Aghtaie, A. Abbaspour, M. Fotuhi-Firuzabad, and E. Hajipour, "A Decomposed Solution to Multiple-Energy Carriers Optimal Power Flow," *IEEE Trans. Power Syst.*, vol. 29, no. 2, pp. 707 – 716, Mar. 2014.

[107] L. Carradore and F. Bignucolo, "Distributed multi-generation and application of the energy hub concept in future networks," in *Proc. 2008 UPEC 43rd Int. Universities Power Engineering Conf.*, Sept. 2008, pp. 1 – 5.

[108] S. Pazouki, M. R. Haghifam, and S. Pazouki, "Short term economical scheduling in an energy hub by renewable and demand response," in *Proc. 2013 3rd Int. Conf. Electric Power and Energy Conversion Systems (EPECS)*, Oct. 2013, pp. 1 – 6.

[109] X. Guan, Z. Xu, and Q. S. Jia, "Energy-Efficient Buildings Facilitated by Microgrid," *IEEE Trans. Smart Grid*, vol. 1, no. 3, pp. 243 – 252, Dec. 2010.

[110] A. Soares, A. Gomes, and C. H. Antunes, "Domestic load characterization for demand-responsive energy management systems," in *Proc. 2012 IEEE Int. Symp. Sustainable Systems and Technology (ISSST)*, May 2012, pp. 1 – 6.

[111] A. Molderink, V. Bakker, M. G. C. Bosman, J. L. Hurink, and G. J. M. Smit, "Management and Control of Domestic Smart Grid Technology," *IEEE Trans. Smart Grid*, vol. 1, no. 2, pp. 109 – 119, Sept. 2010.

[112] I. Sharma, C. A. Cañizares, and K. Bhattacharya, "Smart charging of PEVs penetrating into residential distribution systems," *IEEE Trans. Smart Grid*, vol. 5, no. 3, pp. 1196 – 1209, May 2014.

[113] E. Pouresmaeil, J. M. Gonzalez, C. A. Canizares, and K. Bhattacharya, "Development of a Smart Residential Load Simulator for Energy Management in Smart Grids," pp. 1 – 8, [online]. Available: https://uwaterloo.ca/power-energy-systems-group/downloads/smart-residential-load-simulator-srls.

[114] S. Bahrami, F. Khazaeli, and M. Parniani, "Industrial load scheduling in smart power grids," in *Proc. 22nd Int. Conf. and Exhib. Electricity Distribution (CIRED 2013)*, June 2013, pp. 1 – 4.

[115] I. Sharma, K. Bhattacharya, and C. A. Cañizares, "Smart Distribution System Operations With Price-Responsive and Controllable Loads," *IEEE Trans. Smart Grid*, vol. 6, no. 2, pp. 795 – 807, Mar. 2015.

[116] S. Wang and Z. Ma, "Supervisory and Optimal Control of Building HVAC Systems: A Review," *HVAC&R Research*, vol. 14, no. 1, pp. 3 – 32, Jan. 2008, [online]. Available: http://dx.doi.org/10.1080/10789669.2008.10390991.

[117] F. Zhao, J. Fan, and S. Mijanovic, "PI auto-tuning and performance assessment in HVAC systems," in *Proc. 2013 American Control Conf. (ACC)*, June 2013, pp. 1783 – 1788.

[118] Y. Sun, M. Elizondo, S. Lu, and J. C. Fuller, "The Impact of Uncertain Physical Parameters on HVAC Demand Response," *IEEE Trans. Smart Grid*, vol. 5, no. 2, pp. 916 – 923, Mar. 2014.

[119] M. Anderson, M. Buehner, P. Young, D. Hittle, C. Anderson, J. Tu, and D. Hodgson, "MIMO Robust Control for HVAC Systems," *IEEE Trans. Control Syst. Technol.*, vol. 16, no. 3, pp. 475 – 483, May 2008.

[120] "Peaksaver PLUS Frequently Asked Questions," *Hydro One*, [online]. Available: http://www.hydroone.com/MyHome/SaveEnergy/Pages/peaksaverPLUS_FAQs.aspx.

[121] S. Singla and S. Keshav, "Demand response through a temperature setpoint market in Ontario," in *Proc. 2012 IEEE 3rd Int. Conf. Smart Grid Communications (SmartGridComm)*, Nov. 2012, pp. 103 – 108.

[122] "Energy Savings & Tips," *EnerSource*, [online]. Available: http://www.enersource.com/energy-savings-tips.

[123] S. S. Rao, *Engineering Optimization: Theory and Practice*, 4th ed. New York: John Wiley & Sons, Inc., 2009.

[124] M. Kaplan, "Optimization of Number, Location, Size, Control Type, and Control Setting of Shunt Capacitors on Radial Distribution Feeders," *IEEE Trans. Power App. Syst.*, vol. PAS-103, no. 9, pp. 2659 – 2665, Sept. 1984.

[125] S. Deshmukh, B. Natarajan, and A. Pahwa, "Voltage/VAR Control in Distribution Networks via Reactive Power Injection Through Distributed Generators," *IEEE Trans. Smart Grid*, vol. 3, no. 3, pp. 1226 – 1234, Sept. 2012.

[126] N. Daratha, B. Das, and J. Sharma, "Coordination Between OLTC and SVC for Voltage Regulation in Unbalanced Distribution System Distributed Generation," *IEEE Trans. Power Syst.*, vol. 29, no. 1, pp. 289 – 299, Jan. 2014.

[127] M. A. Azzouz, M. F. Shaaban, and E. F. El-Saadany, "Real-Time Optimal Voltage Regulation for Distribution Networks Incorporating High Penetration of PEVs," *IEEE Trans. Power Syst.*, vol. 30, no. 6, pp. 3234 – 3245, Nov. 2015.

[128] L. Costa and P. Oliveira, "Evolutionary algorithms approach to the solution of mixed integer non-linear programming problems," *Computers & Chemical Engineering*, vol. 25, no. 2 – 3, pp. 257 – 266, Mar. 2001.

[129] G. Levitin, A. Kalyuzhny, A. Shenkman, and M. Chertkov, "Optimal capacitor allocation in distribution systems using a genetic algorithm and a fast energy loss computation technique," *IEEE Trans. Power Del.*, vol. 15, no. 2, pp. 623 – 628, Apr. 2000.

[130] S. Sundhararajan and A. Pahwa, "Optimal selection of capacitors for radial distribution systems using a genetic algorithm," *IEEE Trans. Power Syst.*, vol. 9, no. 3, pp. 1499 – 1507, Aug. 1994.

[131] V. Farahani, B. Vahidi, and H. A. Abyaneh, "Reconfiguration and Capacitor Placement Simultaneously for Energy Loss Reduction Based on an Improved Reconfiguration Method," *IEEE Trans. Power Syst.*, vol. 27, no. 2, pp. 587 – 595, May 2012.

[132] V. Farahani, S. H. H. Sadeghi, H. A. Abyaneh, S. M. M. Agah, and K. Mazlumi, "Energy Loss Reduction by Conductor Replacement and Capacitor Placement in Distribution Systems," *IEEE Trans. Power Syst.*, vol. 28, no. 3, pp. 2077 – 2085, Aug. 2013.

[133] P. Nallagownden, L. T. Thin, N. C. Guan, and C. M. H. Mahmud, "Application of Genetic Algorithm for the Reduction of Reactive Power Losses in Radial Distribution

System," in *Proc. 2006 IEEE Int. Power and Energy Conf. (PECon)*, Nov. 2006, pp. 76 – 81.

[134] W. Fang, B. He, Q. Luo, and N. K. Govindaraju, "Mars: Accelerating MapReduce with Graphics Processors," *IEEE Trans. Parallel Distrib. Syst.*, vol. 22, no. 4, pp. 608 – 620, Apr. 2011.

[135] D. W. Marquardt, "An Algorithm for Least-Squares Estimation of Nonlinear Parameters," *Journal of the Society for Industrial and Applied Mathematics*, vol. 11, no. 2, pp. 431 – 441, June 1963.

[136] J. J. Moré, *The Levenberg-Marquardt algorithm: Implementation and theory*, lecture notes in mathematics ed. Springer-Verlag, 1977, vol. 630, ch. Numerical Analysis, G. A. Watson (editor), pp. 105 – 116.

[137] W. H. Kersting, "Radial distribution test feeders," in *Proc. 2001 IEEE Power Engineering Society Winter Meeting*, vol. 2, Jan. 2001, pp. 908 – 912.

[138] M. Graovac, X. Wang, and R. Iravani, "Integration of Storage in Electrical Distribution Systems and its Impact on the Depth of Penetration of DG," Clean Energy Technology Centre (CTEC), Tech. Rep. 2009-174, May 2008, [online]. Available: https://www.nrcan.gc.ca/sites/www.nrcan.gc.ca/files/canmetenergy/files/pubs/2009-174_RP-TEC_411-IMPACT_Graovac_Wang_Iravani_e.pdf.

[139] D. Greenhalgh and S. Marshall, "Convergence Criteria for Genetic Algorithms," *SIAM Journal on Computing*, vol. 30, no. 1, pp. 269–282, May 2000, [online]. Available: http://dx.doi.org/10.1137/S009753979732565X.

[140] I. Sharma, "Operation of Distribution Systems with PEVs and Smart Loads," Ph.D. dissertation, Department of Electrical and Computer Engineering, University of Waterloo, 2014.

[141] B. V. Solanki, A. Raghurajan, K. Bhattacharya, and C. A. Cañizares, "Including Smart Loads for Optimal Demand Response in Integrated Energy Management Systems for Isolated Microgrids," *IEEE Trans. Smart Grid*, vol. PP, no. 99, pp. 1 – 10, Jan. 2015.

[142] "Linear Transfer Function," *MathWorks*, [online]. Available: http://www.mathworks.com/help/nnet/ref/purelin.html.

[143] T. Facchinetti and M. L. Della Vedova, "Real-Time Modeling for Direct Load Control in Cyber-Physical Power Systems," *IEEE Trans. Ind. Informat.*, vol. 7, no. 4, pp. 689 – 698, Nov. 2011.

[144] W. Zhang, J. Lian, C. Y. Chang, and K. Kalsi, "Aggregated Modeling and Control of Air Conditioning Loads for Demand Response," *IEEE Trans. Power Syst.*, vol. 28, no. 4, pp. 4655 – 4664, Nov. 2013.

[145] A. Mosaddegh, C. A. Cañizares, and K. Bhattacharya, "Optimal Demand Response for Distribution Feeders with Existing Smart Loads," *Submitted to IEEE Trans. Smart Grid*, pp. 1 – 8, Sept. 2016.